A novel MR contrast agent for angiography and perfusion: Hyperpolarized water

Lipsø, Hans Kasper Wigh

Publication date:
2016

Document Version
Publisher's PDF, also known as Version of record

DTU Electrical Engineering
Department of Electrical Engineering

A novel MR contrast agent for angiography and perfusion: Hyperpolarized water

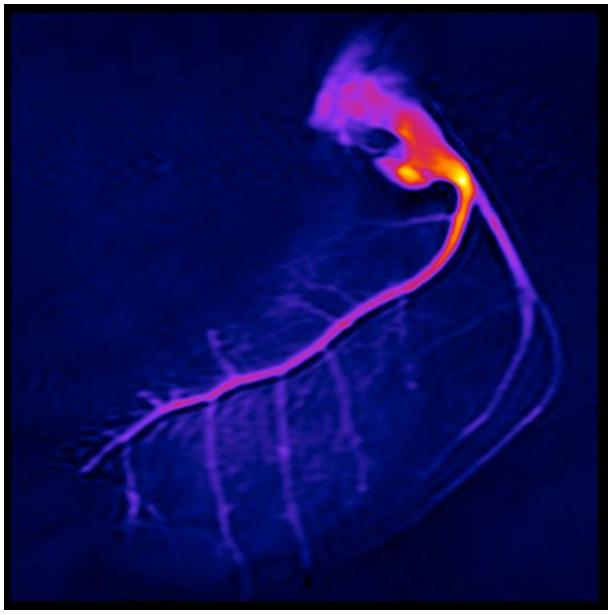

PhD Dissertation

Kasper Wigh Lipsø

November 2016

Front page image: Coronal angiography in a pig imaged by hyperpolarized water MRI.

Abstract

Magnetic Resonance Imaging (MRI) is an important tool in medical imaging, and is widely used for its high spatial and temporal resolution, and low safety concerns. However, the technique has its limitations due to the inherent low sensitivity, making it inferior to Computed Tomography (CT) in terms of spatial and temporal sensitivity and to nuclear medicine methods in terms of molecular imaging sensitivity. By hyperpolarization, the available signal can be enhanced by several orders of magnitude, and potentially close some of these gaps.

In this thesis work, the purpose is to demonstrate that water, hyperpolarized by dissolution Dynamic Nuclear Polarization (d-DNP), can be applied as an MRI contrast agent for angiography and perfusion.

The first part of the project focuses on development of a protocol for production of large samples of hyperpolarized protons in D_2O. The samples are polarized and dissolved in a fluid path compatible with the installed base of commercial polarizers developed for clinical research. The solid-state DNP is optimized at 6.7 T and 1.2 K by microwave frequency modulation. A solid-state polarization of 70% is obtained. The dissolution procedure is optimized by introduction of a fluorinated solvent to accelerate the transition from solid to liquid state, and efficient radical extraction is obtained with a two-phase system of water and heptane. A final liquid state polarization of 13% in samples of 16 mL is obtained, suitable for large animal experiments.

In second part of the project, hyperpolarized water is applied for angiographic imaging and perfusion measurements in a pig model. Renal angiography of 0.55 mm in-plane isotropic resolution is demonstrated and perfusion measurements provides values comparable to conventional Gd-T_1-DCE analysis. Finally, it is demonstrated that the method can be applied to acquire dynamic coronary MR angiography with temporal resolution of less than 1 s, apparent Signal-to-Noise Ratio of 269±169 and coronary sharpness of 0.31±0.086 mm^{-1}, which is superior to coronary MRA available in today's clinical practice.

Resumé

Magnetisk resonans billeddannelse (MRI) er et vigtigt redskab i medicinsk diagnostik, og bliver brugt i stor udstrækning pga. den høje billedopløsning og lave sundhedsrisiko. Metoden har dog sine begrænsninger, da den naturligt har en lav sensitivitet, der gør den underlegen i sammenligning med CT mht. spatiel og temporal opløsning, og med nuklearmedicinsk billeddiagnostik mht. sensitivitet af molekylær billeddannelse. Det tilgængelige signal kan forøges med flere størrelsesordner ved hyperpolarisering.

Formålet med denne afhandling er at demonstrere hvordan vand, hyperpolariseret ved Dynamisk Nuklear Polarisation (DNP), kan anvendes som MRI konstrastvæske til angiografi og perfusionsmålinger.

Den første del af projektet fokuserer på udviklingen af en protokol til produktion af store doser af hyperpolariserede protoner opløst i D_2O. Prøven polariseres og opløses i et aflukket væskesystem (*fluid path*), som er kompatibelt med de kommercielle polarisatorer der i dag er i brug til klinisk forskning. DNP optimeres ved 6.7 T og 1.3 K med mikrobølge-frekvensmodulering, og en faststof polarisation af 70% opnås. Opløsningsprocessen forbedres ved at introducere en fluoreret solvent, der øger hastigheden af overgangen fra fast til flydende form, og effektiv ekstraktion af radikalet opnås med et to-fase system af vand og heptan. Derved opnås 13% polarisation i den opløste prøve á 16 mL; en passende mængde til forsøg i store dyr.

I den anden del af projektet anvendes hyperpolariseret vand til angiografi og perfusionsmålinger i grise. Angiografi i nyren demonstreres med 0.55 mm isotropisk opløsning, og perfusionsmålinger giver værdier sammenlignelige med konventionel Gd-T_1-DCE analyse. Tilsidst demonstreres det, at metoden kan anvendes til at optage dynamisk MR koronarangiografi med tidsopløsning af mindre end et sekund, signal-støj-forhold (aSNR) på 269±169 og koronarskarphed på 0.31±0.086 mm^{-1}, som er overlegent i sammenligning med nuværende kliniske MR koronarangiografier.

Acknowledgements

First of all, I would like to express my gratitude for my mentor and supervisor, Jan Henrik Ardenkjær-Larsen. I am grateful that I have be given this opportunity, and it has been a pleasure working with one of the pioneers of d-DNP, providing excellent advice in every corner of the field, as well as general guidance and inspiration from both industrial and academic approaches. It has been a journey to follow our 3-man research group translating into a state-of-the-art research center of 20+ employees. I would like to thank my colleagues at *Hypermag* for forming a nice work environment. Special thanks to Sean Bowen, who challenged my chemical understanding again and again, to my office mates, Bakri, Oleksandr and Ronja, and to our technician, Jan Kilund, for creative solutions to even my tiniest technical problems, as well as motivational talks.

I have also enjoyed the atmosphere at the DRCMR at Hvidovre Hospital. Thanks to my co-supervisor Lars G. Hanson for his always great mood and sometimes great humor, and for the solid introduction into the world of MRI. I am grateful for the inspiration and support from my co-supervisor Lise Vejby Søgaard, who sadly passed away one year into my PhD. It was a pleasure to work with Sascha Gude, whose joyful personality would always make up for scan sessions way too early in the morning, and thanks to Mette Hauge Lauritzen for encouraging discussions and assistance with my challenges of animals handling.

Thanks to Christoffer Laustsen and the group at the MR Research Centre for great collaboration on our many common projects, and for making my many trips to Århus something I look back upon with pleasure.

I appreciate the funding from The Danish Research Council for funding the project, and the Otto Mønsted Foundation for supporting my travels.

Finally, I would like to thank my family for all their support and involvement during this period. Mette and Rosa, I could not have done this without your love and understanding.

Preface

This thesis is submitted in partial fulfillment of the requirement for obtaining a PhD degree at the PhD school of Electrical Engineering at the Technical University of Denmark (DTU). The project was supervised by Professor Jan Henrik Ardenkjær-Larsen and co-supervisor, Associate Professor Lars G. Hanson.

The thesis present work conducted during my employment at the Department of Electrical Engineering at DTU from December 2012 to June 2016. During the period, I have had several research stays at other DNP facilities in Denmark, namely

- Danish Research Center for Magnetic Research Center (DRCMR), Centre for Functional and Diagnostic Imaging and Research, Copenhagen University Hospital Hvidovre, Denmark
- Department of Clinical Medicine, MR Research Centre, Aarhus University, Aarhus, Denmark
- Department of Clinical Physiology, Nuclear Medicine & PET and Cluster for Molecular Imaging, Rigshospitalet and University of Copenhagen, Denmark

In addition, I have had the pleasure of attending several research meeting, namely

- 4th International DNP Symposium, Elsinore, Denmark, August 2013
- ISMRM 21st Annual Meeting & Exhibition, Milan, Italy, May 2014
- Hyperpolarized Magnetic Resonance, Egmond Aan Zee, Netherlands. August 2015

Furthermore, I have benefitted from teaching in the MSc. course *31590 Biomedical Product Development* as well as assisting in the supervision of the MSc. projects of students Sarah Teuber Henriksen and Sotirios Sarros.

List of Publications

The thesis builds on a basis of the following research papers and conference contributions:

Articles in scientific journals

I. *Dissolution Dynamic Nuclear Polarization capability study with fluid path.*

Ronja Malinowski, Kasper Wigh Lipsø, Mathilde H. Lerche and Jan Henrik Ardenkjær-Larsen.

Journal of Magnetic Resonance, 2016, **272**, 141-146.

II. *Large dose hyperpolarized water with dissolution-DNP at high magnetic field.*

Kasper Wigh Lipsø, Sean Bowen, Oleksandr Rybalko and Jan Henrik Ardenkjær-Larsen.

Accepted manuscript, In Press, Journal of Magnetic Resonance, 2016.

III. *Hyperpolarized ^{13}C MR angiography.*

Kasper Wigh Lipsø, Peter Magnusson and Jan Henrik Ardenkjær-Larsen.

Current Pharmaceutical Design, 2016, **22**, 90-95.

IV. *Renal MR Angiography and Perfusion in the Pig using Hyperpolarized Water.*

Kasper Wigh Lipsø, Esben Søvsø Szocska Hansen, Rasmus Stilling Tougaard, Christoffer Laustsen and Jan Henrik Ardenkjær-Larsen.

Magnetic Resonance in Medicine, 2016.

V. *Dynamic Coronary MR Angiography in the Pig using Hyperpolarized Water.*

Kasper Wigh Lipsø, Esben Søvsø Szocska Hansen, Rasmus Stilling Tougaard, Christoffer Laustsen and Jan Henrik Ardenkjær-Larsen.

Manuscript in preparation.

Conference contributions

VI. *Cerebral Angiography in Rats: Comparison of ^{1}H TOF-MRA, SPIO Enhancement and Hyperpolarized ^{13}C bSSFP.*

Kasper Wigh Lipsø, Peter Magnusson, Lise Vejby Søgaard and Jan Henrik Ardenkjær-Larsen.

Poster presentation. ISMRM 21st Annual Meeting & Exhibition, Milan, Italy. May 2014.

VII. *Magnetic Resonance Angiography in the Pig using Hyperpolarized Water.*

Kasper Wigh Lipsø, Sean Bowen, Christoffer Laustsen, Esben Søvsø Szocska Hansen, Thomas Nørlinger and Jan Henrik Ardenkjær-Larsen

Oral presentation, Hyperpolarized Magnetic Resonance - Joint 5th International DNP Symposium and COST Action EUROHyperPOL Final Meeting, Egmond Aan Zee, Netherlands. August 2015.

VIII. *Hyperpolarized Water Perfusion in the Porcine Brain – a Pilot Study.*

Esben Søvsø Szocska Hansen, Kasper Wigh Lipsø, Rasmus Stilling Tougaard, Christoffer Laustsen, and Jan Henrik Ardenkjær-Larsen.

Submitted abstract. ISMRM 25st Annual Meeting & Exhibition, Honolulu, USA. April 2017.

List of Figures

List of Tables

Abbreviations and Symbols

α	Flip angle
AIF	Arterial Input Function
ASL	Arterial Spin Labelling
aSNR	Apparent signal-to-noise ratio
BBB	Blood-Brain-Barrier
BOLD	Blood-oxygen-level dependent
bSSFP	balanced Steady-State Free Precession
CAD	Coronary Artery Disease
CE	Contrast Enhanced
CNR	Contrast-to-Noise Ratio
CT	Computed Tomography
CTA	Computed Tomography Angiography
d-DNP	dissolution-Dynamic Nuclear Polarization
DCE-MRI	Dynamic contrast-enhanced Magnetic Resonance Imaging
DM	Dissolution Medium
DMSO-d_6	Deuterated Dimethyl Sulfoxide
DNP	Dynamic Nuclear Polarization
ECG	Electrocardiography
EDTA	Ethylenediaminetetraacetic acid
EPA	Electron Paramagnetic Agent
EPR	Electron Paramagnetic Resonance
FWHM	Full Width at Half Maximum
FID	Free Induction Decay
FOV	Field of View
FP	Fluid Path
Gd	Gadolinium
GRE	Gradient Echo
HP	Hyperpolarization/ Hyperpolarized
HP001	bis-1,1-(hydroxymethyl)-[1-^{13}C]cyclopropane-d_8
LAD	Left anterior descending coronary artery
MIP	Maximum Intensity Projection
MR	Magnetic Resonance
MRA	Magnetic Resonance Angiography

MRI	Magnetic Resonance Imaging
N	Number of repetitions
NFBME	Nonafluorobutyl methyl ether
NMR	Nuclear Magnetic Resonance
NSF	Nephrogenic Systemic Fibrosis
OE	Overhauser Effect
PC	Phase Contrast
PEEK	Polyether Ether Ketone
PET	Positron Emission Tomography
PHIP	ParaHydrogen-Induced Polarization
PTFE	Polytetrafluoroethylene
QC	Quality Control
P	Partition coefficient
R_1	Longitudinal Relaxation Rate
R_2	Transverse Relaxation Rate
RF	Radio Frequency
SE	Solid Effect
SNR	Signal-to-Noise Ratio
SPECT	Single-photon emission computed tomography
T_1	Longitudinal relaxation time
T_2	Transverse relaxation time
TE	Echo Time
TEMPO	2,2,6,6-Tetramethylpiperidine-1-oxyl
TM	Thermal Mixing
TOF	Time-Of-Flight
TR	Repetition Time
US	Ultra Sound

Table of Contents

1 Introduction

Hyperpolarized Metabolic MR is an exciting new imaging modality based on Magnetic Resonance Imaging (MRI) and hyperpolarization of biological molecules as probes of changes in cellular metabolism in vivo. The bio-probe is typically labelled with ^{13}C in a chemical position with long relaxation time, and the hyperpolarization is achieved by the d-DNP method. In this way, the magnetic resonance signal can be enhanced by many orders of magnitude. The bio-probe is injected intravenously as a bolus, and allows studying the metabolism of tissues over a time window of approx. a minute to characterize disease. The method has emerged over the last decade and is now in clinical use. About a handful of prominent clinical research institutions have conducted human studies with [1-^{13}C]pyruvate, and almost twenty groups are in the preparation of patient studies. These studies have been enabled by commercial polarizer technology, the SPINlab, from GE Healthcare.

In this thesis, another approach is taken. It is here claimed that hyperpolarized water protons (^{1}H) has the potential to provide superior clinical angiographic and perfusion imaging. It is claimed that hyperpolarization of water protons (^{1}H) by the d-DNP method can provide a nuclear magnetization that exceeds the thermal magnetization at clinical MRI field strengths by more than two orders of magnitude, and thereby allow high resolution, dynamic imaging. It is claimed that angiography and perfusion images of high diagnostic quality can be acquired within the short relaxation time of water protons in vivo when arterial injection in applied.

1.1 Aims

The aim of this thesis work was to investigate the potential of hyperpolarized water as a new contrast agent for angiography and perfusion.

The first aim was to investigate and optimize the hyperpolarization of water by the d-DNP method under conditions compatible with clinical polarizers at collaborator sites, and for a formulation of the hyperpolarized product that is well tolerated. This involves developing a sample preparation method compatible with the SPINlab polarizer (**Study I**). The target was to

demonstrate that a proton magnetization more than hundred-fold above thermal equilibrium at 3 T could be obtained for a volume of more than 10 mL and with a T_1 of more than 10 s (**Study II**).

The second aim was to investigate the behavior of two common imaging sequences, balanced-Steady-State-Free-Precession and Gradient-Recalled-Echo, for angiography (**Study III**). This was done in a small animal model using a ^{13}C-labelled molecule with long relaxation time *in vivo*. This would allow selection of the most suitable imaging sequence in subsequent large animal studies.

The third aim was to demonstrate perfusion (**Study IV**) and coronary angiography (**Study V**) in a large animal model with similar or superior diagnostic quality as state-of-the-art contrast agent based MRI.

1.2 Clinical Motivation

Cardiovascular disease is the leading cause of death worldwide, according to the World Health Organization [1]. It is estimated that 7.4 million people died from Coronary Artery Disease (CAD) in 2012, corresponding to 13% of global deaths.

Imaging of the vasculature is crucial for diagnosis and treatment of CAD. High resolution angiographies are required to diagnose atherosclerosis, a precursor for CAD. In addition, treatment, such as angioplasty and stent placement, must be assessed by post-surgical flow measurements, and tissue blood supply must be validated by perfusion measurements.

Angiographic techniques include magnetic resonance angiography (MRA), computed tomography angiography (CTA), cardiac catheterization using X-ray contrast, and ultrasound (US), each with advantages and downsides regarding which structures can be imaged, the safety and convenience of the patient, etc. Today, CTA is the gold standard for CAD diagnosis, and provides excellent spatial resolution, with the main drawback of exposing patients to ionizing radiation.

MRI has a better soft-tissue contrast, but suffers from inherently low sensitivity. Coronary angiography requires high spatial resolution, while the acquisition time must be short to avoid motion artefacts. MR angiography thus fails to provide images of quality sufficient for CAD diagnosis. By hyperpolarization, the MR signal can be increased by several orders of magnitude.

Hyperpolarized water could overcome both the challenge of high spatial resolution and short acquisition time, while also being compatible with the equipment and MRI sequences already existing in the clinic. Furthermore, the tracer could serve as a perfusion marker for treatment assessment, to form a one-stop shop for CAD diagnosis and assessment.

With the target of complementing existing MRI techniques to achieve a *full MR cardiac package*, a novel contrast agent consisting of hyperpolarized water will be presented. The hypothesis is that the signal of the hyperpolarized nuclei can provide enough sensitivity to produce images of similar resolution and quality as CTA. The main goal of this project was to demonstrate coronary angiography and perfusion using hyperpolarized water MRI in large animals. The hope was to form a basis for future perspectives of a novel CAD diagnostic tool, which could potentially replace CTA and hence save the radiation burden in millions of people every year.

^{13}C-labelled pyruvate is the main research target in the field of hyperpolarization by d-DNP. Pyruvate is the end product of glycolysis, and serves at the precursor to the tricarboxylic acid cycle for ATP production. By spectroscopic imaging or chemical shift imaging, concentrations of metabolism products such as lactate, alanine and bicarbonate, can be monitored, and thus the biochemical pathways can be followed over time. In addition to being a non-invasive, radiation free technology, the method provides otherwise unavailable measures of metabolism.

The method has been applied in preclinical studies for several years [2], and several research groups have initiated clinical research with promising results [3,4].

2 Angiography and Perfusion

Medical imaging is essential in diagnosis and therapy assessment, where MRI and CT are the major modalities with 72 million and 26 million, examinations every year in the US alone [5].

Angiography is the field of visualizing the lumen of blood vessels and organs in the body, and can be achieved by several techniques and modalities.

2.1 Coronary Catheterizations

Every year, millions of people in the United States suspected of having CAD are examined with coronary catheterizations [6]. Coronary catheterizations is a minimally invasive method to obtain images of the coronary arteries, in which a catheter is inserted through an artery in the groin or arm to reach the heart. The end of the catheter is placed in the coronary arteries, where contrast agent is injected during X-ray imaging. An example is shown in Figure 1A.

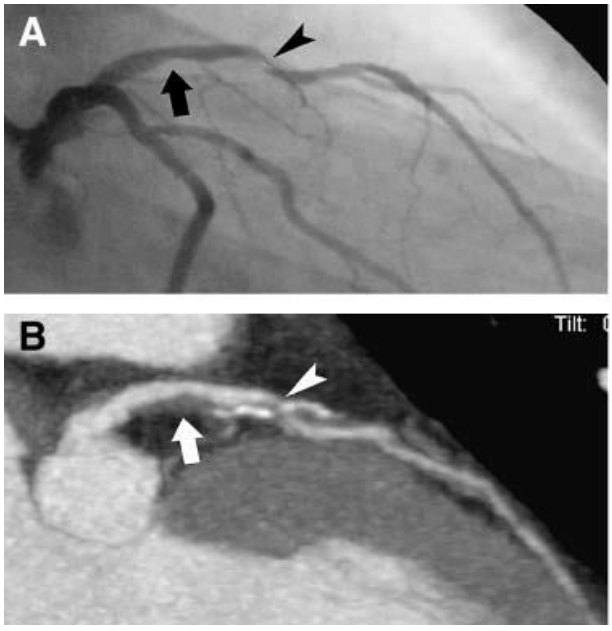

Figure 1: Luminal narrowing in proximal left anterior descending artery (LAD, arrow) and stenosis in middle LAD (arrow head) in a 66 year old male. A) Coronary catheterization X-ray image showing the fine structure of the arterial branches and apparent vessel narrowing. B) Thin-slab maximum intensity projection (MIP) across the LAD plane from a 64-slice multi detector CT scan, showing non-calcified plaque in proximal LAD and mixed calcified and non-calcified atherosclerotic plaque in middle LAD. Reprinted with permission from [7].

The method can provide images of high resolution, and the catheter can be applied for angioplasty and stent placement. However, several complications are associated with coronary catheterization. Smaller risks include infection, allergic reactions to the contrast agent and

abnormal heart rhythms, while serious side effects are stroke and heart attacks, among others. In addition, the radiation dose from fluoroscopy and X-rays adds several mSv [8]. The mortality associated with cardiac catheterization and coronary angiography has been reported to 0.11%, while the incidence of total major complications was 1.7% [9,10].

2.2 Computed Tomography

Computed tomography (CT) applies X-rays from various angles to determine the spatial structure of the body. High resolution images (typically 0.4-0.625 mm in-plane resolution) can be acquired with temporal resolution of 82.5 ms with prospective ECG gating to freeze cardiac motion [11,12]. A valuable feature of CT coronary angiography is the visualization of intravascular plaque, for which calcified and non-calcified plaque can be distinguished (Figure 1B). With modern scanner systems and optimized procedures, angiographies can be acquired with as little as 1.2 mSv radiation dose [8,13]. However, the usefulness of CT coronary angiography still has to be weighed against the increased risk for later cancer development.

2.1 Ultrasound

Intravascular ultrasound assessment of the vessels is often performed in combination with CT angiography. An ultrasound wand is inserted into the artery and moved to the heart, from where images provide spatial information from within the vessels. The method provides visualization of the artery walls and plaques in these [14,15], and the procedure is recommended to determine the need for intervention [16]. The main risk of complications is related to the catheterization, and thus only adds little additional risks in procedures where coronary catheterization is already used.

2.2 Magnetic Resonance Angiography

MRI suffers from low SNR and long imaging time, but distinguishes itself from other diagnostic imaging modalities in that the patient is not exposed to any radiation burden. MRI provides great soft tissue contrast, but the inherently low sensitivity requires several minutes of acquisition to obtain images of adequate diagnostic quality. Whereas extended imaging time is inconvenient, but acceptable for non-moving objects, it complicates the application of traditional MRI for moving organs such as the heart, where the motion results in image artefacts. Thus, cardiac gating must be used to acquire images of moving targets, where sampling is repeated over

several cardiac cycles. With this technique, cine imaging, the heart function can be assessed. However, the image quality is limited, and the resolution of >1.5 mm is inadequate for CAD diagnosis [17,18].

Due to its safety and good soft tissue contrast, MRI is the preferred technique for several types of diagnostic imaging today. However, in one third of the examinations, gadolinium based contrast agents are used. The use of gadolinium-based contrast agents is especially problematic for kidney patients, where development of Nephrogenic Systemic Fibrosis (NSF) since 2006 has been linked with contrast-enhanced MRI in patients with reduced kidney function [19]. A retrospective study of about 370 patients with severe renal insufficiency who had undergone contrast-enhanced MRI with the Gd-based contrast agent *Omniscan* estimated the risk of NSF to 4%. Another study found gadolinium in the tissue of patients with NSF [20], another indication for the link between Gd and NSF. In addition, recent studies have determined high signal intensity in the *dentate nucleus* and *globus pallidus* in T_1-weighted images of the brain for patients who had undergone 6 or more contrast-enhanced MRI examinations. The high signal intensity in these areas are associated with diseases such as multiple sclerosis and hepatitis dysfunction. Thus, new solutions for MRI signal enhancement are called for. Angiographic images using magnetic resonance can be acquired with or without injection of contrast agents. Non contrast-enhanced MRA can be obtained via the time-of-flight (TOF) principle, or by phase contrast (PC) [21–23].

Time-of-flight

TOF techniques change the magnetization of the tissue, so the NMR signal of the spins in the moving blood deviates from the stationary spins. Slabs are oriented orthogonal to the flow direction, and stationary spins in the tissue will lose magnetization from excitation by radio frequency (RF) pulses. Fully magnetized, fresh blood will then flow into the slab, yielding a contrast between tissue and the vascular system. The signal-to-noise (SNR) and contrast-to-noise (CNR) depend on the slab thickness, blood velocity, vessel orientation and the MRI sequence. Typically, a gradient echo sequence with short repetition time (TR) will be applied. A long TR allows more of the blood in the vessel to be replaced, but also allows tissue magnetization to recover between excitations. Thinner slabs will enhance the contrast by allowing more blood to be replaced, at the expense of acquisition time to improve SNR. The same principle can be used with 3D gradient echo

sequence, where a series of thin slices are imaged and stacked after reconstruction. An example is shown in Figure 2.

Phase contrast

In the phase contrast technique, bipolar gradients are used to encode the velocity of the spins. A gradient is applied, and after a delay, a second gradient of equal magnitude, but opposite direction, is turned on. Spins of flowing blood will be phase shifted, because the position in the gradient field has changed from the first to the second gradient. Stationary tissue spins will have zero phase shift. The NMR signal of the moving spins is linearly decreasing with their phase shift. The gradient pair can be applied in all three directions; thus, the flow is imaged in all directions. The phase shifted image is subtracted from an image without velocity encoding, and the resulting angiography provides quantitative information of flow velocity and direction.

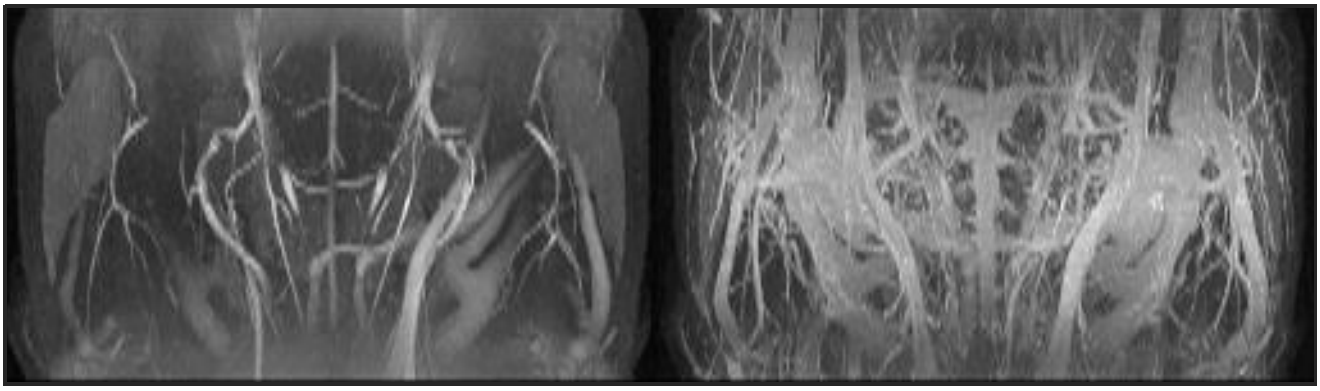

Figure 2: Time-of-flight imaging without (left) and with (right) contrast enhancement. The images are maximum intensity projections (MIP) of a rat cerebral area in a coronal plane, acquired with a 3D gradient echo sequence. The acquisition time was 24 min.

Contrast enhanced angiography

The contrast in the angiographic images can be further enhanced by administration of a T_1 shortening agent such as gadolinium or iron oxide [24,25]. Fluctuating magnetic fields of the unpaired electrons of the agent will interact with the ^{1}H nuclei to contribute to T_1 relaxation. Thus, the effect of the ions (or nanoparticles), rather than the ions themselves are imaged during CE angiography. The agent is typically injected intravenously, and the timing of signal acquisition can be used to determine whether only the arterial network, the entire vasculature or only the venous system is imaged. An image acquired before contrast agent injection can be used for reference, and the subtraction between the two displays the desired vessels. A fast, low angle T_1-weighted

sequence such as FLASH is typically used for CE angiography. An example using the iron based blood pool agent Clariscan™ and a 3D gradient echo sequence is shown in Figure 2.

2.3 Coronary Angiography

Coronary angiography provides imaging of the arteries that supply freshly oxygenated blood to the heart tissue. The coronary arteries have diameter of 2-4 mm in proximal segments and smaller in distal segments (Figure 3), and thus require high resolution imaging to be used for diagnosis.

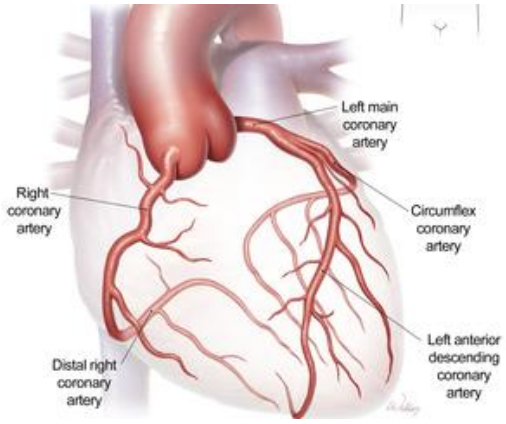

Figure 3: Human coronary artery anatomy (Source: Baylor College of Medicine, credit: Scott Weldon).

Though some studies have provided coronary MRA of sub-millimeter resolution with use of contrast agents [26,27], most recently published coronary MRA studies apply lower resolutions with corresponding loss of details, in order to achieve a sufficient signal-to-noise ratio (SNR) and robustness [28–30]. Coronary contrast enhanced MRA is usually acquired with ECG triggering, where signal is read out during steady periods of the cardiac cycle to avoid motion artefacts, and typically during free breathing. Ahlman et al. obtained apparent Signal-to-Noise Ratio, aSNR, of 24 with 1 mm^3 isotropic resolution using this technique in an optimized setup using gadolinium injections [31]. The total acquisition time is several minutes. Therefore, coronary artery disease is often diagnosed with invasive X-ray cardiac catheterization procedure, or more recently, CT angiography, where high resolution images (0.4-0.5 mm in-plane, isotropic [32,33]) can be acquired fast. However, these techniques have their drawbacks such as patient exposure to ionizing radiation, as well as blooming artefacts from highly attenuating coronary calcification. In summary, coronary MRA is not an established clinical approach, but several approaches for

feasibility are made due to the potential advantages over competing diagnostic technologies [34]. Other interesting tools such as assessment of atherosclerotic disease in vessel walls could follow from high resolution, motion-robust MRA techniques [35].

2.4 Perfusion

In physiology, perfusion is the process of a body delivering blood to a capillary bed in its biological tissue. Perfusion is defined as the passage of fluid through the lymphatic system or blood vessels to an organ or a tissue. Myocardial perfusion provides an accurate means for diagnosing obstructive CAD, and post-surgical flow measurements are an integrated part of a number of treatments for cardiac disease.

Perfusion measurements can be performed with MRI in several ways. The late gadolinium enhancement method images the temporal concentrations of a water soluble gadolinium chelated agent through the changes in relaxation time with a T_1-weighted gradient echo sequence [36]. The main drawback is the gadolinium-related complications discussed earlier, and the low sensitivity. A noninvasive method using Arterial Spin Labelling (ASL) eliminates both catheterization and gadolinium, but the sensitivity is even lower than for the late enhancement method [37].

A method corresponding to the late gadolinium enhancement in MRI is the tracing of iodinated contrast agents using CT [33,38]. The method provides higher sensitivity, but incorporates the safety concerns of CT (cancer development) and adds new complications from toxicity of the iodinated contrast agent [39].

Stress SPECT myocardial perfusion imaging is the most commonly utilized stress imaging technique for patients with suspected or known coronary artery disease [40]. An example of SPECT perfusion, CT perfusion and invasive catheterization is shown in Figure 4 [38]. The perfusion defects detected by CT and SPECT are similar, and may be explained from the occlusion and significant stenosis visualized by cardiac catheterization.

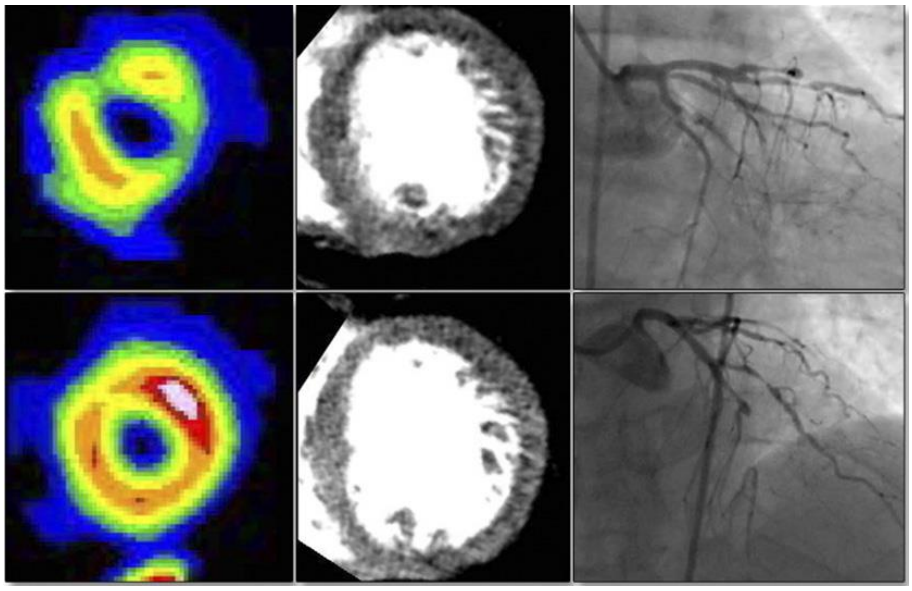

Figure 4: Comparison of SPECT perfusion (left), CT perfusion (center), and invasive coronary angiography (right) in a 55 year-old man in stress (top) and rest (bottom). The perfusion defects detected by CT and SPECT are related to the stenosis in the left circumflex at stress (top, right) and occlusion in the LAD at rest (right, bottom). Reprinted with permission from [38].

PET is another modality for perfusion imaging, and studies suggest that is may provide better diagnostic quality than SPECT [41]. Due to the permeability differences and active transport limitations of contrast agents, it has been attempted to find a suitable tracer based on water molecules. Thus, ^{15}O-labeled water as a tracer for positron emission tomography (PET) imaging has been suggested [42–44], with the main drawbacks of the limited spatial and temporal resolution of PET, the need for an on-site cyclotron, and the risk profile of the radioactive tracer. Other recent suggestions for a water based perfusion tracer include NMR detection of $H_2{}^{17}O$ in the blood after a short $^{17}O_2$ gas inhalation [45].

3 Hyperpolarization

When a sample is allowed to be undisturbed for a long time in a magnetic field, it reaches a state of thermal equilibrium. The populations of nuclear spin states follow the Boltzmann distribution. For a spin *I*, the number of spins in the state m is given by [46]

$$N_m = N_0 \frac{e^{\frac{-E_m}{k_B T}}}{\sum_{n=-I}^{n=I} e^{\frac{-E_n}{k_B T}}}$$

where N_0 is the total spin population, k_B is Boltzmann's constant, *T* is the temperature, and E_m is the energy of the eigenstate *m* given by

$$E_m = -m\,\gamma\,\hbar\,B_0$$

where the state m, in the case of spin ½, can be parallel ($m = +½$) or antiparallel ($m = -½$) to the magnetic field, B_0, γ is the gyromagnetic ratio and $\hbar$ is the reduced Planck's constant. The polarization is defined as the normalized population difference,

$$P = \frac{N_\uparrow - N_\downarrow}{N_\uparrow + N_\downarrow}$$

where $N_\uparrow$ and $N_\downarrow$ are the numbers of spins aligned and anti-aligned with the magnetic field, respectively. The thermal polarization is then given as

$$P = \tanh\left(\frac{\hbar\gamma B}{2k_B T}\right).$$

For ^{1}H and ^{13}C in a clinical MRI system of 3 T at room temperature, the polarization is 10 ppm and 2.5 ppm, respectively.

The potential for sensitivity improvement is therefore tremendous; in principle, close to five orders of magnitude depending on the nucleus and field strength. Since the earliest days of magnetic resonance, various ideas of enhancing the signal-to-noise ratio by increasing the nuclear spin polarization above thermal equilibrium have been investigated. Trivially, the polarization can be increased by raising the magnetic field and lowering the temperature, but there are limited possibilities in conventional NMR and MRI. Currently, the highest magnetic field strength is 23 T

for NMR and 9.4 T for whole body MRI. Only in solid-state NMR is there any room to optimize the sensitivity by lowering the temperature.

Hyperpolarization is the process of polarizing spins beyond the Boltzmann distribution. Hyperpolarization signifies a spin polarization that deviates strongly from thermal equilibrium. A characteristic of hyperpolarization is that the polarization is created *ex situ*, and therefore cannot be restored to the initial state. The polarization decays irreversible by relaxation or signal acquisition. In 2003, a novel method for polarizing nuclear spins in molecules in solution was demonstrated. The method takes advantage of Dynamic Nuclear Polarization (DNP) in the solid state followed by rapid dissolution in a suitable solvent. The polarization is retained almost completely in the dissolution step creating a solution with a non-thermal nuclear polarization approaching unity. Enhancements of more than 10,000 can be achieved using d-DNP (dDNP) [47].

3.1 Dynamic Nuclear Polarization

At low temperatures, electron spins are polarized to almost unity due to their strong magnetic moment. Dynamic Nuclear Polarization (DNP) is the process of transferring the electron spin polarization to nuclear spins. The polarization of electron spins, protons and ^{13}C at a magnetic field of 6.67 T is shown in Figure 5. At 1.2 K, electrons are polarized to 99.97 %, whereas the polarization of the protons is only 0.68 %.

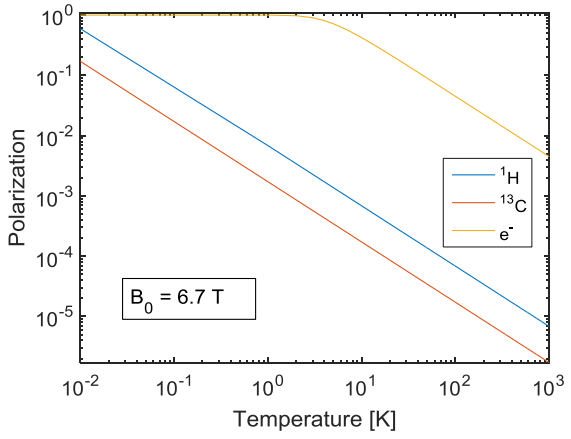

Figure 5: Spin polarization at thermal equilibrium for electrons, protons and ^{13}C nuclei in a magnetic field of 6.67 T.

The spin polarization of the unpaired electrons is transferred to nuclear spins by irradiation with microwaves close to the resonance frequency of the electron spin in the solid state. DNP was predicted by Albert Overhauser in 1953 for conduction electrons in a metal [48], and later, in the same year, Carver and Richter demonstrated the effect experimentally using metallic lithium, and later on using other materials [49,50]. Abragam extended the theory to electron spins in solution [51], and it was soon demonstrated that also nuclear spins in the solid state could be polarized dynamically [52]. Several mechanisms for DNP have been described.

The solid effect invokes the interaction between low concentration free electrons and atomic nuclei by flip-flop transitions induced by the microwave field [53], where double quantum or zero quantum transitions are exited and exploits the hyperfine coupling between electrons and surrounding nuclei. The principle was described by Abragam and Goldman in 1978 [54]. The solid effect is generally observed when the electron paramagnetic resonance (EPR) linewidth is significantly narrower than the NMR frequency.

Thermal mixing is a two-step process. The first step is a single quantum transition, and therefore thermal mixing requires less microwave power than the solid effect. Thermal mixing is efficient when the EPR linewidth is comparable to or larger than the NMR Larmor frequency, and when the electron spin concentration is high enough to ensure a common electron spin temperature through dipolar couplings [55,56].

Thermal mixing breaks down when the electron spin resonance is inhomogeneously broadened and a spin temperature cannot be assigned to the dipolar reservoir. In this situation, the mechanism has been named the cross effect, and the DNP efficiency is reduced. At low temperature, this situation may arise at high magnetic fields where the EPR linewidth is becoming much wider than the electron dipolar couplings. The DNP efficiency may be recovered by increasing the concentration of electron spins to increase the electron-electron dipolar interaction or by MW frequency modulation.

The transfer of polarization from electrons to nuclei can be increased and accelerated by modulation of the microwave frequency. Thurber et al. [57] demonstrated in 2010 that DNP effect and rate can be enhanced by modulation of the magnetic field strength, and Hovav et al. [58] showed that modulation of the microwave frequency at 3.38 T and 30 K can yield even larger

effect, while being more flexible and depositing less heat than modulation of the static magnetic field. Later, Bornet et al. [59] published results on frequency modulation by sinusoidal frequency modulation at 6.7 T magnet and 1.2 K.

The optimal carrier frequency, $f_{\mu w}$, is determined by a frequency sweep. The sinusoidal modulation is characterized by the modulation frequency, f_{mod}, and the modulation range, $\Delta f_{\mu w}$, where the latter is sometimes expressed modulation amplitude $a_{mod} = \Delta f_{\mu w}/2$. A graphical definition is shown in Figure 6.

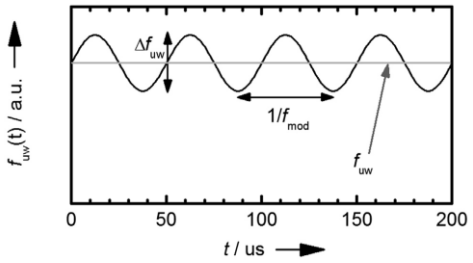

Figure 6: Graphical interpretation of frequency modulation and definition of parameters. Reprinted with permission from [59].

By implementation of frequency modulation in DNP, electron spins packets in a range of resonance frequencies are exited. Thus, the modulation of the microwave frequency should cover a substantial part of the inhomogeneously broadened radical EPR line for maximum efficiency. In addition, the modulation frequency should be higher than the inverse electron T_1 for full utilization of electron polarization.

The electron spin is typically provided by chemical doping with a stable organic radical. Nitroxides are a class of stable radicals with good properties for proton DNP. TEMPO (2,2,6,6-Tetramethylpiperidine-1-oxyl, Figure 7) is an example, which is widely used for DNP due to its EPR properties [60,61] and solubility in hydrophilic solvents.

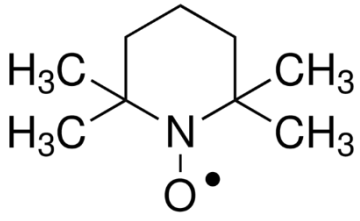

Figure 7: Molecular structure of TEMPO.

Trityls are a group of narrow EPR linewidth radicals that are usually applied for ^{13}C hyperpolarization. The linewidth of the trityl matches closely the Larmor frequency of ^{13}C, and is therefore the best-known radical for direct ^{13}C DNP. However, the narrow EPR line width makes it inefficient for proton polarization, since the solid effect is difficult to drive at high magnetic field and low temperature. The trityl *OX063* is used in **Study III** for hyperpolarization of the ^{13}C labelled compound HP001 (long T_1 quarternary carbon labelling).

Frozen water (ice) is a crystalline sample that will not provide a uniform doping of the electron paramagnetic agent. Thus, a glassing agent such as glycerol or dimethyl sulfoxide (DMSO) is typically used in the sample to ensure good glassing. However, the glassing agent may be omitted and replaced by techniques such as rapid freezing [62]. For *in vivo* studies the glassing agent has to be well tolerated. This limits the choice, and typical options are glycerol, DMSO, ethanol, or mixtures thereof.

3.2 Dissolution-DNP (d-DNP)

D-DNP is the most versatile method for obtaining hyperpolarized nuclear spins in solution. DNP in the solid state at low temperature allows high nuclear polarization of a range of nuclei and molecules. The polarized solid sample is rapidly dissolved without substantially loss of polarization [47,63]. The dissolved sample is transferred for detection in either an NMR spectrometer for *in vitro* experiments, or to an MRI system for imaging *in vivo*. The longitudinal relaxation time, T_1, reduces significantly once the sample has been dissolved, and the transfer from polarizer to detector must therefore be fast. Ardenkjær-Larsen and coworkers demonstrated in 2003 that ^{13}C-urea could be dissolved and transferred to an NMR tube in a spectrometer in less than 6 s [47]. For *in vivo* studies of metabolism, T_1 has to be relatively long. Both from a logistical perspective, but also to ensure enough time for circulation and metabolism. Therefore, ^{13}C-labelling of carboxylic acids or carbonyls in small molecules has been preferred. The longitudinal relaxation time is affected by many parameters. Generally, small molecules (<100 Da) have fast dynamics, averaging interactions such as dipolar and chemical-shift-anisotropy. A high temperature favors fast dynamics, further averaging the interactions. The magnetic field environment has to be favorable; sudden changes of magnetic field orientation in low magnetic fields can be detrimental, if the change is non-adiabatic. Relaxation may be enhanced in low field if the hyperpolarized nuclear spin is coupled to a quadrupolar nucleus or if paramagnetic impurities are present. After

dissolution, the relaxation induced by the paramagnetic agent used for DNP is typically insignificant. This is the case for trityls, and therefore no removal of this radical is necessary. However, nitroxides have higher relaxivity and are used in higher concentrations, and may therefore have to be removed. Likewise, molecular oxygen is paramagnetic and will contribute significantly to water proton relaxation.

For *in vitro* studies with fast transfer systems, nuclear spins with sub-second T_1 has been detected [64]. An automated injection system for *in vivo* studies was published in [65], where it is demonstrated that the time from dissolution to injection can be reduced to 3 s. Recently, Shang et al. suggested a handheld electromagnet carrier to conserve polarization in the dissolved sample by placing it in a >50 G field [66], and others [67] have proposed a magnetic tunnel to prolong T_1.

3.3 Hyperpolarized ^{13}C Angiography and Perfusion

Hyperpolarization of nuclear spins is interesting for angiography and perfusion due to the large magnetization, and hence signal, that can be created. The large signal can be exchanged for high SNR images with high spatial and temporal resolution. ^{13}C-labelled exogenous compounds are favorable due to their long T_1. In 2001, Golman and coworkers [68] demonstrated that ^{13}C can be hyperpolarized with the PHIP method and applied for MRA. A ^{13}C polarization of 4% was obtained, and angiographic imaging of the *vena cava* and its branching veins was demonstrated in the rat. Svensson et al. [69] achieved ^{13}C polarization of 15% of bis-1,1-(hydroxymethyl)-[1-^{13}C]cyclopropane-d_8 (HP001) at time of injection using d-DNP, and acquired angiographies of the head and neck region, as well as the abdominal area, in the rat. In 2006, Olsson et al. [70] published the first study of hyperpolarized MRA in a large animal, when ^{13}C-enriched hydroxyethylproponate polarized to 30% was injected intra-arterially into the coronary artery of a pig to obtain coronary angiographies. The images of ECG triggered acquisition are shown in Figure 8. The LAD in Figure 8c had SNR of 16.

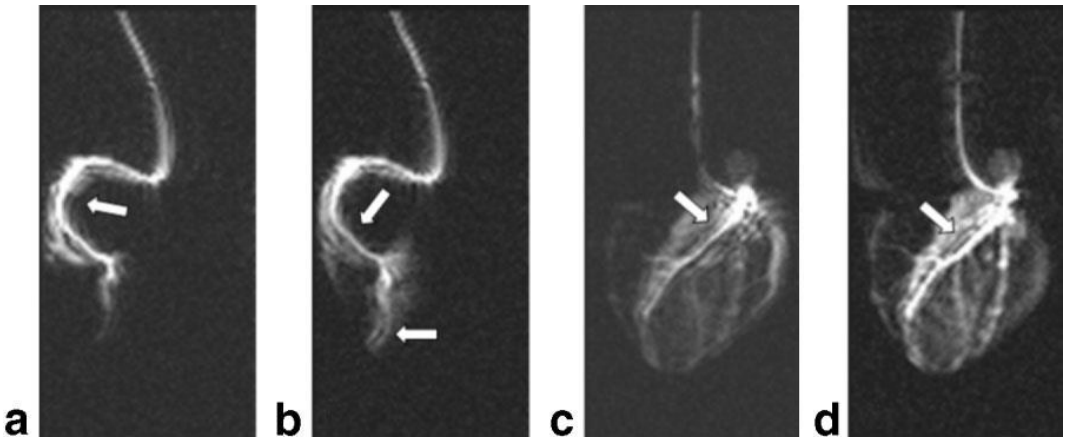

Figure 8: Hyperpolarized ^{13}C angiogram of a pig heart with pixel size 1.5×1.5 mm^2. Injection in left and right coronary arteries. Images were acquired every heartbeat after ECG triggering with acquisition time of 422 ms. Arrows show artefacts, believed to be caused by intensity variation. Reprinted with permission from [70].

In addition to angiography, hyperpolarized ^{13}C compounds have been suggested as perfusion markers. The method was first demonstrated for cerebral perfusion in rats [71,72], and later on used for investigation of rat tumor perfusion [73,74]. Recently, Lau et al. demonstrated that flow sensitizing gradients could be applied to reduce the signal of hyperpolarized ^{13}C urea from the blood pool in the heart, and measure the myocardial perfusion in rats [75], and the same group has used the concept in combination with [1-^{13}C]pyruvate to assess myocardial perfusion and metabolism simultaneously, Figure 9. The intravenously injected agent rapidly reached the cardiac chambers, and was later observed in the myocardium.

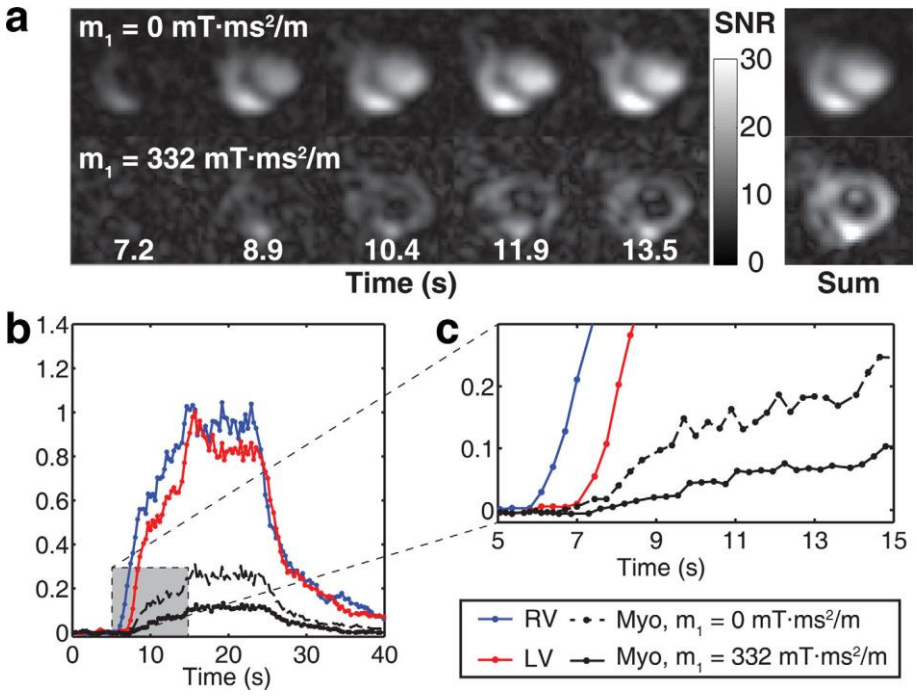

Figure 9: Myocardial perfusion in rats with hyperpolarized ^{13}C urea. a) Images of every 5th frame of an ECG triggered acquisition without (upper row) and with (lower row) flow sensitivity. The in-plane resolution was 1.25×1.25 mm^2. b) and c) Time course for the first pass of urea signal in the right ventricle (RV, blue), left ventricle (LV, red) and myocardium with no flow encoding (dashed, black) and with flow sensitization (solid, black). Reprinted with permission from [75].

3.4 Hyperpolarized Water

Hyperpolarized protons, and water protons in particular, have several advantages over hyperpolarized ^{13}C:

- Large magnetization and sensitivity due to high concentration, large magnetic moment and large gyromagnetic ratio (detection frequency)
- Higher spatial resolution due to larger gyromagnetic ratio for given gradient performance
- Optimized sequences and coils are widely available for ^{1}H imaging.

The disadvantage of hyperpolarized protons is the short T_1, which will limit the available time window significantly. The proton T_1 may be increased by dilution to reduce the efficient proton-proton dipolar relaxation. The most obvious solvent for dilution is D_2O, since deuterium has a low magnetic moment (1/6 of the proton), leading to a square reduction of dipolar relaxation mechanisms. The relaxation time of protons in D_2O is given as

$$\frac{1}{T_1} = \eta \frac{1}{T_{1w}}(\alpha + (1-\alpha)R), \text{where } R = \frac{2}{3}\frac{\gamma^2 I_d(I_d+1)}{\gamma^2 I_p(I_p+1)} = 0.0419$$

I_d and I_p are the spin numbers of deuterium (I_d = 1) and the proton (I_p= 1/2), respectively [76]. The relaxation times of various H_2O/ D_2O ratios are shown in Table 1.

Volume ratio, (V_{H2O}/ V_{D2O})	1.0	0.8	0.6	0.4	0.2	0.1	0.05
T_1 (21.5 °C)	3.2 s	3.9 s	4.7 s	6.7 s	11 s	18 s	25 s

Table 1: Proton relaxation times for H_2O-D_2O mixtures in degassed samples. Data from [76].

Another important factor determining T_1 is the sample temperature. The relaxation times over a range of temperatures are given in Table 2 [77].

Temp.	293K / 20°C	303K / 30°C	313 K / 40°C	323K / 50°C	333K / 60°C	343K / 70°C	353K / 80°C	363K / 90°C	373K / 100°C
T_1	3.0 s	3.8 s	4.8 s	5.8 s	6.8 s	7.9 s	9.1 s	10.3 s	11.6 s

Table 2: Relaxation times for oxygen-free waters. Data from [77].

The relaxation of protons in D_2O was measured as a function of concentration and temperature [78], Table 3. For a concentration of 6 M at 40 °C, the T_1 of protons in deoxygenated D_2O can be as long as 36 s.

***T* (°C)**	**H_2O**	**5% H_2O in D_2O**	**10% H_2O in D_2O**	**4.8% 1:1 (w:w) glycerol:H_2O in D_2O**	**4.8% 1:1 glycerol:H_2O and 30 mM TEMPOL in D_2O**	**+ 100 mM asorbate***	**D_2O**
25	3.3	25	16	26	3.0	20	38
40	5.0	36	22	37	4.3	28	53
60	7.4	51	26	53	6.5	41	76
80	10	64	35	68	9.0	53	93
[H^+]	**111**	**6.26**	**11.8**	**4.56**	**4.56**	**5.30**	**0.74**

Table 3: Longitudinal relaxation time constants (T_1) measured at 9.4 T for ^1H in various sample compositions. All T_1 values are reported in s. The lower row is the proton concentration in M.

Dissolved molecular oxygen, O_2, and the nitroxide radical are two dominant relaxation sources. The relaxivity of dissolved molecular oxygen is given in [79] as R_{O2} = 0.0094 L/mg/s. At 25 °C, water dissolves 8.6 mg/L O_2, and therefore removing 90% of the dissolved oxygen would bring the relaxation rate contribution to 0.008 s^{-1}. It is therefore not too demanding to eliminate this contribution by thorough degassing of all solvents and containers. It should be noted that organic solvents can have much higher solubility of molecular oxygen. Höfer et al. [80] provides a relaxation rate contribution for a nitroxide radical of $R_{Nitroxide}$ = 0.55 $s^{-1}mM^{-1}$ at 25 °C in low field. To have minimal effect on T_1, the relaxation rate contribution should be less than e.g. 0.02 s^{-1}, which means that the concentration of the nitroxide should be less than 40 µM. Several techniques have been applied for minimizing the relaxation from the radical after dissolution. One way is to quench the radical with ascorbic acid. The method has been demonstrated to be useful [78,81], although polarization is lost during the quenching process, because the redox reaction is relatively slow and requires high ascorbic acid concentration. In addition, the ascorbic acid is unstable in the heated solutions, and browning can be observed. Furthermore, the method leaves unwanted residues in the solution, which may be problematic for clinical application. Another method is to filter out the nitroxide by using a cation such as amino-TEMPO, which can be removed with ion exchange. However, few working systems have been demonstrated, and the relaxation of water protons in the filter is unknown. Instead, the radical has been suggested removed by extraction in an organic solvent [61,82]. This method has the advantage that the organic solvent can be used to provide heat for dissolution of the sample, such that the dissolution medium and hence dilution can be minimized.

With dilute water protons, a large initial magnetization can theoretically be achieved. Table 4 calculates the magnetization for three different situations. Relaxation factor is calculated from the T_1 and a transfer time of 15 s. A dilution factor estimates the dilution in the vasculature, for intra-arterial or intravenous injection methods. The tissue water proton signal is taken as reference, assuming a T_1 and repetition time of 1 s. As example, and based on a target T_1 of 20 s, the magnetization of 5 M protons in D_2O is 628 times larger than the tissue proton magnetization at 3 T, if it is assumed that 20% polarization can be achieved. For a ^{13}C-labelled molecule of 500 mM concentration and initial polarization of 50%, the magnetization is 79 times higher than the tissue magnetization, but 8 times smaller than the hyperpolarized proton magnetization.

Depending on assumptions for dilution and relaxation, the effective magnetization at time of imaging can be difficult to predict. However, the fast mixing of the water protons with blood, means that the T_1 will quickly reduce to around 1.6 s, the T_1 of blood at 3 T [83].

Nucleus	Initial conc. [M]	P [ppm]	Initial M_0 [mA/m]	T_1 [s]	Relaxation factor	Dilution factor	M_0 at imaging [mA/m]
^{1}H (H_2O/D_2O)	5	200,000	4,895	20	$e^{-15/20} = 0.5$	0.2	490
^{13}C agent	0.5	500,000	615	60	$e^{-15/60} = 0.8$	0.1	49
Thermal ^{1}H	80	10 @ 3T	7.8	1	0.6	1	4.7

Table 4: Comparison of magnetization for three situations. The proton magnetization of tissue is used as reference.

In 2014, Ardenkjær-Larsen et al. proposed to hyperpolarize the protons of water molecules with d-DNP for angiography [78]. A polarization of 3.5% at a concentration of 3.9 M was measured at time of injection, which proved to be sufficient for angiographies of the head and neck region after intra-arterial injection in the carotid artery, and imaging of the *vena cava* after intravenously injection into a tail vein of a rat. Concurrently, hyperpolarized water has been applied for signal enhancement in biomolecular NMR studies [61,82,84].

4 Safety of the formulation and administration

The formulation that was developed in this thesis work, and used in pig experiments, was approx. 5 M ^{1}H in D_2O with 9 g/L NaCl, 1 mM calcium disodium ethylenediaminetetraacetic acid (EDTA), approx. 25 mM glycerol and trace amount of heptane. No formal safety studies have been performed, but the formulation was well-tolerated in animal studies. The safety concerns with the formulation are discussed only by principle.

The temperature of the formulation was close to body temperature at time of injection, i.e. in the range 35-40 °C. The pH of the formulation was close to physiologic, but unbuffered. Only the weak EDTA concentration provides a minimal buffering capacity. The formulation was adjusted to isotonic with sodium chloride. On these parameters, the formulation was considered optimal and safe. However, it may be that some further optimization of the composition of salts (Ca^{2+}, Mg^{2+}, K^{+}) in the formulation could be introduced similar to iodinated contrast agents [85].

The solubility of heptane in water is 0.0003% (v/v), or 3 ppm, at 25 °C (logP of 4.274). This means that the pig could receive a dose of 45 nL (60 ng) when 15 mL of the formulation is given. The acute oral toxicity of heptane has been determined to >5,000 mg/kg in rat [86]. This means that a high, acute toxicity, safety margin should be present. However, local toxicity at point or organ of injection is unclear and needs to be determined, as well as other long term side effects of heptane. It is a general concern that, potentially, pure heptane could be injected into the animal, if complete separation is not accomplished. Alternatively, an organic solvent with lower solubility and/or better safety profile, may be applied for the extraction.

Deuterium oxide (D_2O) is an inherent and major component of the formulation. Approx. 15 mL of D_2O (3.3 g of deuterium) is given to a pig of 30 kg in the experiments performed as part of this thesis. Deuterium accounts for 0.0156% of all hydrogen, or 0.0312% by mass. A 70 kg person contains approx. 7 kg (10%) [87] of hydrogen and would thus have a natural level of deuterium of 2.2 g. The dose of deuterium given in these experiments are thus at the level of the endogenous level. The injected deuterium will exchange with exchangeable protons in proteins and metabolites as well as be incorporated in molecules by e.g. hydration reactions.

Experiments in mice, rats, and dogs have shown that a degree of 25% deuteration causes (sometimes irreversible) sterility, because neither gametes nor zygotes can develop [88]. High

concentrations of heavy water (90%) rapidly kill fish, tadpoles, flatworms, and Drosophila. Mammals (for example, rats) given heavy water to drink die after a week, at a time when their body water approaches about 50% [89]. The mode of death appears to be the same as that in cytotoxic poisoning (such as chemotherapy) or in acute radiation syndrome (though deuterium is not radioactive), and is due to deuterium's action in generally inhibiting cell division. It is more toxic to malignant cells than normal cells. As in chemotherapy, deuterium-poisoned mammals die of a failure of bone marrow (bleeding and infection) and intestinal-barrier functions (diarrhea and fluid loss). Oral doses of heavy water in the range of several grams, typically 0.2 g D_2O per kg body weight, as well as heavy oxygen, ^{18}O, are routinely used in human metabolic experiments; the double-labelled-water method [90]. It is known from this method that much of the deuterium will be excreted with water by renal elimination.

Cardiac catheterization is a procedure to examine the function of the heart. A thin catheter is inserted into a large blood vessel that leads to the heart. During the procedure, the pressure and blood flow in the heart can be measured. Coronary angiography is done during cardiac catheterization. A contrast dye visible in X-rays is injected through the catheter. X-ray images show the dye as it flows through the heart arteries. This shows where arteries are blocked. The chances that problems will develop during cardiac catheterization are low. A small number of people have minor problems. Some develop bruises where the catheter had been inserted (puncture site). Overall, arterial line placement is considered a safe procedure, with a rate of major complications that is below 1% [91]. It is not entirely without risks, however, and it requires appropriate knowledge of the anatomy and procedural skills. Arterial lines can be placed in multiple arteries, including the radial, ulnar, brachial, axillary, posterior tibial, femoral, and dorsalis pedis arteries. In 1995, a total of approx. 1 million patients underwent cardiac catheterization in Europe alone [92].

5 Studies and Results

5.1 Study I: Dissolution Dynamic Nuclear Polarization capability study with fluid path

5.1.1 Introduction

The aim of this study was to develop a method for filling of the fluid path that allows reuse, and to determine the capability of the fluid path system for d-DNP by validation of the reproducibility of the produced sample properties.

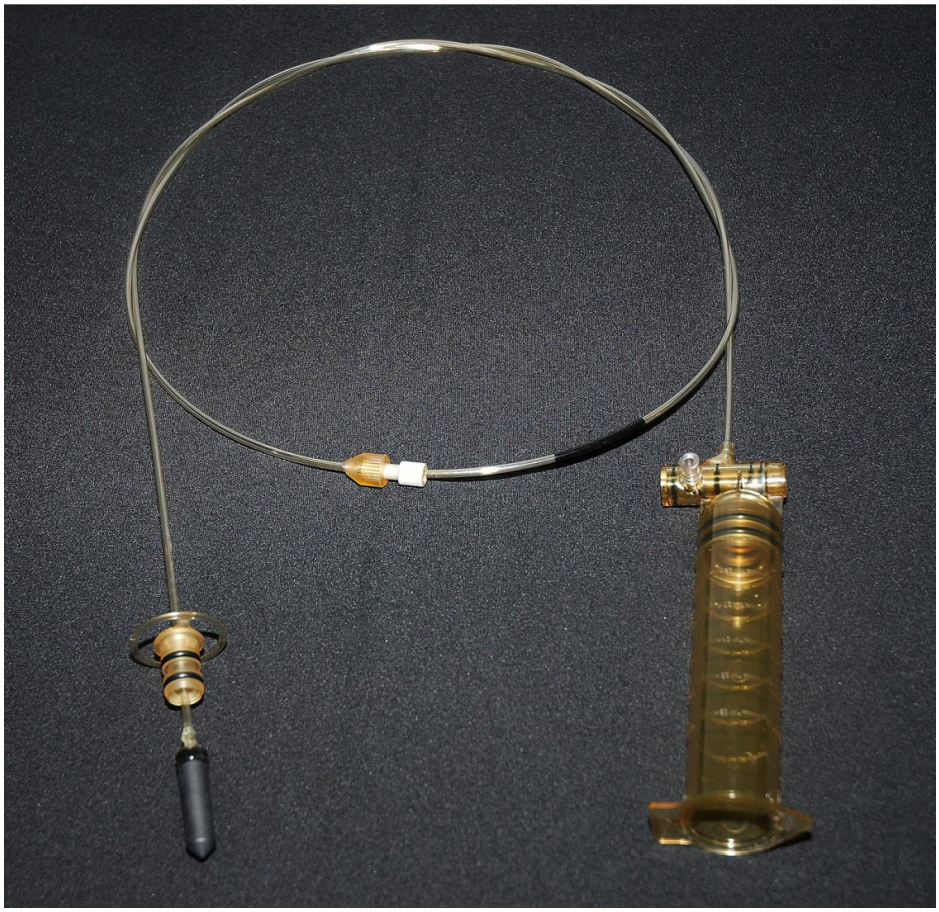

Figure 10: Fluid path for d-DNP for research purposes. Dissolution medium is heated and pressurized in the syringe (right) before transfer through the inner concentric tube to the sample vial (right), and the dissolved sample is transferred back through the outer concentric tube, where an exit tube can be attached.

The fluid path was introduced in 2011 [93]. In contrast to the earlier vapor pressure driven dissolution systems [94,95], the fluid path dissolution is driven by pressure driven piston in the syringe. The primary purpose of the fluid path was to provide a sterile environment during polarization and dissolution, and the technology is now being used in 20 SPINlab facilities worldwide.

The fluid path exists in two different versions. One version, the fluid path for research purposes, Figure 10, applies a ferrule union, and the sample vial and lower outer tube can thus be replaced, to facilitate reuse of the rest of the fluid path. During initial testing, variation in the dissolution time was observed. The union was believed to be the main source of variation, because the manually tightened ferrule would manipulate the geometry of the outer concentric tube, and thus hinder the flow. Even though a system using a torque wrench was established to avoid this issue, the modification of the tube and irreproducible dissolution times were still observed. The fluid path for research purposes has successfully been applied in numerous hyperpolarization experiments. However, for hyperpolarization of water, the dissolution time is crucial for obtaining high final polarization, because of the short relaxation time, the need for fast dilution in D_2O, and rapid radical extraction. Hence, the variation was unacceptable for these studies. The fluid path for clinical purpose has no union. Instead, the concentric tubes are uninterrupted from syringe to sample vial and back. The standard filling protocol implies one time use of expensive, sometimes limited available fluid paths, where the sample is pipetted into the sample vial before attaching the vial to the outer tube with a UV-curing adhesive.

In the method developed in this study, a filling tube is guided through the inner tube for dispersion of the sample. By introduction of the method, fluid paths can be reused, which is a large asset for labs using the system. In addition, the need for UV cured gluing is only needed for the first time use of a fluid path.

The method was originally developed and optimized for hyperpolarization of water. Later on, it was expanded to pyruvate hyperpolarization, to accommodate the general need in modern d-DNP. The main difference between fluid path use for water and pyruvate is the need for degassed solvents to minimize the T_1 of water samples.

5.1.2 Methods

Fluid path system

A fluid path system was used for dissolution of samples polarized in a homebuilt and a clinical polarizer. It was made up of two parts, as shown in Figure 11; Part A consisted of a syringe for dissolution medium, concentric tubes leading the dissolution medium to the sample placed in a vial and back to a valve in the syringe, and an exit tube leading the dissolved sample to a receiver.

Part B consisted of a receiver, an EPA filter, and a quality control module for assessment of the dissolved sample.

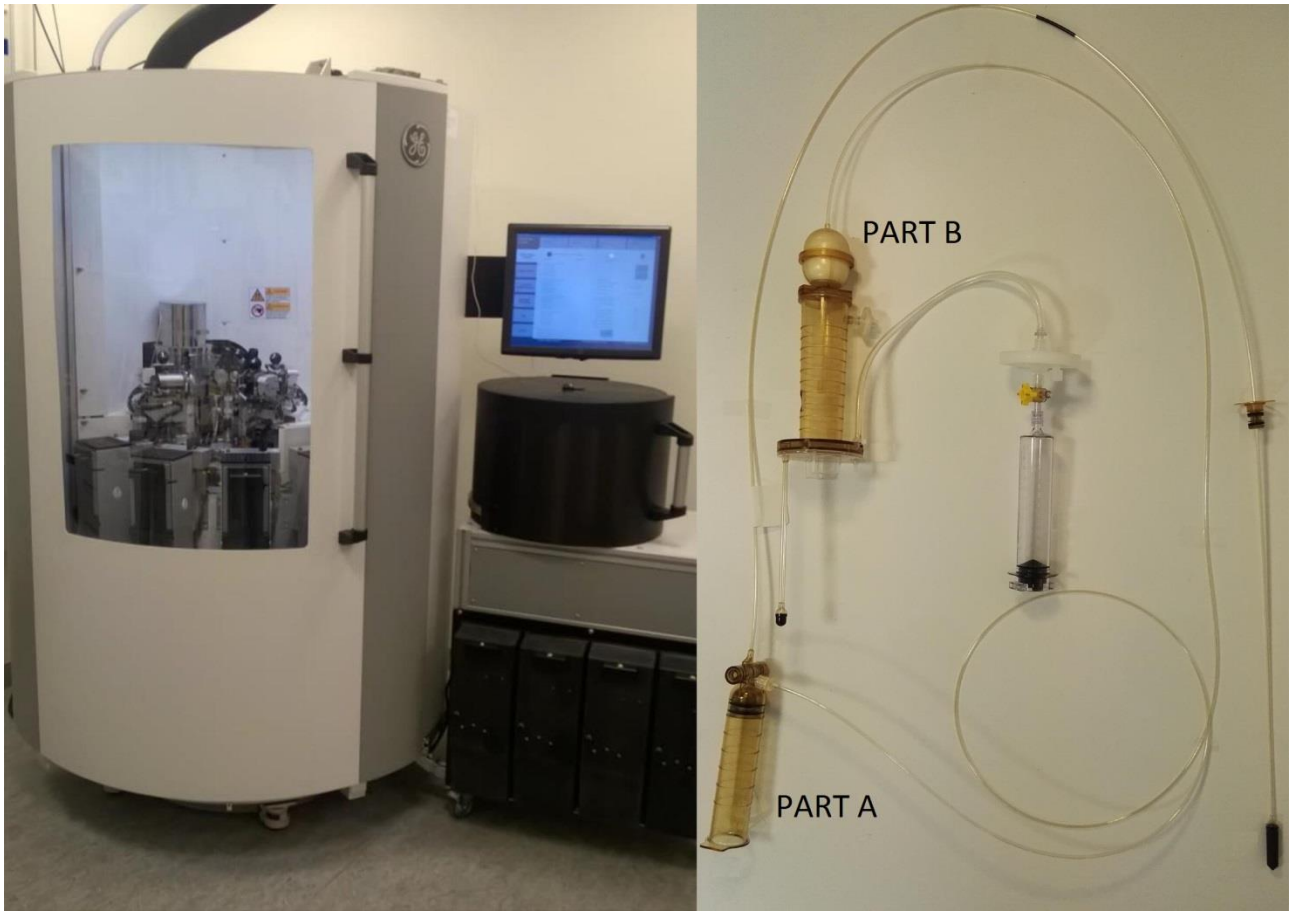

Figure 11: SPINlab and fluid path for clinical use, consisting of Part A and Part B.

A PEEK tube of outer diameter 1/32” and inner diameter 0.5 mm was found applicable for the filling purpose. It was found that the end should be cut in a slanted manner to better enter the inner tube and fit though the nozzle, as well as to minimize the size of the last droplet, which was drawn back into the tube to not contaminate inner walls at retraction. The tube was adequately rigid for insertion through the entire inner tube of >1.5 m, and sufficiently bendable to fit through the dissolution syringe valve bore and inner tube entrance without buckling.

The sample was drawn into the filling tube. The tube was wiped off and inserted into the inner concentric tube and guided to the vial, where the sample was injected. The exact position of the tube outlet was indicated by a mark.

Large Samples

1.47 g µL [1-^{13}C]pyruvic acid containing Electron Paramagnetic Agent (EPA, 15 mM AH111501) was injected into the sample vial with the filling tube. 38.0 g ultra-pure water with 0.1 g/L EDTA was added to the dissolution syringe. 26.2 g ultra-pure water with 0.1 g/L EDTA and 15.0 g 0.72 M NaOH, 0.4 M TRIS base, 0.1 g/L EDTA were added to the receiver of the fluid path Part B.

The samples were polarized a clinical polarizer (SPINlab, GE Healthcare) operating at 5 T and 0.85 K and dissolved in a fluid path Part A with an attached Part B receiver with EPA filter.

The quality control (QC) module measured 6 parameters of the dissolved sample in 15 s without direct contact.

6.7 T Homebuilt Polarizer

The initial aim of **Study** 1 and **Study II** was to develop filling techniques and protocols for hyperpolarized water. Hence, a 6.7 T magnet (Magnex, Oxford, UK) was adapted to facilitate the fluid path technology, so that the methods could be transferred to SPINlab polarizers for preclinical imaging. The magnet was modified with a flow-type variable temperature insert. A microwave source provided 55 mW microwaves at 188.0±0.6 GHz. A heater-pressure module was implemented for heating the dissolution medium and driving dissolution. A valve was implemented to keep a pressure of 12 bar during heating, adequate to sustain the vapor pressure of the heated solvents. At dissolution, the pressure was increased to 16 bar and the dissolution medium syringe valve was opened. Solid-state NMR was performed with a saddle coil connected to an NMR console. The operating temperature was 1.1-1.2 K. The dissolution process was controlled by a LabVIEW program, and the various phases of polarizing, dissolution medium heating, and dissolution process could be controlled individually.

Small Samples

40 µL [1-^{13}C]pyruvic acid containing 15 mM AH111501 was injected into the sample vial with the filling tube. The filling tube was connected to a helium gas source to flush remaining sample into the vial. 13.3 g 0.2 M tris-hydroxymethyl aminomethane (TRIS base) with 0.1 g/L EDTA and 138 µL NaOH (10 M) was added to the dissolution syringe.

The samples were polarized in the homebuilt polarizer for one hour. Liquid state NMR data was acquired on a 9.4 T spectrometer. ^{13}C polarization and relaxation time was measured with excitations of $\alpha = 3^o$ every 2 s, starting approx. 10 s post dissolution. The thermal signal was acquired by adding 15 µL Omniscan to reduce T_1 to <1 s with 2000 averages of repetition delay 0.5 s and $\alpha = 3^o$.

5.1.3 Results

Two sample size were tested in the study.

1) A human dose for clinical studies of 1.47 g pyruvic acid/EPA was polarized and dissolved in a clinical polarizer, aiming for 40 mL 250 mM pyruvate sample, reaching an average polarization of 34.2%. Six quality control parameters were measured online on the SPINlab. The relevant measures and standard deviations are shown in Table 5.

	Average	**Standard deviation**	**Relative STD (%)**
PA/EPA added (g)	1.47	0.02	1.4
DM in syringe (g)	38.0	0.1	0.2
DM in receiver (g)	25.8	0.3	1.0
NM in receiver (g)	14.3	0.2	1.4
PA/NaOH mol ratio	1.6	0.002	0.2
Pyruvate conc. (mM)	246	19	7.7
pH	7.71	0.17	2.2
EPA conc. (µM)	1.17	0.28	24
Temperature (^{o}C)	32.0	1.3	4.0
Volume (mL)	>40 mL		
Polarization (%)	34.2	2.9 (n = 3)*	8.5

Table 5: Results from dissolutions with large sample filling (n = 11).

2) A smaller dose for small animal preclinical studies of 40 mg pyruvic acid/EPA was polarized and dissolved in a homebuilt polarizer aiming for 5 mL 80 mM pyruvate sample, reaching an average polarization of 43.7%.

Six quality control parameters were measured: Final pyruvate concentration, pH, EPA concentration, temperature, output volume and polarization, Table 6. They all showed high

reproducibility with low standard deviations, and concentrations 3-10 times smaller than the acceptance criteria for clinical studies.

	Average	**Standard deviation**	**Relative STD (%)**
PA/EPA added (mg)	40		
DM in syringe (g)	13.4	0.6	4.5
NaOH (10M) syringe (g)	0.138		
Pyruvate conc. (mM)	70	7.4	11
pH	7.8	0.1	2
EPA conc. (µM)	70.5	7.5	11
Product in receiver (g)	5.3	0.6	12
Temperature (^{o}C)	54	2.6	5
Polarization (%)	43.7	5.5 (n = 4)	13
T_1	53.8	2.0 (n = 4)	4
Recovery (%)	82	12	15

Table 6: Results from dissolutions with small sample filling (n = 7).

5.1.4 Discussion

The filling method was developed to be able to reuse the fluid paths. The optimization of the protocol for hyperpolarized water has required hundreds of dissolutions in the fluid path. With the high purchase cost of the sterile fluid path, this would not have been possible with a PhD project budget, if each system could only be used once. Thus the method has facilitated a trial-and-error investigation of dissolution parameters and new ideas such as radical extraction solvents, as well as a systematic optimization of the system.

The method is complicated, because the insertion of the filling tube requires know-how for how to get the tip into the inner tube though the geometry of the dissolution medium syringe, and a steady hand to get the tube through the inner tube nozzle without buckling. The best way to learn the technique may be from the videos published as supplemental material to *Paper I*. Several aggregates were 3D printed and tested to guide the tube into the system and make the procedure more straightforward, but none were successful. Thus, buckling and rupture of the filling tubes was experienced occasionally.

Despite of these difficulties, it is believed that the method and the reproducibility of the sample properties can be an asset for research sites using the fluid path technology.

5.1.5 Conclusion

A novel fluid path filling method has been developed. The method facilitates reproducible polarization and low variance in the quality control parameters. In addition, the method allows multiple reuses of the fluid path, and potentially saves preparation time, because the UV cured gluing or laser welding process is only needed for first time usage.

5.2 Study II: Large dose hyperpolarized water with dissolution-DNP at high magnetic field

5.2.1 Introduction

The aim of this study was to develop a protocol for production of hyperpolarized water samples of volumes suitable for large animal experiments, and to optimize polarization, relaxation time and radical removal.

The end goal is to deliver a safe sample of highest possible polarization at time of injection into the animal. The latter requires a high solid-state polarization, efficient dissolution with minimal polarization loss, and long relaxation time to conserve polarization during the transfer and injection. The fluid path system described in **Study I** is applied to be able to use the method in clinical setups with SPINlab facilities.

Dipolar relaxation is the main source of relaxation in the sample. Pure water has a T_1 of 3.2 s, due to the dipolar relaxation between neighboring protons. The polarized sample is therefore dissolved in D_2O. Due to its smaller magnetic moment, which enters quadratically in the relaxation process, a deuteron should be about ten times less effective for the relaxation of neighboring protons than another proton [76]. The relaxation times of various H_2O/ D_2O ratios were shown in Table 1. Determination of the proton concentration in the dissolved sample is a balance between achieving long relaxation time, while keeping the protons concentrated to get the highest possible signal. A sample size of 1 mL sample was determined to achieve sample sizes suited for large animal experiments. In order to secure a uniform radical distribution in the sample, half of the sample volume was substituted for glycerol. By dissolution in 16 mL D_2O dissolution medium, the final H_2O volume fraction is 0.031. Thus, the relaxation from neighboring protons alone will give a T_1 of more than 25 s, which is acceptable.

The radical is another contributor to relaxation. In the low magnetic field, the sample is exposed to during the transfer and injection time, nitroxide relaxation rate contribution of $R_{\text{Nitroxide}}$ = 0.55 $s^{-1}mM^{-1}$ at 25 °C has been reported [80]. For the 1 mL 30 mM TEMPO sample dissolved in 16 mL dissolution medium, the radical would result in a T_1 of less than 1 s, if not removed. Several techniques has been discussed earlier to minimize relaxation from the radical. Quenching of the radical by ascorbic acid has been successfully applied in other studies [78,81], but the process takes time and leaves unwanted products in the final sample. Filtration of the radical is another

solution, but few working systems have been demonstrated, and the relaxation mechanisms in the filtering process are unknown. Therefore, the radical was extracted in an organic phase.

The relaxation contribution from the oxygen in the system originating from air in the fluid path and dissolved in the solvents contributes to the relaxation rate with 0.0094 L/mg/s [79]. The concentration of dissolved oxygen in air saturated water at 25 °C is around 8.6 mg/L, which leads to a relaxation rate contribution of 0.081 s^{-1}. The corresponding oxygen concentrations in the organic solvents used for extraction, heptane and NFBME, are a factor of 10 and 20 higher, respectively [96,97]. The dissolution medium and the extraction solvent were therefore degassed before use. The dissolved sample relaxation from the oxygen originating from the 1 mL sample is negligible. However, the oxygen can affect the DNP, and was therefore investigated by comparing degassed and non-degassed samples.

5.2.2 Methods

The standard water sample consisted of 30 mM TEMPO (2,2,6,6-Tetramethylpiperidine 1-oxyl) in H_2O/glycerol 1:1 (w/w). In addition, corresponding 20 mM TEMPO in water/glycerol and 30 mM TEMPO in H_2O/dimethyl sulfoxide-d_6 (DMSO-d_6) 1:1 (w/w), were prepared. 1100 mg sample (~1 mL) was filled in the sample vial as described for **Study I**. The dissolution medium syringe was filled with 7.60 g (5 mL) nonafluorobutyl methyl ether (NFBME) and 17.72 g (16 mL) dissolution medium, consisting of D_2O with 1 mM calcium disodium ethylenediaminetetraacetic acid (EDTA) and 9 g/L NaCl. The solvents were degassed in the syringe by bubbling with helium gas for 10 minutes through an adapter, leading the wet vapor away from the inner tube to prevent ice blockage when cooled in the magnet.

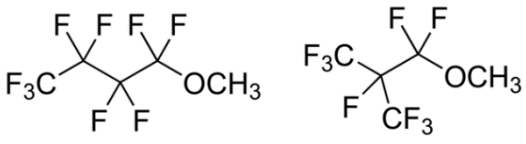

Figure 12: The two isomers of nonafluorobutyl methyl ether, used to accelerate dissolution and extraction process.

Samples to be degassed with the freeze-pump-thaw method were exposed to 3 cycles of freezing, vacuum and melting. The fluid path was sealed off to prevent condensation of moist air,

and the sample was frozen by placing the vial in a liquid nitrogen bath for 2 minutes, before the fluid path was flushed with helium gas and checked for pressure leaks.

The samples were polarized in the homebuilt polarizer described in **Study I** at 188 GHz. Only Part A of the fluid path system was used. A sealed separatory funnel with 25 mL degassed heptane was used as receiver. The funnel was shaken vigorously during dissolution, extracting most of the TEMPO radical. The lower, denser, aqueous phase was drawn into a 25 mL disposable syringe, and injected into a 5 mm NMR tube placed in the NMR spectrometer through 1 m tubing. Funnel, syringe, tubing and NMR tube had all been flushed with helium gas and sealed off.

NMR acquisition

Liquid state NMR data was acquired on a 9.4 T spectrometer. Hyperpolarized water samples were excited with a 1° flip angle (α) for a series of 200 spectra of 1 s intervals. The proton concentration in the samples was measured by addition of 0.2 M potassium formate before thermal scans with α = 90°.

Absorbance for radical quantification

The radical extraction was evaluated by optical absorbance spectroscopy of the dissolved samples. Data was acquired with a light source (Ocean Optics DH-2000) and a UV- spectrometer (Ocean Optics USB2000+UV-VIS) in quartz cuvettes of 10 mm path length. The dark spectrum was recorded, and a quartz cuvette with reference medium was inserted. The reference spectrum was recorded after letting the light source stabilize for 30 minutes. The cuvette was flushed with the relevant solution 3 times before the transmitted spectrum was recorded.

5.2.3 Results

Solid-state polarization

The solid-state polarization was quantified by letting a sample polarize for 19 hrs towards thermal equilibrium, and the corresponding background signal was acquired with an empty sample vial, Figure 13.

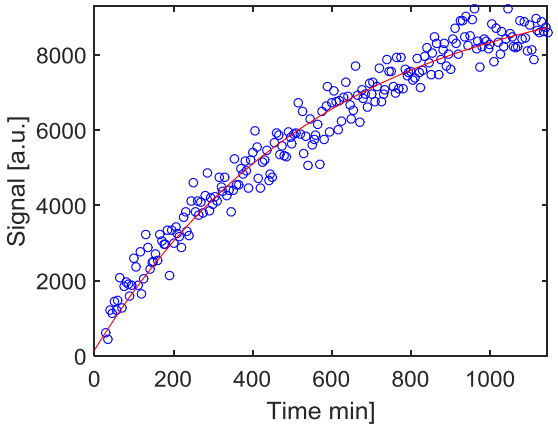

Figure 13: Thermal polarization build-up of a 30 mM TEMPO in water/glycerol 1:1 (w/w) sample at 6.7 T after subtraction of background signal. The time constant was T_1 = 583 min.

The background signal was subtracted from the sample signal, and the NMR signal time series, $S(t)$, was fitted with a function

$$S(t) = P_{\text{thermal}}\left[1 - \exp\left(\frac{-t}{T_1}\right)\right]$$

yielding a T_1 of 583±62 min. The constant P_{thermal} corresponds to the thermal equilibrium value,

$$P_{\text{thermal}} = \tanh\left(\frac{\hbar\gamma B}{2k_B T}\right) = 0.61\%$$

where $\hbar$ is the Planck constant, γ is the proton gyromagnetic ratio, B is the magnetic field, k_B is the Boltzmann constant, and T is the temperature.

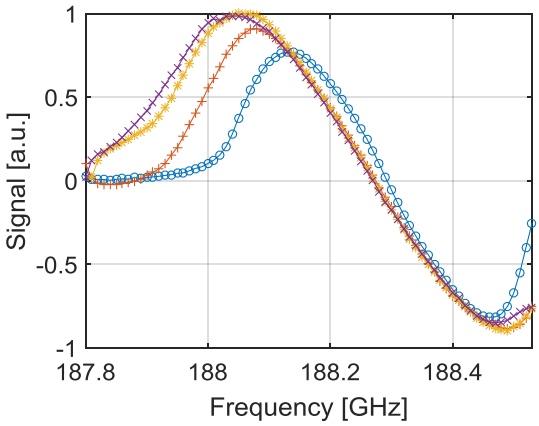

Figure 14: Frequency sweep of 30 mM TEMPO in water/glycerol 1:1 (w/w) with no frequency modulation (○) and modulation amplitude of 25 MHz (+), 50 MHz (*) and 75 MHz (x). Modulation frequency f_{mod} = 1 kHz.

The effect of frequency modulation was investigated by acquiring frequency sweeps with 60 s DNP for each frequency step for a series of 4 different modulation amplitudes, Figure 14. The optimal modulation amplitude of 50 MHz yielded an increase of 30% compared to no modulation.

The signal of the thermally polarized sample was used to quantify the DNP build-ups shown in Figure 15. An overview of the polarization after one hour and the fitted build time constants are stated in Table 7. The standard sample of 1100 mg 30 mM TEMPO in water/glycerol polarized at 188.12 GHz with 50 MHz modulation amplitude and 1 kHz modulation frequency showed a polarization of 63.1±3.7% after 1 hr (N = 4), whereas the corresponding 20 mM TEMPO sample only reached 48.1±4.9% after one hour, with a longer buildup time of 37±5 min. The solid-state polarization increased to 71.5±4.5% when the sample was degassed before DNP.

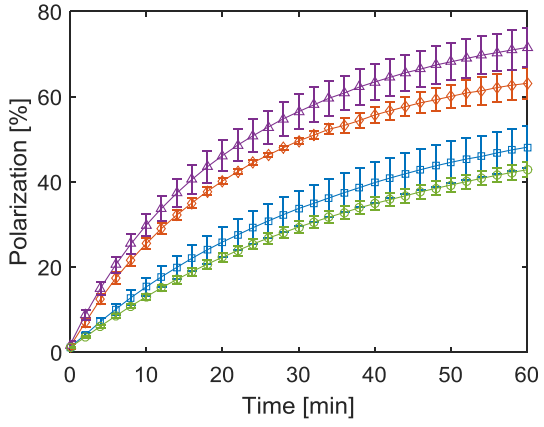

Figure 15: DNP build-up curves for 20 mM TEMPO in water glycerol at 188.12 GHz (□), 30 mM TEMPO in water/glycerol at 188.12 GHz (◊), degassed 30 mM TEMPO in water/glycerol at 188.06 GHz (Δ) and degassed 30 mM TEMPO in water/DMSO-d_6 at 188.06 GHz (○). All with frequency modulation of a_{mod} = 50 MHz and f_{mod} = 1 kHz.

Experiment	*N*	*P*(1 hr) [%]	DNP time const.
20 mM TEMPO in water/glycerol	6	48.1 ± 4.9	37 ± 5 min
30 mM TEMPO in water/glycerol	4	63.1 ± 3.7	24 ± 4 min
Degassed 30 mM TEMPO in water/glycerol	5	71.5 ± 4.5	23 ± 2 min
Degassed 30 mM TEMPO in water/DMSO-d_6	3	42.8 ± 1.7	41 ± 2 min

Table 7: DNP results for various sample compositions and polarization parameters.

Liquid state polarization

The dissolution resulted in 16±1 mL (*N* = 8) hyperpolarized water with a temperature of 50±2 °C (*N* = 6). The free induction decay (FID) of the first hyperpolarized signal decays rapidly due to radiation damping (Figure 16a). The time constant of the FID fit was 0.25 ms, implying a linewidth of more than 1200 Hz due to radiation damping. The integral of each acquisition is shown in Figure 16b. The polarization was measured by comparing the first signal to the thermal signal. On average, the standard experiments of 30 mM TEMPO in water/glycerol 1:1 (w/w) showed a polarization of 7.8±3.3 %, and the data were fitted to a T_1 of 17.0±0.9 s (*N* = 6). A validation experiment where the fully relaxed sample was introduced into the 9.4 T magnet 5 min later, yielded consistent T_1 of 16.6 s, Figure 16b.

The results of the dissolutions are shown in Table 8.

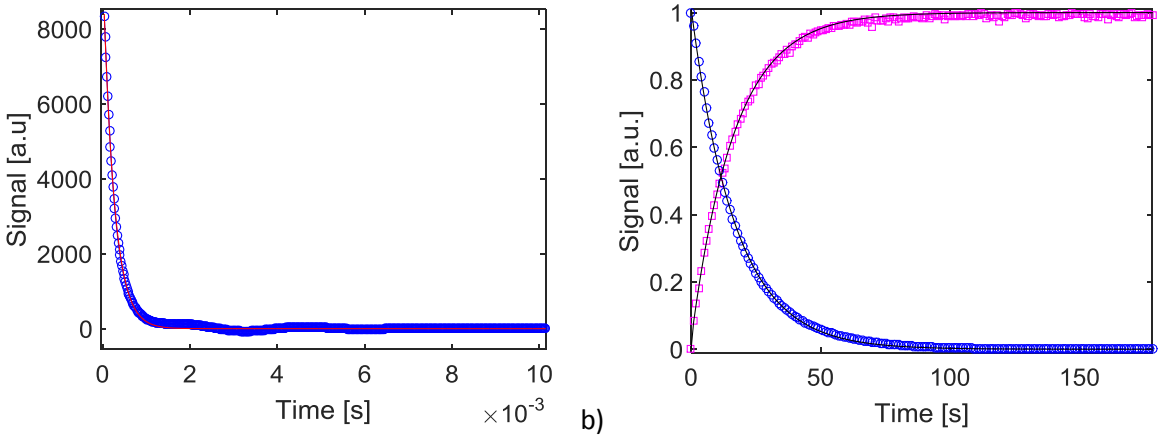

Figure 16: a) FID of first hyperpolarized signal fitted with a decaying exponential function b) Normalized NMR signal of hyperpolarized 30 mM TEMPO in water/glycerol 1:1 (w/w) sample (○) and build-up of relaxed sample at 9.4 T to validate T_1 (□). The signal from the first point was 3761 times that at thermal equilibrium. The time constant for hyperpolarized relaxation was 17.0 s, whereas the validation measurement of thermal build-up was T_1 = 16.6 s.

Experiment	*N*	Pol. [%]	T_1 [s]
20 mM TEMPO in water/glycerol 1:1 (w/w)	5	8.6 ± 1.5	16.1 ± 1.0
30 mM TEMPO in water/glycerol 1:1 (w/w)	6	7.8 ± 3.3	17.0 ± 0.9
Degassed 30 mM TEMPO in water/glycerol 1:1 (w/w)	3	13.0 ± 0.9	15.7 ± 1.2
Degassed 30 mM TEMPO in water/DMSO-d_6 1:1 (w/w)	2	7.2 ± 1.3	18.8 ± 1.6
30 mM TEMPO in water/glycerol 1:1 (w/w) without NFBME, long exit tube	2	2.4 ± 0.6	19.6 ± 0.8
30 mM TEMPO in water/glycerol 1:1 (w/w) without NFBME, short exit tube	2	4.8 ± 0.5	20.1 ± 1.3

Table 8: Liquid state polarization and T_1 at 9.4 T.

5.2.3.1 Radical Quantification

The radical concentration in the dissolved sample solution was quantified with optical absorption spectroscopy measurements. TEMPO has an absorbance peak around 240 nm, and no other substances in the composition has significant absorbance around this range. Thus the absorbance *A* at 240 nm follows the Beer-Lambert law and scales linearly with concentration,

$$A_\lambda = \varepsilon_\lambda c\, l$$

where A_λ is the absorbance at wavelength λ, ε_λ is the extinction coefficient at wavelength λ, c is the concentration of the absorbing molecule and l is the optical path length. The linearity is valid in the range A = [0.1:1]. The measurement is repeated 3 times, and the absorbance spectrum is calculated as

$$A_\lambda = -\log_{10}\left(\frac{S_\lambda - D_\lambda}{R_\lambda - D_\lambda}\right)$$

where S_λ is the sample intensity at wavelength λ, R_λ is the reference intensity at wavelength λ, and D_λ is the dark intensity at wavelength λ.

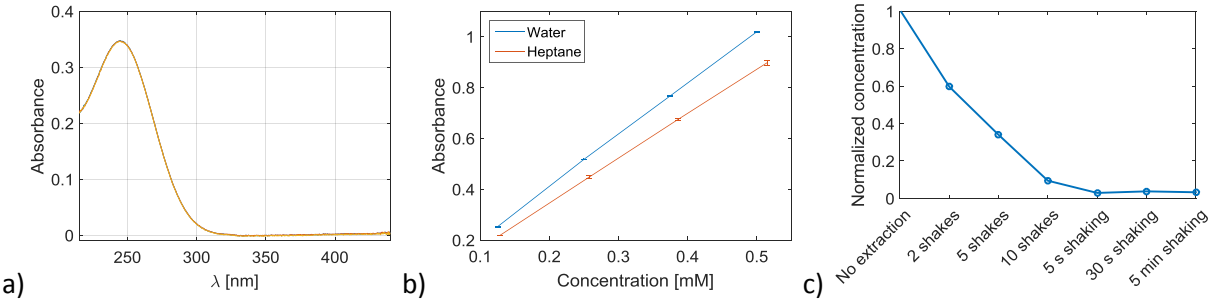

Figure 17: a) Absorbance spectra of example measurement. The spectra of the three repetitions overlap. b) The standard curves for TEMPO in water and heptane (N = 3 for each point). c) The TEMPO concentration in the water phase after extraction in heptane for various degree of shaking (N = 3 for each point).

The absorbance spectra of an experiment are shown in Figure 17a. The 3 spectra in the figure cover each other, confirming the reproducibility. Absorbance spectra of known concentrations of TEMPO in water and heptane was used to produce the standard curves shown in Figure 17b. Having established the relation between concentration and absorbance, the equilibrium value of concentrations in the two phases, the partition coefficient *P*, could be determined. The partition coefficient of TEMPO in water and heptane was $P_{Heptane}$ = 22 at room temperature, where extraction from TEMPO in water reference sample into equal volume of heptane in separatory funnel was measured. The corresponding partition coefficient in NFBME was P_{NFBME} = 23, and extraction in a 25% NFBME/75% heptane mixture showed partition coefficient between the two other reported values.

The extraction was tested for different schemes of shaking in the separatory funnel. Using the volumes of dissolved sample and heptane volumes in dissolution experiments, extraction was tested for 2, 5 and 10 individual shakes, and for 5 s, 30 s and 5 min continuous shaking, respectively (3 repetitions each, Figure 17c). It appears that maximum extraction was obtained after 5 s of continuous shaking, and that no further gain could be achieved by longer shaking. In dissolution-DNP experiments, the extraction should be started as soon as the front of the dissolved sample reaches the heptane in the receiver, but continue long enough to obtain maximum extraction of the latest arriving drop of the sample. 10 s of shaking from dissolution start was chosen to meet these requirements. This fits conveniently with a popping sound when the valve controlling the dissolution is closed (valid for both the homebuilt polarizer and GE SPINlab clinical polarizers).

A final TEMPO concentration of 50±12 µM (30 mM TEMPO in water/glycerol 1:1 (w/w), *N* = 5) was measured in the dissolution experiments. This is compared to the theoretical value of final water phase concentration

$$c_{WP} = c_{Sample} \frac{V_{Sample}}{V_{DM} + V_{Sample} + P\, V_{Heptane}} = 53\ \mu\text{M}$$

for the sample concentration of c_{Sample} = 30 mM, sample volume of V_{Sample} = 1 mL, dissolution medium volume of V_{DM} = 16 mL, heptane volume $V_{Heptane}$ = 25 mL, and partition coefficient P = 22. The small amount of NFBME reaching the receiver was ignored in this calculation.

Proton Concentration

The proton concentration in the dissolved sample is a delicate balance, where a high concentration increases the magnetization of the sample, but simultaneously increases the relaxation rate by dipole-dipole relaxation. The proton concentration was measured by quantitative NMR after addition of a potassium formate reference solution. A spectrum is shown in Figure 18. The formate peak (left) and water peak (right) were integrated (red regions) to 5.0±0.5 M (*N* = 18).

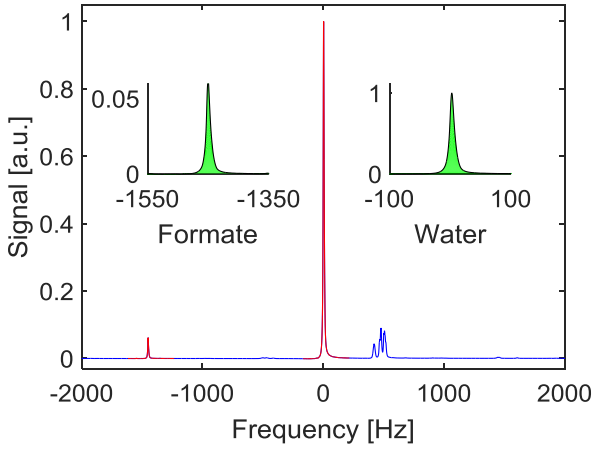

Figure 18: Proton concentration measurement. Large integrated peak of water in the dissolved sample, and small integrated peak of 0.2 M formate for reference. Other peaks represent the glycerol in the sample. The proton concentration was estimated to 5.0 M.

5.2.4 Discussion

The liquid state polarization of the 20 mM sample was higher than for the 30 mM sample. Although the T_1 after radical extraction was marginally lower than for the 30 mM sample, the

relaxation in the important time window of 1-2 s from dissolution of the sample to extraction of the radical could be the explanation. Yet, it should be noted that the differences in polarization and T_1 are within the uncertainty range of the measurements, where only five 20 mM sample dissolutions and six 30 mM sample dissolutions were conducted.

The NFBME was added to accelerate the dissolution process, so that the time from sample melting to dilution and radical extraction was shortened, and the relaxation was reduced. The volume of NFBME was tested with volumes of 5, 8 and 11 mL, where the lower volume yielded the most controlled and efficient dissolution, and highest polarization in the liquid state. The effect of the NFBME was examined by replacing it with additional dissolution medium. The polarization of the dissolved sample decreased to 4.8±0.5%. The main drawback of using NFBME is the weakening of the otherwise chemically stable polyphenylsulphone, which the fluid path is made of. Extended heating time with fluid path exposure to NFBME during polarization was observed to cause bursting dissolution medium syringes in several occasions. Other nonpolar solvents were tested to replace the NFBME. 1-Octanol stressed the syringes even more than NFBME and was discarded. Another fluorinated, organic solvent (3M™ Novec™ HFE-7500 Engineered fluid) with boiling point of 130 °C and density similar to NFBME (ρ = 1.559 g/mL) yielded a decrease of 35% in the observed polarization in dissolved state in comparison, indicating that the driving force of the superheated NFBME is important for quick extraction of the radical (identical solvent volumes and parameters, 3 repetitions each).

It was determined that the final radical concentration of 50 µM matched the theoretical value for the given solvent volumes in equilibrium. Hence, the 10 s shaking may be more than needed, and a few seconds may be saved without affecting the relaxation time. As the maximum possible radical extraction has been achieved with the applied shaking scheme, further extraction would require increased heptane volume. In this case, heated heptane would be required to conserve a high sample temperature for relaxation considerations.

An important feature for the final sample polarization is the length of the exit tubing. The standard exit tubes are longer than 2 m to fit the clinical polarizers and reach the QC module. For hyperpolarized ^{13}C compounds with long T_1, the long exit tube transfer time is not a problem. However, for hyperpolarized water with short T_1 and need for rapid dilution and radical extraction,

the transfer time of the concentrated, radical containing sample is crucial, and the cooling of long tubes should be minimized. The experiments showed that the final polarization was halved for standard exit tubes, compared to 50 cm exit tubes.

5.2.5 Conclusions

The method succeeded in producing large volumes, 16 mL, of hyperpolarized water suitable for large animal experiments. The sample was polarized to 71.5% for the most efficient sample composition and optimized frequency modulation. The liquid state polarization was 13.0%, indicating that most polarization is lost during dissolution. This is unavoidable, but the dissolution and radical extraction may be further optimized to provide injectable samples of higher polarization.

A standard deviation of more than 40% in liquid state polarization was experienced for some experiments. The dissolution in a two-phase system of D_2O and organic solvents yielded rapid radical extraction of 97.2%±0.7%, but the manual shaking may be the main contributor to the irreproducibility. Thus, an automated extraction scheme or a radical filtering system may be beneficial.

5.3 Study III: Hyperpolarized ^{13}C MR Angiography

5.3.1 Introduction

The aim of this study was to establish optimal conditions for hyperpolarized ^{13}C angiography, by comparing the behavior of two common sequences, balanced-Steady-State-Free-Precession (bSSFP) and Gradient-Recalled-Echo (GRE). In addition, the study was performed to provide in house data as a benchmark for the later work on hyperpolarized water angiography.

The ^{13}C compound HP001 (Bis-1,1-(hydroxymethyl)-[1-^{13}C]cyclopropane-D8, Figure 19), was selected to yield a high polarization and long relaxation time (in vitro, 2.35 T: $T_1 \approx 82$ s, $T_2 \approx 18$ s; in vivo, 2.35 T: $T_1 \approx 38$ s, $T_2 \approx 1.3$ s [69]) to optimize angiographic image quality in a preclinical facility.

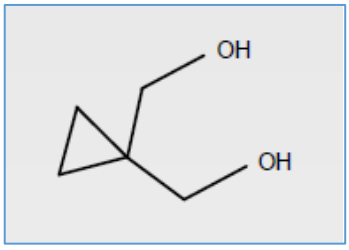

Figure 19: Molecular structure of HP001.

5.3.2 Methods

Healthy male Sprague Dawley rats of 240-320 g were catheterized in the carotid artery (N = 18) or tail vein (N = 5) before administration of hyperpolarized HP001.

The preclinical polarizer (HyperSense, Oxford Instruments) operated at 3.35 T and 1.4 K. 18.0 mg trityl (OX063), 500 mg HP001, 180 mg water and 15 µL Dotarem (1:10 dilution) was prepared. 100 µL sample was dissolved in 1 mL PBS buffer with 0.01 g/L EDTA diluted in 3 mL NaCl (9 g/L). The polarization of the sample was 20-25% at time of injection.

A preclinical scanner of 4.7 T (Agilent, Direct Drive, VnmrJ 4.0) equipped with a ^{1}H/^{13}C volume transmit/receive and 4-channel surface array ^{13}C receive coil setup was used.

HP-^{13}C, bSSFP: The hyperpolarized signals were acquired using a single-shot bSSFP sequence with $\alpha = 110°$. An $\alpha/2$ preparation pulse was implemented at time TR/2 before the first excitation pulse to approach a steady-state like situation faster, and a corresponding flip-back pulse was implemented at the end of each image acquisition to restore the longitudinal magnetization for the following time frame. The angiographic images had a FOV of 70×35 mm^2 and a slab thickness of 30 mm placed coronal in the head and neck region. The matrix size was 128×64. The repetition time and echo time were set to minimum, TR/TE = 6.95/3.48 ms. A

bandwidth of 50 kHz yielded a total image acquisition of 450 ms for each image. The sequence was started when the solution had been fully injected to capture the maximum possible signal.

HP-^{13}C-MRA, GRE: The GRE sequence was applied with an FOV of 70×35 mm^2, a slab thickness of 20 mm and with matrix size 256×128. The pulse length was 2 ms and the repetition and echo times were TR/TE = 10.16/5.10 ms. The total acquisition time for an image was 1300 ms with α = 5° and imaging was repeated over 30 time frames. Acquisition was started when injection was initiated to capture the maximum signal strength.

^{1}H MRA: Proton angiographic images were acquired with a ^{1}H quadrature coil with inner diameter of 35 mm. A 3D GRE sequence with TR/TE = 90/2.47 ms, α = 40°, FOV of 30×35×20 mm^3, matrix size 256×256×64 was used after an intravenous injection of 50 µL Clariscan™. The total acquisition time was 25 minutes.

5.3.3 Results

A gradient echo (GRE) sequence of α = 5° was determined as optimal for carotid artery injections, producing images of the right vascular arterial and venous network (Figure 20, left). 18 injections in 10 animals yielded SNR of 17.6±4.5. The GRE sequence was not efficient for intravenous injections, where the hyperpolarized agent is diluted in the vasculature before reaching the cerebral network, yielding SNR <10. A bSSFP sequence proved more useful for intravenous injection, where the venous structure of the rat head appeared, and larger veins could be identified (Figure 20, center). 5 injections in 4 different animals yielded SNR of 31.3±20.0. The sequence was optimized on a thermal ^{13}C phantom, finding α = 110° the optimum. This was confirmed by initial tests with intravenous injections of hyperpolarized HP001 in the tail vein (Figure 21). A 128×128 matrix with FOV = 60×60 mm^2 was used in these experiments.

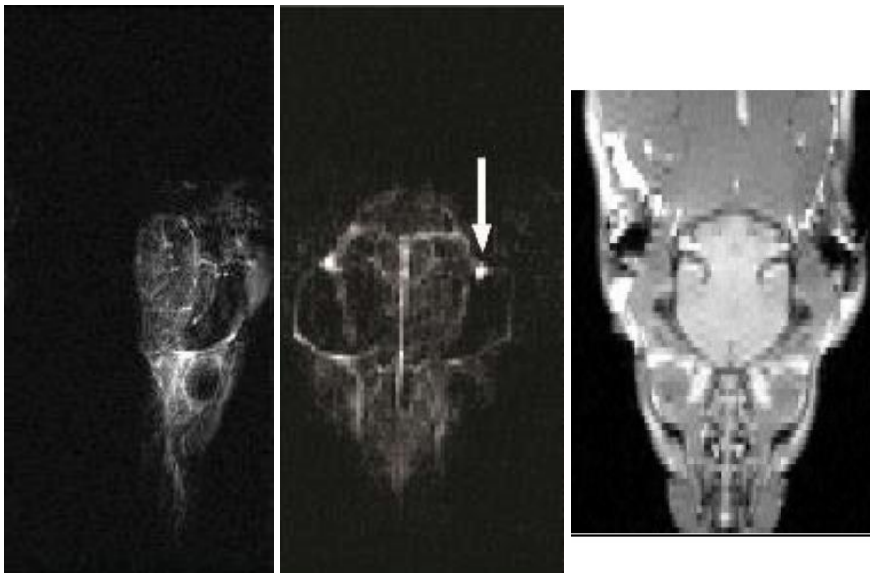

Figure 20: Rat cerebral angiography after hyperpolarized injection in the carotid artery, imaged with a GRE sequence (left) and tail vein imaged with a bSSFP sequence (center). The images are coronal planes, with the brain in the center and the eyes underneath, and the nose in the bottom of the FOV. The right pane shows an anatomical spin echo ^{1}H image for navigation.

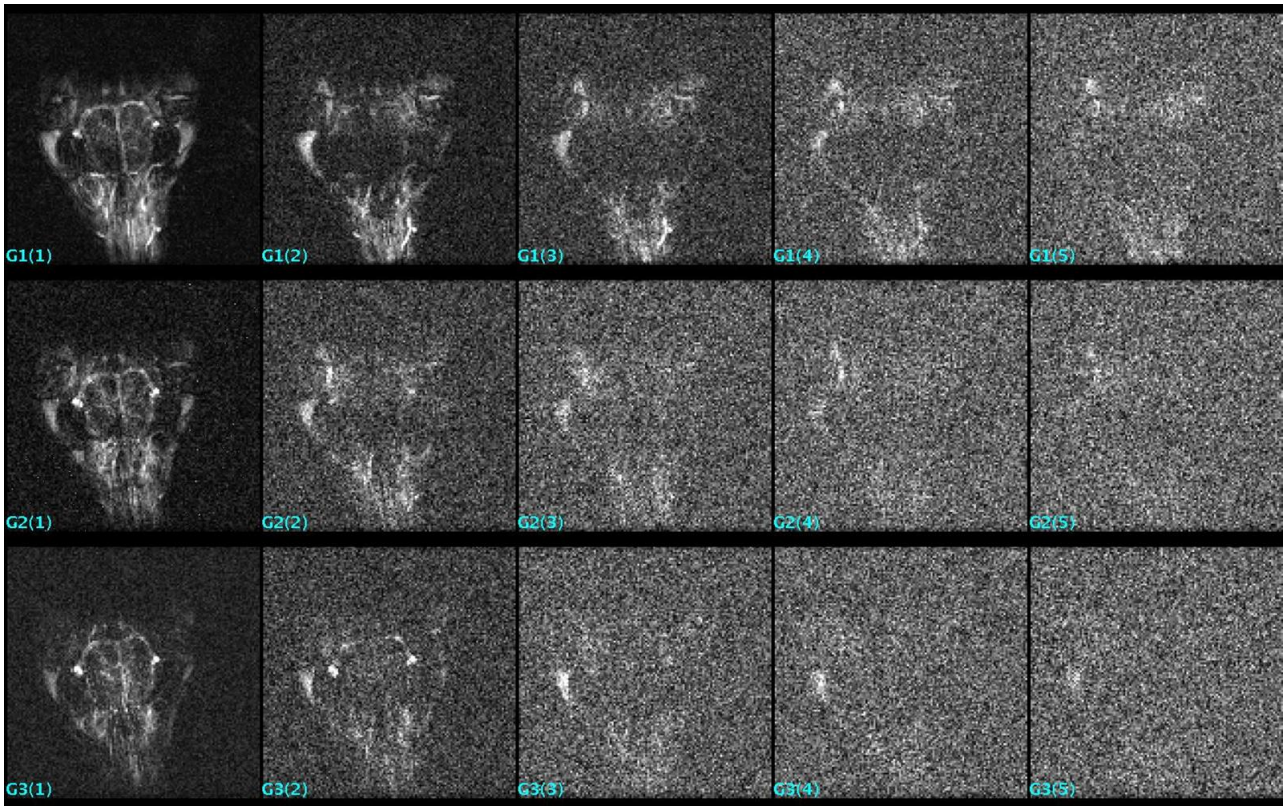

Figure 21: Time series of bSSFP imaging of intravenous injections of hyperpolarized HP001. The image quality and SNR was highest for α = 110° (top row), lower for α = 60° (middle row), and further decreased for α = 30° (bottom row). These images were acquired in a 128×128 matrix with FOV = 60×60 mm^2.

5.3.4 Discussion

It was unclear why the bSSFP sequence was unsuccessful for imaging of the intra-arterial injections. The sequence optimally would produce images with higher signal, and for the minimal background signal, higher CNR. However, the images were unusable due to the artefacts. The artefacts were believed to origin from movements of the arteries, which could be either from mechanical impacts from the catheter, or from physiological reactions.

The hyperpolarized ^{13}C MR angiography study was designed to be a precursor for hyperpolarized ^{1}H coronary angiography in rats, which could later be translated into a clinical setup with large animals. However, the study was complicated for several reasons. Working in small animals with fine vascular system requires high spatial resolution. In addition, the physiological dynamics are faster than in large animals, challenging the temporal measurements such as flow and diffusion.

Furthermore, issues of a preclinical scanner without modern imaging tools and with challenging artefacts in many images, were the main arguments for following another path for the hyperpolarized water studies. It was determined to design the ^{1}H hyperpolarization methodology for doses for large animals, and applicable to the currently existing polarizers at clinical facilities.

5.3.5 Conclusion

The bSSFP sequence was useful for intravenous injections, where SNR of 31.3±20 was observed with 0.55×0.55 mm^2 pixel size, although the large standard deviation indicated that the method yielded unstable results. The gradient echo sequence yielded SNR <10 with intravenous injections. Comparing the results of the two sequences for intravenous injections, the bSSFP would be preferred for achieving high signal for intra-arterial injections. However, the bSSFP sequence proved unsuitable for intra-arterial injections, where artefacts prevented useful images.

Angiographies of the right carotid arterial network of rats were acquired with a gradient echo sequence at 4.7 T with resolution of 0.27×0.27 mm^2 pixel size, and SNR of 17.6±4.5 resulting in a high image quality.

5.4 Study IV: Renal MR Angiography and Perfusion in the Pig using Hyperpolarized Water

5.4.1 Introduction

The aim of this study was to demonstrate hyperpolarized water MR angiographies and perfusion maps in a large animal model.

Whereas the target of the project was coronary angiography and myocardial perfusion, the kidney serves as an easier accessible organ for catheterization, and without the complications of cardiac motion. Renal investigations therefore served as a precursor to the cardiac study. However, development of a gadolinium and radiation free angiography and perfusion technique of the kidney has its own justification as well.

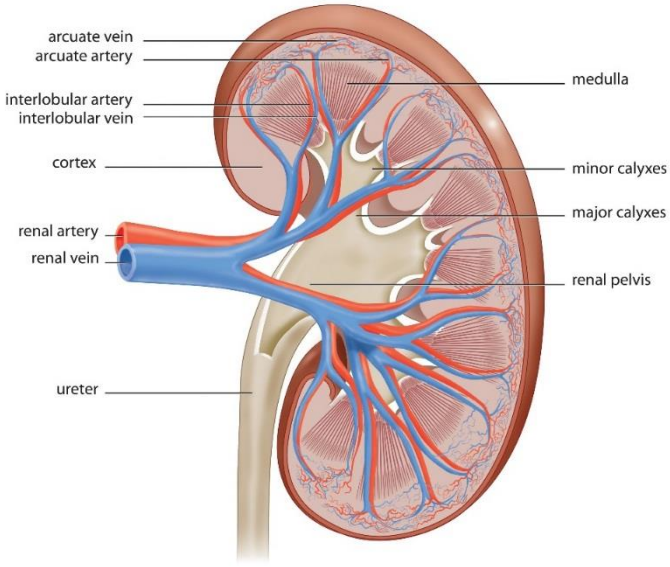

Figure 22: Anatomy of the human kidney. The renal artery and arteries are shown in red. Figure from [98].

The kidney is supplied with oxygenated blood through the renal artery (Figure 22). Renal artery stenosis is prevalent in 6.8% of the elderly population, and is associated with progressive, decreased kidney function and renal failure [99]. Hence, studies of renal MRA is regularly gaining attention [100,101], since early diagnosis can form the basis of preventive surgery or medical treatment before development of renal failure [102]. In addition to renal angiography, the extravasation into the renal tissue provides valuable information, in that renal perfusion is linked to hypertension. Several methods for perfusion measurements exist, but most employ imaging of other molecules than water. Direct assessment of water atoms diffusing into the vascular bed has

been asked for, and suggested by $H_2{}^{15}O$ PET imaging [103,104], again with the exposure to ionizing radiation. Hyperpolarized water as a perfusion marker could solve both of these issues.

5.4.2 Methods

Hyperpolarization

The 30 mM TEMPO in H_2O/glycerol 1:1 (w/w) sample was prepared as described for **Study II**. Due to bursting of the dissolution syringes during extended time of heating while exposure to organic solvents, the NFBME was left out and replaced by additional dissolution medium to a total of 31.01 g (28 mL). The fluid path was prepared with sample, dissolution medium and heptane as described for **Study I** and **Study II**. A 50 cm exit tube was used.

The sample was polarized in a SPINlab for one hour. Since the SPINlab only has ^{13}C channels installed, the electron resonance frequency was determined from a ^{13}C sample.

Animals

Healthy 30 kg female Danish domestic pigs were sedated and anesthetized before catheterization of the main renal artery for administration of 12-15 mL hyperpolarized water. The catheter was placed using fluoroscopy (Figure 23).

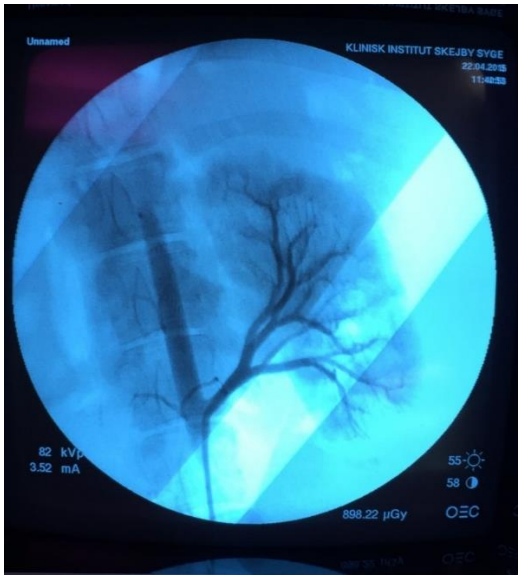

Figure 23: Renal arterial tree imaged by fluoroscopy during insertion of catheter.

Imaging

Hyperpolarized water angiographies in pigs and phantom scans were acquired on a 3 T scanner (HDx, GE) with an 8-channel cardiac array receiver coil. Phantom experiments were performed by placing the filled sample syringe next to a saline filled syringe in the scanner, before acquisition with a gradient echo sequence of α = 1°, matrix size 128×128, field-of-view, FOV = (24 mm)^2 in a slab of 40 mm with TR = 3 ms, TE = 0.784 ms. The acquisition time of each frame was 450 ms, and images were acquired with a time delay of one second.

Axial and coronal images covering the kidneys of the pig were acquired to allow for planning of the angiography slab for hyperpolarized water imaging. The sequence was as follows: a 3D T_1 weighted sequence with a standard steady-state free precession sequence (TE = 1.1 ms, TR = 2.7 ms, flip angle α = 35°, image matrix 256×256, FOV = 340x340 mm^2, in-plane resolution 1.3 mm, slice thickness 3 mm).

Angiographies were acquired in the coronal plane of the left kidney. Following the conclusions of **Study III**, a gradient echo sequence gave high signal and was robust towards artefacts for intra-arterial injections. Hence, a gradient echo sequence with α = 5°, slice thickness 40 mm, TR = 3.4 ms, TE = 0.984 ms, 256×256 matrix, FOV = 140×140 mm^2 was used. The acquisition time was 870 ms. The Gd-perfusion sequence was executed with the following parameters: spoiled gradient echo, inversion time = 850 ms, α = 10°, slice thickness 50 mm, TR = 2 s, TE = 1.4 ms, 128×128 matrix, FOV = 290×290 mm^2.

5.4.3 Results

Four phantom scans of sample polarized in a clinical polarizer were performed, giving average polarizations of 5.3±0.9% and T_1 of 24±1 s (Figure 24). The proton concentration of the 18 mL samples was 3.84±0.22 M (N = 10).

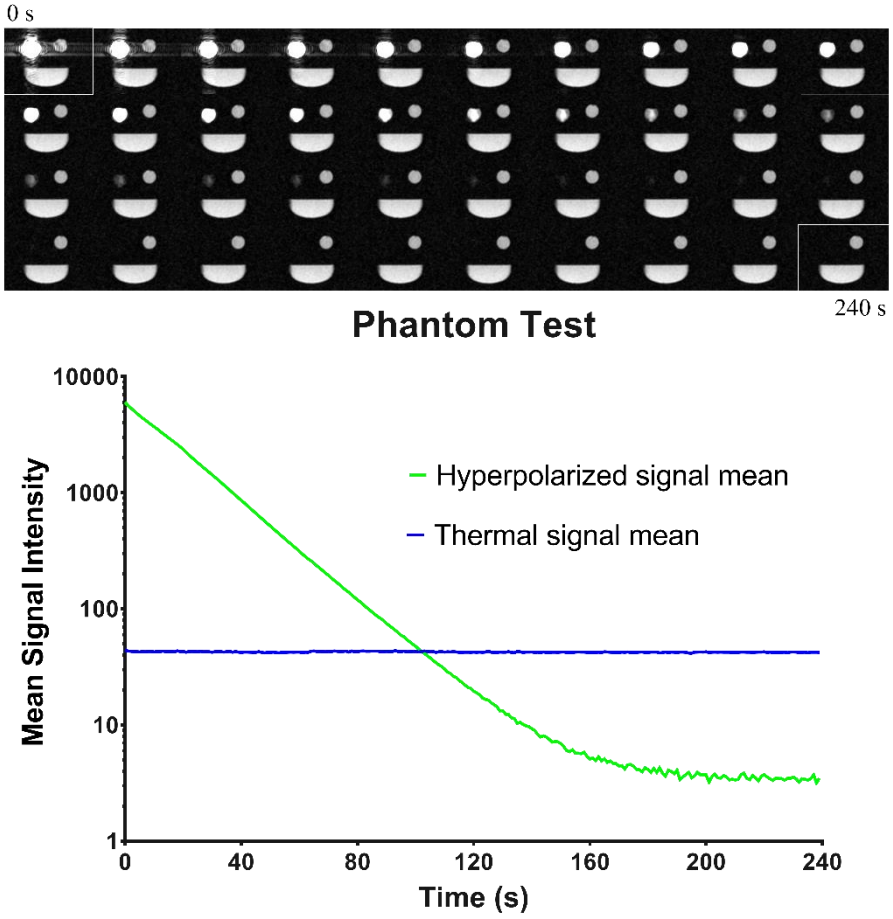

Figure 24: Hyperpolarized water phantom experiment. The phantoms consisted of two syringes. Stacked images (same scale) are shown from 0 to 240 s with an image every second. The graph shows ROI signal means of the hyperpolarized ^1H in D_2O (green, decaying signal) and the H_2O thermal phantoms (blue, steady signal). The hyperpolarized MR signal is initially 211 times stronger than the thermal H_2O signal, and the T_1 of the decay is 24 s. The hyperpolarized signal decays into the noise since the ^1H density is ca 20 times lower than the thermal H_2O sample.

Angiographies of the left kidney arterial system were produced in 4 animals with high contrast from kidney tissue. A time series with 2 s intervals is shown in Figure 25. The second frame shows the highest signal in the arteries, where the contrast agent has filled the main arteries after 5 s. The signal dereases in the followin frames due to relaxation and washout. This trend is visualized in the plot, where the time trends of the mean signal intensity in the input site and cortex are shown. Whereas the input signal depicts a step function with high intensity during the injection, the filling of the vascular bed increases continoulsy, before relaxation and washout occurs.

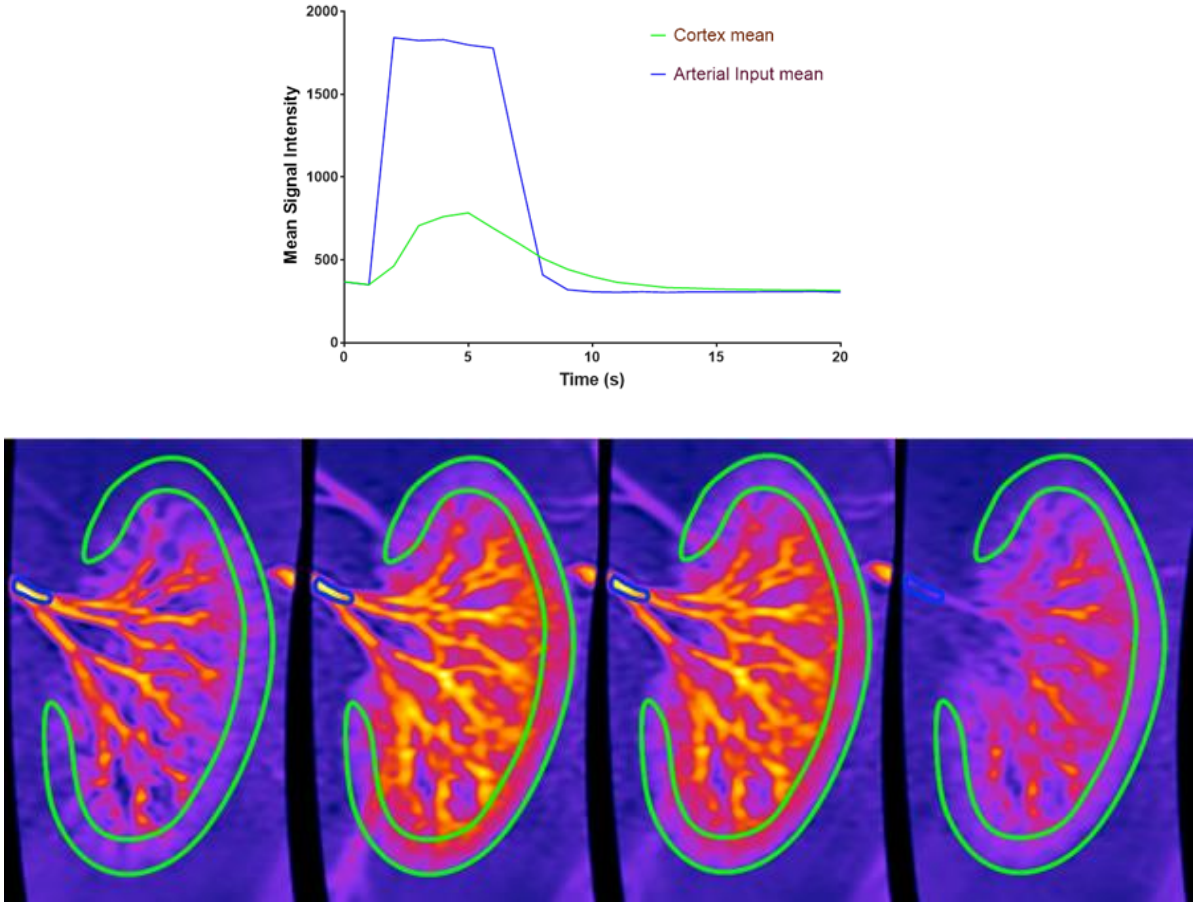

Figure 25: Renal angiographies in a pig at 3, 5, 7 and 9 s after injection of 15 mL hyperpolarized water. The color maps show the signal intensity from no signal (blue) to high signal (yellow) in arbitrary units. The mean signal in the input ROI (blue) and cortex ROI (green) are plotted versus time.

The perfusion maps derived from the time series are shown in Figure 26. The average perfusion in the cortex was 504±123 mL/100 mL/min (green circumference), in agreement with Gd-T_1-DCE analysis of 450±57.3 mL/100 mL/min (N = 2), and values reported in the literature.

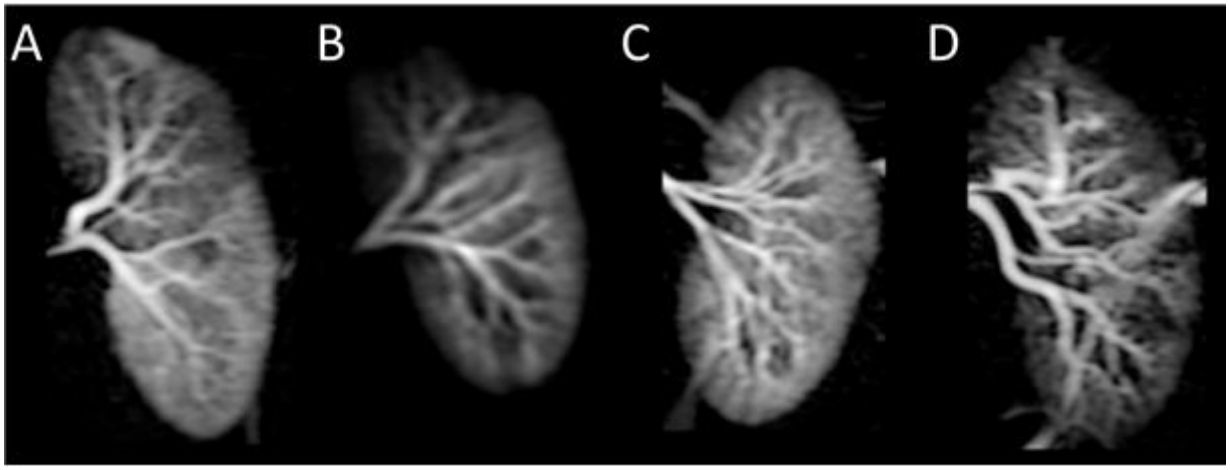

Figure 26: Perfusion maps of the kidney of four individual pigs after injection of 15 mL hyperpolarized water. The time series of Figure 25 is the data used for frame C.

5.4.4 Discussion

Hyperpolarized water MR angiography has been demonstrated in the pig kidney. The dynamics of the time series was used to produce perfusion maps, which provided perfusion values comparable to the standard Gd-T_1-DCE method. The study opens for direct measurement of water in the tissue, instead of tracing perfusion of e.g. gadolinium complexes with other perfusion characteristics. In addition, the method saves the burden of NFS related complications from Gd based contrast agents.

During injection and mixing with the blood in the arteries, the relaxation time of the protons is reduced to around 1.6 s, the T_1 of blood at 3 T [83]. This is important for the perfusion analysis, and should be validated experimentally, and taken into account in a prospective automated perfusion data analysis.

The main drawback is the need for renal catheterization, an invasive procedure. However, avoiding traditional contrast agents or, alternatively, radiation burden from CT scan may justify this. Comparing to state-of-the-art renal MR angiography of in-plane resolution 0.8×0.8 mm^2 [105,106], the presented method provides 0.55×0.55 mm^2 resolution without the burden of

gadolinium-based contrast agent, which is problematic for kidney patients in particular. Whereas conventional MRA may be a suitable screening tool for renal artery stenosis detection, the increased resolution of hyperpolarized water MRA may also be feasible for stenosis grading.

The protocol for hyperpolarized water was developed on a system, where several parameters could be controlled individually. However, using the SPINlab, the hyperpolarization process is automated. As a consequence, the dissolution syringes are pressurized and heated during the entire polarization. Even though the pressure and temperature in the homebuilt system mimicked those of the SPINlab, the extended heating time resulted in several breakings of the syringes. The breaking is problematic in terms of losing the sample, but can also result in damage of the polarizer and person damage from squirting of hot solvents. Thus, it was necessary to replace the NFBME in the syringe with additional dissolution medium. This may be the main reason for the lower polarization than that of the homebuilt polarizer. Other relevance differences between the two systems are the field strength (5 T of SPINlab vs. 6.7 T of the Magnex), temperature (0.8 K of SPINlab vs. 1.2 K of the Magnex), and the absence of frequency modulation on the SPINlab.

The SPINlab is designed for application of the full fluid path system, where Part A is connected to part B through an almost 2 m exit tube (see Figure 11). The system is closed off during polarization and dissolution. However, as determined in **Study II**, shortening of the exit tube is important to achieve high polarization. Thus, it was necessary to remove the protective Plexiglas plate, and run the short exit tube directly out through the window (Figure 11).

5.4.5 Conclusion

MR angiography in large animals using hyperpolarized water was demonstrated feasible for the first time. The method yielded reproducible results in 4 different animals, and the derived perfusion maps gave values corresponding to those of conventional methods. The protocol for hyperpolarized water developed in **Study II** was transferable to a clinical environment, although substantial loss in polarization was observed for the SPINlab experiments.

5.5 Study V: Dynamic Coronary MR Angiography in the Pig using Hyperpolarized Water

5.5.1 Introduction

Cardiovascular magnetic resonance imaging is an efficient tool for radiation free diagnosis of cardiac diseases, and is routinely used in clinical praxis. However, coronary magnetic resonance angiography is troublesome due to the fine structure of the coronary arterial network, and the cardiac and respiratory motion. Thus, coronary MRA remains an unresolved challenge for cardiac disease diagnosis.

The aim of this study was to demonstrate that hyperpolarized water can be used as a contrast agent to obtain coronary angiographies in a large animal model. The major challenge was the heart beating, where sampling within the diastole is required to avoid motion artefacts, and thus to acquire adequate signal to obtain a satisfactory resolution within less than a cardiac cycle.

The method provides direct tracing of water molecules, contrary to established techniques which measures perfusion of radioactive nuclei, iodine contrast, or MR relaxation compounds.

5.5.2 Methods

The 1 mL 30 mM TEMPO in water/glycerol 1:1 (w/w) sample was prepared as described in **Study II** and filled in the fluid path using the method developed in **Study I**. The sample was polarized as described in **Study IV**.

Images were acquired in a tilted plane covering the LAD with equipment and parameters as in **Study IV**. A gradient echo sequence of matrix size 256×256 and FOV = 140×140 mm^2 yielded isotropic resolution of 0.55 mm. The acquisition time was 870 ms.

Animals

Healthy 30 kg female Danish domestic pigs were sedated and anesthetized before catheterization of the coronary artery (N = 3), for administration of 15 mL hyperpolarized water.

5.5.3 Results

A gradient echo sequence was used to produce dynamic time series of the coronary perfusion with frame acquisition time of 870 ms after hyperpolarized water injection in the coronary artery with 3 successful injections in each of the 3 animals. Angiographies of each animal are shown in Figure 27. The injection site, the LAD and the left circumflex appear with the highest intensity, and some flow into their smaller branches is observed.

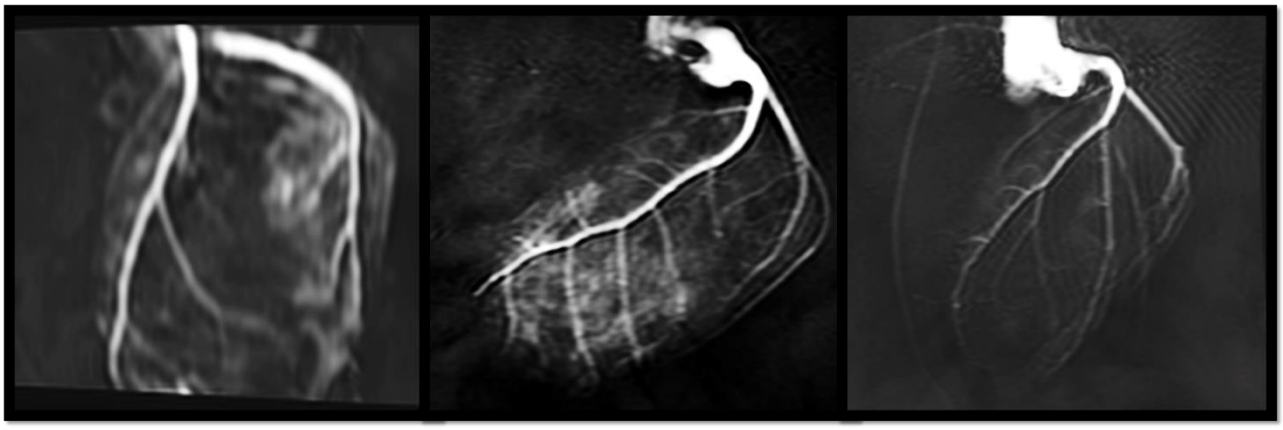

Figure 27: Coronary angiographies after hyperpolarized water injections in three different animals. Images 5 s after injection of sample.

The apparent SNR, aSNR, defined as the ratio between the mean signal intensity in the vessel and the standard deviation of a background ROI, in left main stem was 269±169. The coronary sharpness, defined as the mean of the inverse distances between the 20% and 80% point on both sides of the 1D cross-section profile of a coronary segment in the proximal LAD, was 0.31±0.086 mm^{-1}.

A dynamic time series is shown in Figure 28. Since no cardiac triggering was applied, motion artefacts were observed in some time frames (Frames 3, 4, 6 and 7, in particular). Frame 1 shows the first detection of hyperpolarized signal. The signal rapidly increases in the injection site, the proximal LAD, in Frame 2. The signal distributes throughout the main arteries, and later throughout the arterial branches. From Frame 5, the extravasation in the myocardial tissue appears. No hyperpolarized signal was observed after 14 s.

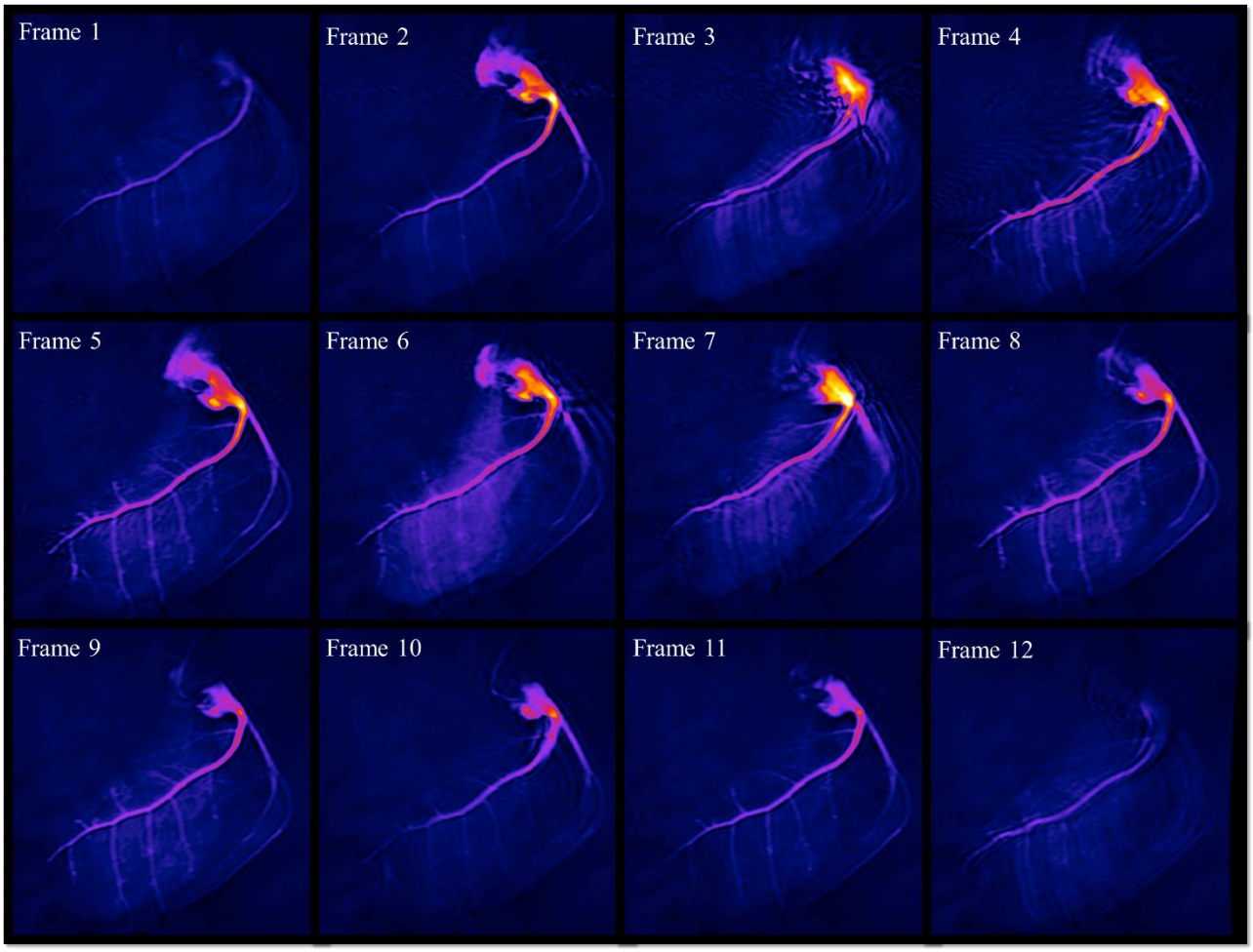

Figure 28: Time series of consecutive images acquired every second from injection of sample. Major and minor vessels of the coronary tree can easily be identified. The frames are scaled collectively, with blue indicating no signal and yellow indication maximum signal. The animal of this time series is the center pane of Figure 27.

The signal in the injection site, the main arteries and the distal branches all have different time delays from injection to signal increase and subsequent signal decrease due to relaxation and washout. The temporal profiles of average signal in these sites are shown in Figure 29. The rapid increase in the injection site (the proximal LAD) and the later increase in the smaller branches describe the perfusion into the coronary vasculature.

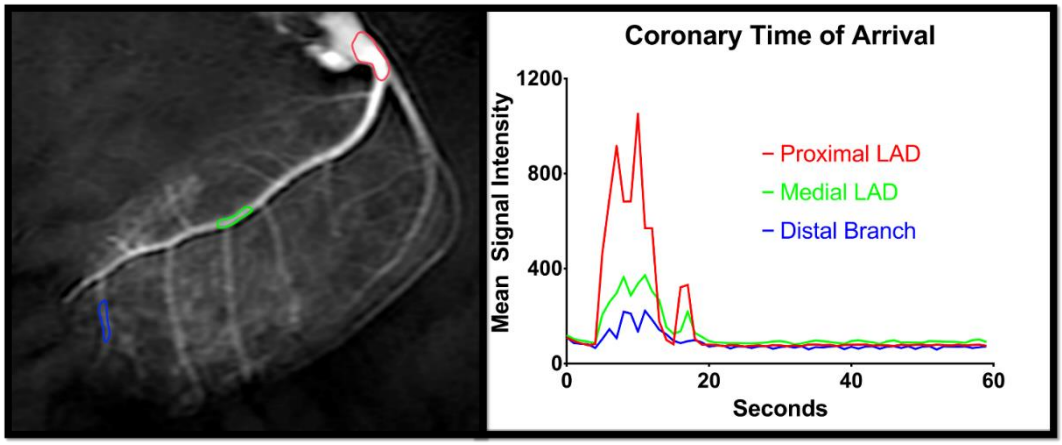

Figure 29: Time of arrival of hyperpolarized water at proximal LAD, medial LAD and at a distal branch of LAD.

5.5.4 Discussion

The method for MR angiography using hyperpolarized water demonstrated in **Study IV** translated successfully into coronary angiography. The method demonstrated high resolution dynamic MR coronary angiography for the first time.

The method was robust; three consecutive injections of hyperpolarized water in an animal yielded reproducible results. The method is believed to be translational into clinical practice, because the samples can be produced in a sterile environment, with the safety profile discussed in Chapter 4. The safety of the formulation should be investigated thoroughly before human studies. The main drawback of the method is the invasive nature of the coronary catheterization. However, in combination with other examinations and treatments that requires catheterization, such as angioplasty and stent placement, the method may be feasible.

The high temporal resolution provided detailed information about the perfusion of the vasculature and tissue. However, the lab did not facilitate ECG triggering, and hence movements of the heart, and artefacts were observed in several time frames. In a setup of ECG triggered imaging and respiratory control, the method is believed to provide data suitable for automated perfusion analysis, which could be of great value for CAD treatment assessment.

Several optimizations are believed to potentially enhance the image quality further. The 5% proton polarization was adequate for 0.55 mm^2 isotropic resolution with aSNR in the left main stem of 269±169, superior to value in the literature of 25.3, obtained in the right coronary artery

of humans with Gd enhanced MRI [31]. The large standard deviation is believed to be a result of the different positioning of the 3 animals.

By enhancing the solid-state polarization, optimizing the dissolution and extending the relaxation time, a potential 50% polarization could improve the image quality dramatically. In combination with a clinical setup suited for cardiac images, the method could provide angiographies matching the resolution of CTA, and cardiac perfusion analysis with the advantages of direct water perfusion measurement and avoidance of ionizing radiation and toxic contrast agents.

5.5.5 Conclusion

The main finding of this study was the feasibility of coronary MR angiography using hyperpolarized water. Images were acquired in less than 1 s, allowing for cardiac triggering, and providing detailed information about the extravasation into the myocardial tissue. It was demonstrated, that the aSNR, and with that, image quality, was superior to that of other coronary MR angiographic methods. The method can be improved in several ways, to provide state-of-the-art perfusion data of the myocardium.

6 Discussion

This chapter discusses the main findings and their relevance, and recommendations for future research is presented. The largest obstacles for clinical translation are discussed. The main purpose of this project was to investigate if hyperpolarized water could be applied as an MRI contrast agent for coronary angiography and perfusion measurements in large animal models.

The major challenge is the fast relaxation of the polarization of the water protons, which has led to a skepticism for the application of hyperpolarized water for angiography and perfusion imaging [107]. Overhauser enhanced water provides low magnetization and short T_1 [107]. Water polarization by parahydrogen has been proposed [108], but without success so far. The advantage of d-DNP, and the method proposed in this thesis, is the dilution of the protons in D_2O to achieve a long T_1 before injection, and the high polarization achievable by DNP.

The solid-state ^1H polarization obtained in this study was 70% in good agreement with literature under similar experimental conditions (6.7 T and 1 K). Higher proton polarization has been reported for similar polarizer conditions, up to 90%, but for samples with lower proton density to reduce the heat capacity of the proton spin bath. It could be investigated if lower proton density, e.g. by deuteration of the glycerol (glycerol-d_5 or glycerol-d_8) would lead to higher polarization. However, further reduction of the proton density would increase the required sample size beyond practical for a clinical/large animal dose. In this thesis, a 1 mL sample was polarized to produce 15 mL of hyperpolarized solution. The fluid path would in principle accommodate up to 2 mL of solid sample, but further than that would require major hardware modifications.

The DNP build-up time constant was typically more than 30 min, and limited by the available microwave power. However, final polarization was fully saturated, and microwave frequency modulation was found to be very efficient in overcoming the inhomogeneous broadening of the nitroxide EPR line at high magnetic field. Microwave frequency modulation is particular preferable to increase electron-electron dipolar couplings in this context, compared to increasing the nitroxide concentration (leading to relaxation losses in dissolution and liquid state). Reduction of the microwave attenuation of the waveguide transmission system or exchanging the microwave source with a higher power source is feasible, and could improve the throughput of d-DNP by shortening the build-up time. It was found that degassing the solid sample leads to

significant improvement of the DNP efficiency. This is consistent with literature, and is explained by the increased relaxation times of the nitroxide when molecular oxygen is removed. The shortening of the nitroxide relaxation times by oxygen cannot be overcome by increased microwave power. It was verified that the degassing did not lead to an increase of the T_1 of the protons after dissolution, i.e. it is not an effect of insufficient degassing of the final product. The degassing of the solid sample was omitted in preclinical studies with the SPINlab due to practical limitations at the hospital site.

There are recent developments within the field of d-DNP that can further advance the method. It has been demonstrated that non-persistent radicals can be created by photo induction of ^{13}C-labelled pyruvic acid [109,110]. UV radicals generated from pyruvic acid in water [109] could be thermally annihilated and radical free solutions could be obtained. In [111], 70% proton polarization in the solid state in water/pyruvic acid 1:1 (v/v) was demonstrated. Liquid state proton polarization has not yet been demonstrated by this method, but it would eliminate the need for radical extraction and hence eliminate the heptane. Lower losses in dissolution and longer T_1 may also be expected with this method since the paramagnetic centers are eliminated in the solid state prior to dissolution. Hirsh et al. demonstrated that a brute force polarized sample (without paramagnetic centers) could conserve polarization during a 10 min. transfer from polarizing site to imaging site by keeping it in the solid state and only dissolve immediately before imaging [112]. This may also open up new perspectives for hyperpolarized water, even though the solid-state T_1 of protons should be significantly shorter than for ^{13}C. Finally, parawater has been a “hot topic” in magnetic resonance for the past many years [108]. So far, no one has succeeded, but a long-lived singlet state would open up for intravenous administration and more reliable perfusion and angiography. Another, possibly more likely, way of maintaining the magnetization for longer, would be to encapsulate the hyperpolarized water in liposomes or similar, to prevent the dilution with blood and shortening of T_1.

The fluorinated solvent proposed to accelerate the dissolution process resulted in a large enhancement of the liquid state polarization, but failed the translation into preclinical use. The reason was that the heating time could not be controlled manually on the SPINlab, and syringes burst from the extensive exposure to the solvent under high temperature and pressure. The dissolution acceleration was omitted from the protocol for imaging experiments, and a substantial

part of polarization was lost when the fluorinated solvent was compensated by increasing the amount of D_2O in the dissolution syringe. Other methods for dissolution acceleration could be desirable for further enhancement of the polarization. In particular, if even larger samples are used. The two-phase extraction system was optimized to ensure almost complete extraction of the nitroxide. However, it may be further improved by increasing the heptane volume, which would require heating of the heptane to retain long relaxation time. An alternative for extraction of the radical, could be implementation of an inline filter (solid-phase extraction) in the exit tube, or acidic precipitation for radicals such as 4-carboxy-TEMPO. The solid-phase-extraction was not attempted, and could lead to significant proton relaxation. It is, however, recommended to investigate this method in further studies. Precipitation of the nitroxide could be challenging, since even the protonated 4-carboxy-TEMPO has water solubility. The two-phase extraction could be optimized by an automated stirring system, which could also eliminate the variability of manual shaking as well as reduce the transfer time.

An automated injection system could control the injection rate of the hyperpolarized product into the animal. This could also ensure that no heptane droplets were injected (by proper quality control), which would be critical for clinical translation. The delivery to the patient has to be as fast and efficient as possible. In this thesis, it is shown that a manual transfer can be done in approx. 25 s. This is longer than the approx. 20 s T_1 of the formulation, and accounts for most of the loss from solid state (P = 70%) to time of measurement in the liquid state (P = 13%). An automated transfer and injection system may potentially reduce the transfer time to 10 s as shown in [65], and thereby increase the polarization by a factor two.

In this project, it was demonstrated that the technique can be applied for perfusion measurements in the pig kidney, and that the obtained perfusion values are in agreement with existing literature based on DCE-MRI. This demonstrates that despite the short T_1 of the hyperpolarized proton signal, reliable perfusion values can be calculated by standard dynamic contrast enhanced models. Furthermore, it was demonstrated that the dynamic coronary MR angiography time series could be acquired using hyperpolarized water; something that that no other method has provided. The 5% proton polarization was adequate for 0.55 mm^2 in plane resolution with aSNR in the left main stem of 269, superior to reported clinical numbers of typically 25 in the right coronary artery with Gd enhanced MRI. Although other works have

demonstrated that hyperpolarized water could be applied for angiography in rats [78,113], the technique has here been translated into a clinical setup, producing large sample volumes in clinical polarizers for large animal imaging. Some artefacts and tissue movement were observed in the coronary angiography time series. Implementation of cardiac and respiratory triggering could eliminate these and is straight forward, and thus may enable perfusion measurements of the cardiac tissue as well as higher quality angiograms. Optimally, this would be in a new, state-of-the-art clinical MRI setup suited for cardiac imaging, including an MRI system with cardiac package, suitable heart array coils, and optimized sequences for 3D coverage of the heart.

The method was also tested for cerebral angiography in the pig [114]. Although great established techniques for cerebral angiography already exist [115], the direct perfusion measurement from hyperpolarized water may offer new insight into cerebral cardiovascular disease and its diagnosis. Since water crosses readily the blood-brain-barrier (BBB), it is an "ideal" contrast agent for investigating changes in the permeability of the BBB and water dynamics, e.g. in patients after a stroke.

Catheterization of the coronary arteries is an invasive technique that is only used in patients with severe cardiovascular disease. However, as previously mentioned, the annual number of arterial catheterizations amounts to millions worldwide. A major step forward would be if new methods of hyperpolarization could provide higher polarization and longer relaxation time, which opens for intravenous injection, without the risk of occluding the coronary vessels or other morbidity associated with catheterization.

With the fluid path filling method presented in **Study I**, a sterile contrast agent can be provided using the SPINlab technology. This will enable human studies if sufficient safety profile can be documented for the formulation. A more controlled radical extraction method than the manual separatory funnel shaking can provide more efficient and reproducible extraction, as well as validation of a heptane free, injectable sample suitable for humans.

The term *Hyperpolarized water* may be misleading. The 0.5 mL H_2O sample is dissolved in 16 mL D_2O. The protons and deuterons exchange rapidly, and will reach an equilibrium distribution long before injection. Assuming a statistical distribution, and ignoring the exchangeable protons of the glycerol, the injected sample will be composed of 0.1% H_2O, 5.9% HDO and 94% D_2O. The final

low radical concentration and the amount of deuterium are of some concern for human usage [116]. However, based on the existing literature safety data, the 0.5 g deuterium per kg body weight used in the pig experiments is not far from the typical 0.2 g/kg dose, given with the water double labelling method. In the studies presented here, multiple injections were given in the same animal with no observed adverse events. The toxicology of the formulation should be investigated carefully before clinical research can be initiated. However, it is our opinion that further development of the method will lead to significant changes to the formulation. Thus, formal safety studies would be premature at this stage.

7 Conclusion

In this thesis work, it has been demonstrated that hyperpolarized water can be applied for coronary angiography in a large animal model, and shows potential for myocardial perfusion measurements.

A technique for preparation and hyperpolarization of large volumes of water was presented and optimized. Solid-state polarization >70% was achieved with frequency modulated microwaves, and a fluid path was used for efficient dissolution to reach a signal enhancement of 4,000 times above thermal equilibrium, corresponding to a liquid state polarization of 13%, with T_1 of 16 s. A radical extraction system was designed, demonstrating removal of 97% of the nitroxide used for DNP. The properties of the sample were suitable for preclinical experiments, although it is believed that they could be further optimized to achieve even higher liquid state polarization.

The hyperpolarization method was implemented in a preclinical setup based on the SPINlab technology. This, in principle, allows clinical translation of the method. Liquid state polarization of 5.3% with T_1 of 24 s was obtained. The lower polarization in these experiments was due to omitting the degassing of the solid sample, and the less efficient dissolution without the fluorinated solvent.

First, renal angiography and perfusion was demonstrated. It was concluded that high resolution, 0.55 mm isotropic, was obtainable, and that the image time series could be applied to derive perfusion measurements in agreement with values reported in the literature.

The central result of the project was the realization of dynamic coronary MR angiography in large animals, something that has not been achieved before. The images are considered to have diagnostic quality, and the dynamics in the time series is believed to be suitable for perfusion measurements, when obstacles such as cardiac triggering can be realized.

The results may impact the field of CAD diagnosis and treatment assessment, as it potentially provides complementary parts to a full MR cardiac package, where both pre- and post-surgical examinations can be achieved with high accuracy and low safety profile.

A novel method for filling of fluid paths for hyperpolarized samples was developed and tested. A filling tube inserted through the inner tube enabled reuse of the fluid path, and facilitated

reproducible sample sizes and control parameters with standard deviations 3–10 times smaller than the acceptance criteria intervals in clinical studies. The method is useful in experiments using the fluid path technology, and was an important element in the later preclinical studies.

Bibliography

[1] World Health Organization, Cardiovascular Diseases Fact Sheet, (2016). http://www.who.int/mediacentre/factsheets/fs317/en/ (accessed November 14, 2016).

[2] M.J. Albers, R. Bok, A.P. Chen, C.H. Cunningham, M.L. Zierhut, V.Y. Zhang, S.J. Kohler, J. Tropp, R.E. Hurd, Y.F. Yen, S.J. Nelson, D.B. Vigneron, J. Kurhanewicz, Hyperpolarized 13C lactate, pyruvate, and alanine: Noninvasive biomarkers for prostate cancer detection and grading, Cancer Res. 68 (2008) 8607–8615. doi:10.1158/0008-5472.CAN-08-0749.

[3] S.J. Nelson, J. Kurhanewicz, D.B. Vigneron, P.E.Z. Larson, A.L. Harzstark, M. Ferrone, M. Van Criekinge, J.W. Chang, R. Bok, I. Park, G. Reed, L. Carvajal, E.J. Small, P. Munster, V.K. Weinberg, J.H. Ardenkjaer-larsen, A.P. Chen, R.E. Hurd, L. Odegardstuen, F.J. Robb, J. Tropp, J. a Murray, Metabolic Imaging of Patients with Prostate Cancer Using Hyperpolarized [1- 13 C]Pyruvate, Sci. Transl. Med. 5 (2013) 198ra108. doi:10.1126/scitranslmed.3006070.

[4] C.H. Cunningham, J.Y. Lau, A.P. Chen, B.J. Geraghty, W.J. Perks, I. Roifman, G.A. Wright, K.A. Connelly, Hyperpolarized 13 C Metabolic MRI of the Human Heart: Initial Experience, Circ. Res. In press (2016). doi:10.1161/CIRCRESAHA.116.309769.

[5] A. Berrington de González, M. Mahesh, Projected Cancer Risks From Computed Tomographic Scans Performed in the United States in 2007, Arch Intern Med. 169 (2009) 2071–7. doi:10.1001/archinternmed.2009.440.

[6] A.S. Go, D. Mozaffarian, V.L. Roger, E.J. Benjamin, J.D. Berry, M.J. Blaha, S. Dai, E.S. Ford, C.S. Fox, S. Franco, H.J. Fullerton, C. Gillespie, S.M. Hailpern, J.A. Heit, V.J. Howard, M.D. Huffman, S.E. Judd, B.M. Kissela, S.J. Kittner, D.T. Lackland, J.H. Lichtman, L.D. Lisabeth, R.H. Mackey, D.J. Magid, G.M. Marcus, A. Marelli, D.B. Matchar, D.K. McGuire, E.R. Mohler, C.S. Moy, M.E. Mussolino, R.W. Neumar, G. Nichol, D.K. Pandey, N.P. Paynter, M.J. Reeves, P.D. Sorlie, J. Stein, A. Towfighi, T.N. Turan, S.S. Virani, N.D. Wong, D. Woo, M.B. Turner, Heart Disease and Stroke Statistics--2014 Update: A Report From the American Heart Association, 2014. doi:10.1161/01.cir.0000441139.02102.80.

[7] U. Hoffmann, M. Ferencik, R.C. Cury, A.J. Pena, Coronary CT Angiography, J. Nucl. Med. 47 (2006) 797–806. doi:10.1148/radiol.2441052145.

[8] K.C. Leung, C.J. Martin, Effective doses for coronary angiography, Br. J. Radiol. 69 (1996) 426–431.

[9] K. Vijayalakshmi, D. Kelly, C.-L. Chapple, D. Williams, R. Wright, M.J. Stewart, J. a Hall, A. Sutton, A.

Davies, J. Haywood, M. a de Belder, Cardiac catheterisation: radiation doses and lifetime risk of malignancy., Heart. 93 (2007) 370–371. doi:10.1136/hrt.2006.098731.

[10] A.J. Einstein, K.W. Moser, R.C. Thompson, M.D. Cerqueira, M.J. Henzlova, Radiation dose to patients from cardiac diagnostic imaging, Circulation. 116 (2007) 1290–1305. doi:10.1161/CIRCULATIONAHA.107.688101.

[11] K.K. Kumamaru, B.E. Hoppel, R.T. Mather, F.J. Rybicki, CT Angiography: Current Technology and Clinical Use, Radiol Clin North Am. 48 (2010) 213–235. doi:10.1016/j.rcl.2010.02.006.CT.

[12] L.W. Goldman, Principles of CT: multislice CT., J. Nucl. Med. Technol. 36 (2008) 57-68-76. doi:10.2967/jnmt.107.044826.

[13] J. Hausleiter, T. Meyer, F. Hermann, M. Hadamitzky, M. Krebs, T.C. Gerber, C. McCollough, S. Martinoff, A. Kastrati, A. Schömig, S. Achenbach, Estimated radiation dose associated with cardiac CT angiography, JAMA. 301 (2009) 500–507. doi:10.1001/jama.2009.54.

[14] S.E. Nissen, J.C. Gurley, C.L. Grines, D.C. Booth, R. Mcclure, M. Berk, C. Fischer, A.N. Demaria, Intravascular Ultrasound Assessment of Lumen Size and Wall Morphology in Normal Subjects and Patients With Coronary Artery Disease, Circulation. 84 (1991) 1087–1099.

[15] P. Schoenhagen, S. Nissen, Understanding coronary artery disease: tomographic imaging with intravascular ultrasound, Heart. 88 (2002) 91–96. doi:10.1136/heart.88.1.91.

[16] G. Montalescot, U. Sechtem, S. Achenbach, ..., 2013 ESC guidelines on the management of stable coronary artery disease, Eur. Heart J. 34 (2013) 2949–3003. doi:10.1093/eurheartj/eht296.

[17] B. a Herzog, J.P. Greenwood, S. Plein, M. Motwani, A. Kidambi, A. Uddin, MR Imaging of Cardiac Tumors and Masses : A Review of Methods, Radiographics. 268 (2013) 26–46. doi:10.1148/radiol.13121239/-/DC1.

[18] S. Srinivasan, D.B. Ennis, Optimal flip angle for high contrast balanced SSFP cardiac cine imaging, Magn. Reson. Med. 73 (2015) 1095–1103. doi:10.1002/mrm.25228.

[19] T. Grobner, Gadolinium – a specific trigger for the development of nephrogenic brosing dermopathy and nephrogenic systemic brosis?, Nephrol Dial Transpl. 21 (2006) 1104–1108. doi:10.1093/ndt/gfk062.

[20] W.A. High, R.A. Ayers, J. Chandler, G. Zito, S.E. Cowper, Gadolinium is detectable within the tissue of patients with nephrogenic systemic fibrosis, J. Am. Acad. Dermatol. 56 (2007) 21–26.

doi:10.1016/j.jaad.2006.10.047.

[21] D.G. Nishimura, Time-of-flight MR angiography, Magn. Reson. Med. 14 (1990) 194–201. doi:10.1002/mrm.1910140206.

[22] T. Reese, D. Bochelen, A. Sauter, N. Beckmann, M. Rudin, Magnetic resonance angiography of the rat cerebrovascular system without the use of contrast agents, NMR Biomed. 12 (1999) 189–196. doi:10.1002/(SICI)1099-1492(199906)12:4<189::AID-NBM557>3.0.CO;2-O.

[23] M. Miyazaki, M. Akahane, Non-contrast enhanced MR angiography: Established techniques, J. Magn. Reson. Imaging. 35 (2012) 1–19. doi:10.1002/jmri.22789.

[24] S. Kinner, S. Maderwald, N. Parohl, J. Albert, C. Corot, P. Robert, J. Barkhausen, F.M. Vogt, Contrast-enhanced magnetic resonance angiography in rabbits: evaluation of the gadolinium-based agent p846 and the iron-based blood pool agent p904 in comparison with gadoterate meglumine., Invest. Radiol. 46 (2011) 524–529. doi:10.1097/RLI.0b013e31821ae21f.

[25] S.J. Riederer, C.R. Haider, E. a. Borisch, P.T. Weavers, P.M. Young, Recent advances in 3D time-resolved contrast-enhanced MR angiography, J. Magn. Reson. Imaging. 42 (2015) 3–22. doi:10.1002/jmri.24880.

[26] N.O. Addy, R.R. Ingle, H.H. Wu, B.S. Hu, D.G. Nishimura, High-resolution variable-density 3D cones coronary MRA, Magn. Reson. Med. 74 (2015) 614–621. doi:10.1002/mrm.25803.

[27] A.M. Gharib, K.Z. Abd-Elmoniem, V.B. Ho, E. Födi, D. a Herzka, J. Ohayon, M. Stuber, R.I. Pettigrew, The Feasibility of 350 µm Spatial Resolution Coronary Magnetic Resonance Angiography at 3 T in Humans., Invest. Radiol. 47 (2012) 339–45. doi:10.1097/RLI.0b013e3182479ec4.

[28] S. Kato, K. Kitagawa, N. Ishida, M. Ishida, M. Nagata, Y. Ichikawa, K. Katahira, Y. Matsumoto, K. Seo, R. Ochiai, Y. Kobayashi, H. Sakuma, Assessment of Coronary Artery Disease Using Magnetic Resonance Coronary Angiography, J. Am. Coll. Cardiol. 56 (2010) 983–991. doi:10.1016/j.jacc.2010.01.071.

[29] D. Piccini, P. Monney, C. Sierro, T. Rutz, A. Littmann, Respiratory Self-navigated Postcontrast Whole-Heart Coronary MR Angiography: Initial Experience in Patients, Radiology. 270 (2014) 378–386.

[30] M. Henningsson, T. Hussain, M.S. Vieira, G.F. Greil, J. Smink, G. v. Ensbergen, G. Beck, R.M. Botnar, Whole-heart coronary MR angiography using image-based navigation for the detection of coronary anomalies in adult patients with congenital heart disease, J. Magn. Reson. Imaging. 43 (2016) 947–955. doi:10.1002/jmri.25058.

[31] M.A. Ahlman, F.S. Raman, J. Pang, F. Zemrak, V. Sandfort, S.R. Penzak, Z. Fan, S. Liu, D. Li, D.A. Bluemke, Part 2 – Coronary angiography with gadofosveset trisodium: a prospective intra-subject comparison for dose optimization for 100 % efficiency imaging, BMC Cardiovasc. Disord. 16 (2016) 58. doi:10.1186/s12872-015-0152-8.

[32] C.E. Rochitte, R.T. George, M.Y. Chen, A. Arbab-Zadeh, M. Dewey, J.M. Miller, H. Niinuma, K. Yoshioka, K. Kitagawa, S. Nakamori, R. Laham, A.L. Vavere, R.J. Cerci, V.C. Mehra, C. Nomura, K.F. Kofoed, M. Jinzaki, S. Kuribayashi, A. de Roos, M. Laule, S.Y. Tan, J. Hoe, N. Paul, F.J. Rybicki, J.A. Brinker, A.E. Arai, C. Cox, M.E. Clouse, M.F. Di Carli, J.A.C. Lima, Computed tomography angiography and perfusion to assess coronary artery stenosis causing perfusion defects by single photon emission computed tomography: the CORE320 study, Eur. Heart J. 35 (2014) 1120–1130. doi:10.1093/eurheartj/eht488.

[33] R.T. George, A. Arbab-zadeh, R.J. Cerci, A.L. Vavere, M. Dewey, C.E. Rochitte, A.E. Arai, N. Paul, J. Frank, A.C. Lardo, M.E. Clouse, J. a C. Lima, Diagnostic Performance of Combined Noninvasive Coronary Angiography and Myocardial Perfusion Imaging Using 320- MDCT: The CT Angiography and Perfusion Methods of the CORE320 Multicenter Multinational Diagnostic Study, Am J Roentgenol. 197 (2011) 829–837. doi:10.2214/AJR.10.5689.

[34] H. Sakuma, Coronary CT versus MR angiography: the role of MR angiography., Radiology. 258 (2011) 340–349. doi:10.1148/radiol.10100116.

[35] C.M. Kramer, J. Narula, Atherosclerotic Plaque Imaging: The Last Frontier for Cardiac Magnetic Resonance, JACC Cardiovasc. Imaging. 2 (2009) 916–918. doi:10.1016/j.jcmg.2009.05.002.

[36] W.I. Tseng, M.M. Su, Y.E. Tseng, Introduction to Cardiovascular Magnetic Resonance: Technical Principles and Clinical Applications, (2016) 129–144. doi:10.6515/ACS20150616A.

[37] M. Essig, M.S. Shiroishi, T.B. Nguyen, M. Saake, J.P. M., D. Enterline, N. Anzalone, A. Dörfler, À. Rovira, M. Wintermark, M. Law, Perfusion MRI: The Five Most Frequently Asked Technical Questions, AJR Am J Roentgenol. 200 (2013) 24–34. doi:10.2214/AJR.12.9543.Perfusion.

[38] T. Techasith, R.C. Cury, Stress myocardial ct perfusion: An update and future perspective, JACC Cardiovasc. Imaging. 4 (2011) 905–916. doi:10.1016/j.jcmg.2011.04.017.

[39] J. Singh, A. Daftary, Iodinated contrast media and their adverse reactions., J. Nucl. Med. Technol. 36 (2008) 69-74-77. doi:10.2967/jnmt.107.047621.

[40] A. Abidov, A. Rozanski, L. Shaw, J. Min, R. Hachamovitch, X. Kang, D. Berman, G. Germano, S. Hayes,

J. Friedman, L. Thomson, P. Slomka, SPECT/PET myocardial perfusion imaging versus coronary CT angiography in patients with known or suspected CAD, Q. J. Nucl. Med. Mol. Imaging. 54 (2010) 177–200.

[41] A. Flotats, P.E. Bravo, K. Fukushima, M.A. Chaudhry, J. Merrill, F.M. Bengel, 82Rb PET myocardial perfusion imaging is superior to 99mTc-labelled agent SPECT in patients with known or suspected coronary artery disease, Eur. J. Nucl. Med. Mol. Imaging. 39 (2012) 1233–1239. doi:10.1007/s00259-012-2140-x.

[42] P. Herscovitch, J. Markham, M.E. Raichle, Brain Blood Flow Measured with Intravenous H215O.: I. Theory and Error Analysis, J Nucl Med. 24 (1983) 782–789.

[43] M.E. Raichle, W.R.W. Martin, P. Herscovltch, M.A. Mintun, J. Markham, Brain Blood Flow Measured with Intravenous H215O.: II. Implementation and Validation, J Nucl Med. 24 (1983).

[44] J. Maddahi, R.R.S. Packard, Cardiac PET perfusion tracers: Current status and future directions, Semin. Nucl. Med. 44 (2014) 333–343. doi:10.1053/j.semnuclmed.2014.06.011.

[45] X.-H. Zhu, Y. Zhang, H. Wiesner, K. Ugurbil, W. Chen, In vivo measurement of CBF using 17 O NMR signal of metabolically produced H217 O as a perfusion tracer, Magn. Reson. Med. 70 (2013) 309–314. doi:10.1002/mrm.24469.

[46] M. Levitt, Spin Dynamics, 2nd ed., John Wiley & Sons, 2008.

[47] J.H. Ardenkjaer-Larsen, B. Fridlund, A. Gram, G. Hansson, L. Hansson, M.H. Lerche, R. Servin, M. Thaning, K. Golman, Increase in signal-to-noise ratio of > 10,000 times in liquid-state NMR., Proc. Natl. Acad. Sci. U. S. A. 100 (2003) 10158–10163. doi:10.1073/pnas.1733835100.

[48] A.W. Overhauser, Polarization of Nuclei in Metals, Phys. Rev. 92 (1953) 411–415.

[49] T.R. Carver, C.P. Slichter, Polarization of nuclear spins in metals, Phys. Rev. 92 (1953) 212–213. doi:10.1103/PhysRev.92.212.2.

[50] T.R. Carver, C.P. Slichter, Experimental verification of the overhauser nuclear polarization effect, Phys. Rev. 102 (1956) 975–980. doi:10.1103/PhysRev.102.975.

[51] A. Abragam, Overhauser effect in nonmetals, Phys. Rev. 98 (1955) 1729–1735. doi:10.1103/PhysRev.98.1729.

[52] C.D. Jeffries, Polarization of nuclei by resonance saturation in paramagnetic crystals, Phys. Rev. 106 (1957) 164–165. doi:10.1103/PhysRev.106.164.

[53] W.T. Wenckebach, The solid effect, Appl. Magn. Reson. 34 (2008) 227–235. doi:10.1007/s00723-008-0121-9.

[54] A. Abragam, M. Goldman, Principles of dynamic nuclear polarisation, Reports Prog. Phys. 41 (1978) 395–467. doi:10.1088/0034-4885/41/3/002.

[55] T. Wenckebach, Essentials of Dynamic Nuclear Polarization, Spindrift Publications, 2016.

[56] V.A. Atsarkin, A. V. Kessenikh, Dynamic Nuclear Polarization in Solids: The Birth and Development of the Many-Particle Concept, Appl. Magn. Reson. 43 (2012) 7–19. doi:10.1007/s00723-012-0328-7.

[57] K.R. Thurber, W.-M. Yau, R. Tycko, Low-temperature dynamic nuclear polarization at 9.4 T with a 30 mW microwave source., J. Magn. Reson. 204 (2010) 303–13. doi:10.1016/j.jmr.2010.03.016.

[58] Y. Hovav, A. Feintuch, S. Vega, D. Goldfarb, Dynamic nuclear polarization using frequency modulation at 3.34 T, J. Magn. Reson. 238 (2014) 94–105. doi:10.1016/j.jmr.2013.10.025.

[59] A. Bornet, J. Milani, B. Vuichoud, A.J. Perez Linde, G. Bodenhausen, S. Jannin, Microwave Frequency Modulation to Enhance Dissolution Dynamic Nuclear Polarization, Chem. Phys. Lett. 602 (2014) 63–67. doi:10.1016/j.cplett.2014.04.013.

[60] S. Jannin, A. Bornet, R. Melzi, G. Bodenhausen, High field dynamic nuclear polarization at 6.7T: Carbon-13 polarization above 70% within 20min, Chem. Phys. Lett. 549 (2012) 99–102. doi:10.1016/j.cplett.2012.08.017.

[61] G. Olsen, E. Markhasin, O. Szekely, C. Bretschneider, L. Frydman, Optimizing water hyperpolarization and dissolution for sensitivity-enhanced 2D biomolecular NMR, J. Magn. Reson. 264 (2016) 49–58. doi:10.1016/j.jmr.2016.01.005.

[62] B. Lama, J.H.P. Collins, D. Downes, A.N. Smith, J.R. Long, Expeditious dissolution dynamic nuclear polarization without glassing agents, NMR Biomed. 29 (2016) 226–231. doi:10.1002/nbm.3473.

[63] J. Wolber, F. Ellner, B. Fridlund, a. Gram, H. Jóhannesson, G. Hansson, L.H. Hansson, M.H. Lerche, S. Månsson, R. Servin, M. Thaning, K. Golman, J.H. Ardenkjær-Larsen, Generating highly polarized nuclear spins in solution using dynamic nuclear polarization, Nucl. Instruments Methods Phys. Res. Sect. A Accel. Spectrometers, Detect. Assoc. Equip. 526 (2004) 173–181. doi:10.1016/j.nima.2004.03.171.

[64] S. Bowen, C. Hilty, Time-resolved dynamic nuclear polarization enhanced NMR spectroscopy, Angew. Chemie - Int. Ed. 47 (2008) 5235–5237. doi:10.1002/anie.200801492.

[65] T. Cheng, M. Mishkovsky, J. a M. Bastiaansen, O. Ouari, P. Hautle, P. Tordo, B. Van Den Brandt, A. Comment, Automated transfer and injection of hyperpolarized molecules with polarization measurement prior to in vivo NMR, NMR Biomed. 26 (2013) 1582–1588. doi:10.1002/nbm.2993.

[66] H. Shang, T. Skloss, C. von Morze, L. Carvajal, M. Van Criekinge, E. Milshteyn, P.E.Z. Larson, R.E. Hurd, D.B. Vigneron, Handheld electromagnet carrier for transfer of hyperpolarized carbon-13 samples, Magn. Reson. Med. 922 (2015) 917–922. doi:10.1002/mrm.25657.

[67] J. Milani, B. Vuichoud, A. Bornet, P. Miéville, R. Mottier, S. Jannin, G. Bodenhausen, A magnetic tunnel to shelter hyperpolarized fluids, Rev. Sci. Instrum. 86 (2015). doi:10.1063/1.4908196.

[68] K. Golman, O. Axelsson, H. Jóhannesson, S. Månsson, C. Olofsson, J.S. Petersson, Parahydrogen-induced polarization in imaging: Subsecond 13C angiography, Magn. Reson. Med. 46 (2001) 1–5. doi:10.1002/mrm.1152.

[69] J. Svensson, S. Månsson, E. Johansson, J.S. Petersson, L.E. Olsson, Hyperpolarized 13C MR angiography using trueFISP, Magn. Reson. Med. 50 (2003) 256–262. doi:10.1002/mrm.10530.

[70] L.E. Olsson, C.M. Chai, O. Axelsson, M. Karlsson, K. Golman, J.S. Petersson, MR coronary angiography in pigs with intraarterial injections of a hyperpolarized 13C substance, Magn. Reson. Med. 55 (2006) 731–737. doi:10.1002/mrm.20847.

[71] E. Johansson, S. Månsson, R. Wirestam, J. Svensson, J.S. Petersson, K. Golman, F. Ståhlberg, Cerebral Perfusion Assessment by Bolus Tracking Using Hyperpolarized 13C, Magn. Reson. Med. 51 (2004) 464–472. doi:10.1002/mrm.20013.

[72] A.K. Grant, E. Vinogradov, X. Wang, R.E. Lenkinski, D.C. Alsop, Perfusion imaging with a freely diffusible hyperpolarized contrast agent, Magn. Reson. Med. 66 (2011) 746–755. doi:10.1002/mrm.22860.

[73] C. Von Morze, P.E.Z. Larson, S. Hu, H. a I. Yoshihara, R. a. Bok, A. Goga, J.H. Ardenkjaer-Larsen, D.B. Vigneron, Investigating tumor perfusion and metabolism using multiple hyperpolarized 13C compounds: HP001, pyruvate and urea, Magn. Reson. Imaging. 30 (2012) 305–311. doi:10.1016/j.mri.2011.09.026.

[74] I. Park, C. von Morze, J.M. Lupo, J.H. Ardenkjaer-Larsen, A. Kadambi, D.B. Vigneron, S.J. Nelson, Investigating tumor perfusion by hyperpolarized 13C MRI with comparison to conventional gadolinium contrast-enhanced MRI and pathology in orthotopic human GBM xenografts, Magn. Reson. Med. (2016). doi:10.1002/mrm.26155.

[75] A.Z. Lau, J.J. Miller, M.D. Robson, D.J. Tyler, Cardiac perfusion imaging using hyperpolarized 13 c urea using flow sensitizing gradients, Magn. Reson. Med. 75 (2016) 1474–1483. doi:10.1002/mrm.25713.

[76] J.T. Anderson, W. A.; Arnold, Proton Relaxation Times in H2O-D2O Mixtures, Phys. Rev. 101 (1956) 511–512. doi:10.1103/PhysRev.101.511.

[77] H.Y. Simpson, J. H.; Carr, Diffusion and Nuclear Spin Relaxation in Water, Phys. Rev. 111 (1958) 1201–1202. doi:10.1103/PhysRev.111.1201.

[78] J.H. Ardenkjaer-Larsen, C. Laustsen, S. Bowen, R. Rizi, Hyperpolarized H2O MR angiography, Magn. Reson. Med. 71 (2014) 50–56. doi:10.1002/mrm.25033.

[79] N. Nestle, T. Baumann, R. Niessner, Oxygen determination in oxygen-supersaturated drinking waters by NMR relaxometry, Water Res. 37 (2003) 3361–3366. doi:10.1016/S0043-1354(03)00211-2.

[80] P. Höfer, G. Parigi, C. Luchinat, P. Carl, G. Guthausen, M. Reese, T. Carlomagno, C. Griesinger, M. Bennati, Field dependent dynamic nuclear polarization with radicals in aqueous solution, J. Am. Chem. Soc. 130 (2008) 3254–3255. doi:10.1021/ja0783207.

[81] P. Miéville, P. Ahuja, R. Sarkar, S. Jannin, P.R. Vasos, S. Gerber-Lemaire, M. Mishkovsky, A. Comment, R. Gruetter, O. Ouari, P. Tordo, G. Bodenhausen, Scavenging free radicals to preserve enhancement and extend relaxation times in NMR using dynamic nuclear polarization, Angew. Chemie - Int. Ed. 49 (2010) 6182–6185. doi:10.1002/anie.201000934.

[82] T. Harris, O. Szekely, L. Frydman, On the potential of Hyperpolarized Water in Biomolecular NMR Studies, J. Phys. Chem. B. 118 (2014) 3281–3290. doi:10.1021/jp4102916.

[83] X. Zhang, E.T. Petersen, E. Ghariq, J.B. De Vis, A.G. Webb, W.M. Teeuwisse, J. Hendrikse, M.J.P. Van Osch, In vivo blood T1 measurements at 1.5 T, 3 T, and 7 T, Magn. Reson. Med. 70 (2013) 1082–1086. doi:10.1002/mrm.24550.

[84] Q. Chappuis, J. Milani, B. Vuichoud, A. Bornet, A.D. Gossert, G. Bodenhausen, S. Jannin, Hyperpolarized Water to Study Protein–Ligand Interactions, J. Phys. Chem. Lett. 6 (2015) 1674–1678. doi:10.1021/acs.jpclett.5b00403.

[85] J. Besjakov, L. Baath, A.N. Oksendal, T. Almen, Reduced Risk of Ventricular Fibrillation by Balancing Sodium, Calcium, Potassium and Magnesium Added to Nonionic Contrast Media: An Investigation in the Isolated Rabbit Heart, Acta Radiol. 34 (1993) 246–251. doi:10.1177/028418519303400309.

[86] NIH, TOXNET, Toxicology Data Network, U.S. Natl. Libr. Med. (n.d.). https://toxnet.nlm.nih.gov/cgi-bin/sis/search/a?dbs+hsdb:@term+@DOCNO+90 (accessed November 21, 2016).

[87] J. Emsley, The Elements, 3rd ed., Clarendon Press, Oxford, 1998.

[88] D.J. Kushner, a Baker, T.G. Dunstall, Pharmacological uses and perspectives of heavy water and deuterated compounds., Can. J. Physiol. Pharmacol. 77 (1999) 79–88. doi:10.1139/y99-005.

[89] J.F. Thomson, Physiological Effects of D2O in Mammals, Ann. N. Y. Acad. Sci. 84 (1960) 736–744. doi:10.1111/j.1749-6632.1960.tb39105.x.

[90] J.R. Speakman, Doubly Labelled Water: Theory and Practice, Springer US, 1997.

[91] B. Scheer, A. Perel, U.J. Pfeiffer, Clinical review: complications and risk factors of peripheral arterial catheters used for haemodynamic monitoring in anaesthesia and intensive care medicine, Crit Care. 6 (2002) 199–204. doi:10.1186/cc1489.

[92] S. Windecker, B.J. Meyer, T. Bonzel, J. Fabian, G. Heyndrickx, M.C. Morice, V. Mu, F. Piscione, M. Rothman, W. Wijns, M. Van Den Brand, Working Group Report: Interventional cardiology in Europe 1995, 20 (1999) 484–495.

[93] J.H. Ardenkjaer-Larsen, A.M. Leach, N. Clarke, J. Urbahn, D. Anderson, T.W. Skloss, Dynamic nuclear polarization polarizer for sterile use intent, NMR Biomed. 24 (2011) 927–932. doi:10.1002/nbm.1682.

[94] A. Comment, J. Rentsch, F. Kurdzesau, S. Jannin, K. Uffmann, R.B. van Heeswijk, P. Hautle, J.A. Konter, B. van den Brandt, J.J. van der Klink, Producing over 100 ml of highly concentrated hyperpolarized solution by means of dissolution DNP, J. Magn. Reson. 194 (2008) 152–155. doi:10.1016/j.jmr.2008.06.003.

[95] S. Bowen, J.H. Ardenkjaer-Larsen, Enhanced performance large volume dissolution-DNP, J. Magn. Reson. 240 (2014) 90–94. doi:10.1016/j.jmr.2014.01.009.

[96] R. Battino, T.R. Rettich, T. Tominaga, The Solubility of Oxygen and Ozone in Liquids, J. Phys. Chem. Ref. Data. 12 (1983) 163–178. doi:10.1063/1.555680.

[97] Michael G. Costello, R.M. Flynn, J.G. Owens, 3M Company, Fluoroethers and Fluoroaminies, Kirk-Othmer Encyclopedia of Chemical Technology, 5th ed., John Wiley & Sons, 2005. doi:10.1002/0471238961.

[98] Human Anatomy Diagram, The Anatomy of Kidney, With Leslie Samuel, (n.d.). http://anatomy-

bodychart.us/anatomy-of-kidney/anatomy-of-kidney-the-anatomy-of-a-kidney-interactive-biology-with-leslie-samuel/ (accessed November 20, 2016).

[99] K.J. Hansen, M.S. Edwards, T.E. Craven, G.S. Cherr, S.A. Jackson, R.G. Appel, G.L. Burke, R.H. Dean, Prevalence of renovascular disease in the elderly: A population-based study, J. Vasc. Surg. 36 (2002) 443–451. doi:10.1067/mva.2002.127351.

[100] K.L. Wright, G.R. Lee, P. Ehses, M.A. Griswold, V. Gulani, N. Seiberlich, Three-dimensional through-time radial GRAPPA for renal MR angiography, J. Magn. Reson. Imaging. 40 (2014) 864–874. doi:10.1002/jmri.24439.

[101] C. Sebastià, A.D. Sotomayor, B. Paño, R. Salvador, M. Burrel, A. Botey, C. Nicolau, Accuracy of unenhanced magnetic resonance angiography for the assessment of renal artery stenosis, Eur. J. Radiol. Open. 3 (2016) 200–206. doi:10.1016/j.ejro.2016.07.003.

[102] K. Jamerson, W. Henrich, D.M. Reid, D.J. Cohen, A.H. Matsumoto, M. Steffes, M.R. Jaff, M.R. Prince, D. Ph, E.F. Lewis, K.R. Tuttle, J.I. Shapiro, J.H. Rundback, J.M. Massaro, R.B.D. Agostino, Stenting and Medical Therapy for Atherosclerotic Renal-Artery Stenosis, New Engl. J. Med. 370 (2013) 1–10. doi:10.1056/NEJMoa1310753.

[103] S.R. Bergmann, P. Herrero, J. Markham, C.J. Weinheimer, M. Norine, Noninvasive Quantitation of Myocardial Blood Flow in Human Subjects With Oxygen-15 Labeled Water and Positron Emission Tomography, J. Am. Coll. Cardiol. 14 (1989) 639–652. doi:10.1016/0735-1097(89)90105-8.

[104] A.J. de Langen, V.E.M. van den Boogaart, J.T. Marcus, M. Lubberink, Use of H2(15)O-PET and DCE-MRI to measure tumor blood flow., Oncologist. 13 (2008) 631–644. doi:10.1634/theoncologist.2007-0235.

[105] S.O. Schoenberg, J. Rieger, C.H. Weber, H.J. Michaely, T. Waggershauser, C. Ittrich, O. Dietrich, M.F. Reiser, High-Spatial-Resolution MR Angiography of Renal Arteries with Integrated Parallel Acquisitions: Comparison with Digital Subtraction Angiography and US, Radiology. 235 (2005) 687–698.

[106] U.I. Attenberger, J.N. Morelli, S.O. Schoenberg, H.J. Michaely, Assessment of the kidneys: magnetic resonance angiography, perfusion and diffusion., J. Cardiovasc. Magn. Reson. 13 (2011). doi:10.1186/1532-429X-13-70.

[107] P. Mark D. Lingwood, B. Ting Ann Siaw, P. Napapon Sailasuta, M. Osama A. Abulseoud, M. Henry R. Chan, M. Brian D. Ross, P. Pratip Bhattacharya, P. Songi Han, Hyperpolarized Water as an MR

Imaging Contrast Agent: Feasibility of in Vivo Imaging in a Rat Model, Radiology. 265 (2012) 418–425. doi:10.1148/radiol.12111804.

[108] D. Mammoli, N. Salvi, J. Milani, R. Buratto, A. Bornet, A.A. Sehgal, E. Canet, P. Pelupessy, D. Carnevale, S. Jannin, G. Bodenhausen, Challenges of preparing, preserving and detecting para-water in bulk: overcoming proton exchange and other hurdles., Phys. Chem. Chem. Phys. (2015) 26819–26827. doi:10.1039/C5CP03350K.

[109] T.R. Eichhorn, Y. Takado, N. Salameh, A. Capozzi, T. Cheng, J.-N. Hyacinthe, M. Mishkovsky, C. Roussel, A. Comment, Hyperpolarization without persistent radicals for in vivo real-time metabolic imaging., Proc. Natl. Acad. Sci. U.S.A. 110 (2013) 18064–9. doi:10.1073/pnas.1314928110.

[110] A. Capozzi, J.-N. Hyacinthe, T. Cheng, T.R. Eichhorn, G. Boero, C. Roussel, J.J. van der Klink, A. Comment, Photoinduced Nonpersistent Radicals as Polarizing Agents for X-Nuclei Dissolution Dynamic Nuclear Polarization, J. Phys. Chem. C. 119 (2015) 22632–22639. doi:10.1021/acs.jpcc.5b07315.

[111] A. Capozzi, Methods to hyperpolarize nuclear spins via dissolution and sublimation DNP at high magnetic field, École Polytechnique Fédérale de Lausanne, 2016.

[112] M.L. Hirsch, B.A. Smith, M. Mattingly, A.G. Goloshevsky, M. Rosay, J.G. Kempf, Transport and imaging of brute-force 13C hyperpolarization, J. Magn. Reson. 261 (2015) 87–94. doi:10.1016/j.jmr.2015.09.017.

[113] E.R. McCarney, B.D. Armstrong, M.D. Lingwood, S. Han, Hyperpolarized water as an authentic magnetic resonance imaging contrast agent., Proc. Natl. Acad. Sci. U. S. A. 104 (2007) 1754–1759. doi:10.1073/pnas.0610540104.

[114] E.S.S. Hansen, K.W. Lipsø, R. Stilling, C. Laustsen, J.H. Ardenkjær-larsen, Hyperpolarized Water Perfusion in the Porcine Brain – a Pilot Study, in: ISMRM 25st Annu. Meet. Exhib. Submitt. Abstr., Honolulu, USA, 2017.

[115] M.E. MacDonald, R. Frayne, Cerebrovascular MRI: a review of state-of-the-art approaches, methods and techniques, NMR Biomed. 28 (2015) 767–91. doi:10.1002/nbm.3322.

[116] C. Ewy, E. Babcock, J. Ackerman, Deuterium nuclear magnetic resonance spin-imagin of D2O: A potential exogenous MRI label, Magn. Reson. Imaging. 4 (1986) 407–411.

Appendix: Article Collection

The peer reviewed journals papers are presented on the following pages.

Papers I-IV have all been published, although *Paper I* only in an unformatted edition at time of writing. Paper V is a late stage manuscript in preparation for submission.

Paper I

Journal of Magnetic Resonance 272 (2016) 141–146

Journal of Magnetic Resonance

Dissolution Dynamic Nuclear Polarization capability study with fluid path

Ronja M. Malinowski [a], Kasper W. Lipsø [a], Mathilde H. Lerche [a,b], Jan H. Ardenkjær-Larsen [a,c,⇑]

[a] Department of Electrical Engineering, Technical University of Denmark, Kgs. Lyngby, Denmark [b] Albeda Research, Ole Maaloes vej 3, 2200 København N, Denmark [c] GE Healthcare, Denmark

ARTICLE INFO

Article history:
Received 11 August 2016
Revised 20 September 2016
Accepted 21 September 2016
Available online 22 September 2016

Keywords:
Hyperpolarization
Dynamic Nuclear Polarization
Dissolution-DNP
Polarizer

ABSTRACT

Signal enhancement by hyperpolarization is a way of overcoming the low sensitivity in magnetic resonance; MRI in particular. One of the most well-known methods, dissolution Dynamic Nuclear Polarization, has been used clinically in cancer patients. One way of ensuring a low bioburden of the hyperpolarized product is by use of a closed fluid path that constitutes a barrier to contamination. The fluid path can be filled with the pharmaceuticals, i.e. imaging agent and solvents, in a clean room, and then stored or immediately used at the polarizer. In this study, we present a method of filling the fluid path that allows it to be reused. The filling method has been investigated in terms of reproducibility at two extrema, high dose for patient use and low dose for rodent studies, using [1-13C]pyruvate as example. We demonstrate that the filling method allows high reproducibility of six quality control parameters with standard deviations 3–10 times smaller than the acceptance criteria intervals in clinical studies.

1 Introduction

Increase of the NMR signal of molecules by hyperpolarization is a technique, which has many applications in the field of NMR spectroscopy and imaging. The most commonly used method is dissolution-Dynamic Nuclear Polarization (d-DNP) [1], in which the hyperpolarized nuclear spins are transferred from the solid state to the liquid state by a quick dissolution while retaining the nuclear spin polarization.

In this study, the d-DNP technique will be demonstrated by hyperpolarization of pyruvate; being a key intersection in various metabolic pathways, [1-^{13}C]pyruvate is by far the most common molecule for studies with d-DNP [2,3]. It has an advantageously long relaxation time T_1 and high polarization levels can be achieved [4]. Other molecules can be used to probe biological pathways as well; [U-^{13}C;U-^{2}H]glucose [5], [1,4-$^{13}C_2$]fumarate [6], [1-^{13}C]bicarbonate [7] among many other biologically relevant molecules. Similarly, hyperpolarized ^{13}C-labelled biologically inert molecules have been applied for angiography and perfusion studies [8,9]. Besides the bioprobe, an electron paramagnetic agent (EPA) should be present to enable Dynamic Nuclear Polarization. The commonly used EPAs for hyperpolarization are OXO63 [10], BDPA [11] and TEMPO [12]. In this study, AH111501 is used, a stable trityl radical, which precipitates in low pH and can be removed by filtration in the receiver previous to the neutralization step. In 2013, the first clinical study with hyperpolarized [1-^{13}C] pyruvate was published, demonstrating technical feasibility and showing promising results in the phase I trial on patients with prostate cancer [13].

Studies on the performance of the d-DNP process with the aim of demonstrating efficient dissolution, i.e. high concentration and large volume with minimal loss of polarization have been published [14,15]. The principle of dissolution in these studies is the use of a solvent that is heated to an elevated temperature to create a vapor pressure that can drive the flow of solvent past the cold, polarized sample. In the case of aqueous dissolutions, a temperature of 180 C is typically used, creating a vapor pressure of 10 bar. Another principle of dissolution was introduced in 2011 [16], where the concept of a closed fluid path (FP) was presented. The primary objective of the closed FP was to secure a sterile environment throughout the polarization and dissolution process [16]. In terms of dissolution capability, two key principal differences between the FP and previous designs should be noted: (1) the solvent is not driven by the vapor pressure at the given temperature, but by a syringe, (2) the independent inlet and outlet tubes are replaced by two concentric tubes with the inlet as the inner lumen and with return flow in the outer lumen. From the first point follows that solvent temperature can be

* Corresponding author at: Technical University of Denmark, Ørsteds Plads, Bldg. 349, Room 126, 2800 Kgs. Lyngby, Denmark. E-mail address: jhar@elektro.dtu.dk (J.H. Ardenkjær-Larsen).

http://dx.doi.org/10.1016/j.jmr.2016.09.015 1090-7807/ 2016 Elsevier Inc. All rights reserved.

controlled independently of solvent flow rate. In [17] it was shown that a syringe and solvent temperature of 130 C and piston drive pressure of 16 bar was optimal for the dissolution. These conditions are extreme for most plastic materials, but is tolerated by e.g. polyphenylsulfones or polyetheretherketones. The second point is expected to affect dissolution efficiency, but was introduced to facilitate a dynamic seal that allows sample introduction into the cryostat through an air lock without raising the pressure of the 1 K sample space to atmospheric pressure. The FP consists of two major parts: part A, which contains sample and solvent, and allows the hyperpolarized solution to leave the polarizer through an open ended tube, and part B, that consists of a receiver connecting to the exit tube of part A, allowing non-contact quality control of the dissolved product. Part B also includes a filter that removes the EPA in-line with the dissolution process. The EPA precipitates in aqueous solution at acidic pH and can be removed effectively by mechanical filtration.

The objective of this work was to study the dissolution capability of the FP for two different sample sizes of [1-^{13}C]pyruvic acid. (1) A sample of 1.47 g, producing a human dose, dissolved in dissolution medium (DM) and neutralized with Neutralization Medium (NM) to a target concentration of 250 mM [1-^{13}C]pyruvate using the SPINlab polarizer and quality control system (involving FP part A and B). (2) A sample of 40 mg, producing a small animal dose, dissolved in DM to a target concentration of 80 mM, using a home-built polarizer involving only part A of the FP.

2 Materials and methods

2.1 Polarizer

Large samples were polarized on a SPINlab (GE Healthcare), Fig. 1, operating at 5 T and 0.85 K. Small samples were polarized on a home built polarizer [1] operating at 6.7 T and 1.1–1.2 K modified to accommodate the fluid path dissolution system.

2.2 Sample

[1-^{13}C]pyruvic acid (PA) (GE Healthcare, Norway) containing 15 mM AH111501 (EPA), 94.9% purity (GE Healthcare, USA).

2.3 Dissolution medium (DM)

Large sample: Ultra pure water (CHROMASOLVPlus HPLC grade, Sigma Aldrich) with 0.1 g/L ethylenediaminetetraacetic acid disodium salt dihydrate (EDTA) (VWR).

Small sample: 0.2 M tris-hydroxymethyl aminomethane (TRIS base) (VWR) with 0.1 g/L EDTA.

2.4 Neutralization Medium (NM)

Large samples: 0.72 M NaOH (MERCK), 0.4 M TRIS base, 0.1 g/L EDTA.

Small sample: NaOH (10 M).

2.5 Fluid path (FP)

The FP (type 1293, GE Healthcare, USA) used for this study is shown in Fig. 1. Part A of the fluid path consists of a vial which can hold up to 2 mL of sample, the dynamic seal that allows the tubing to move inside the polarizer under vacuum, the co-axial tubing for DM inlet and outlet, the valve that opens the inlet and outlet simultaneously and the dissolution syringe that can hold up to 60 mL of solvent. Fig. 2B and C shows the vial with the position of the inner tube. The inner tube has a nozzle to provide a more efficient dissolution as demonstrated in [15,17]. Part B of the FP, Fig. 1, consists of the transfer tube, the EPA filter, receiver vessel with quality control (QC) appendage, the sterile assurance filter and a Medrad 65 mL MR syringe (Bayer, Denmark). On first use of the FP, the vial was attached to the outer tube by the use

Fig. 1. (A) SPINlab polarizer. The polarizer operates at 5 T and 0.9 K [16]. The polarizer has four independent channels that allow simultaneous polarization of up to four samples (fluid paths). The QC module (cylindrical black unit) is seen to the right of the photo below the touch screen. (B) Fluid Path (FP). Part A: (1) vial, (2) dynamic seal, (3) co-axial tube, (4) valve, (5) dissolution syringe. Part B: (6) transfer tube, (7) EPA filter, (8) receiver vessel, (9) QC appendage, (10) sterile assurance filter, (11) Medrad 65 mL MR syringe. Part A loads into the polarizer (behind the sliding door). The vial is inserted into one of the four airlock and the dissolution syringe is inserted into the corresponding heater-pressure module. After some pump-flush cycles, the airlock gate-valve will open and the vial can be pushed through the dynamic seal to the 0.9 K sample space. Part B is initially loaded into the corresponding warmer module seen to the lower right in (A). Shortly before dissolution part B is moved from the warmer to the QC module.

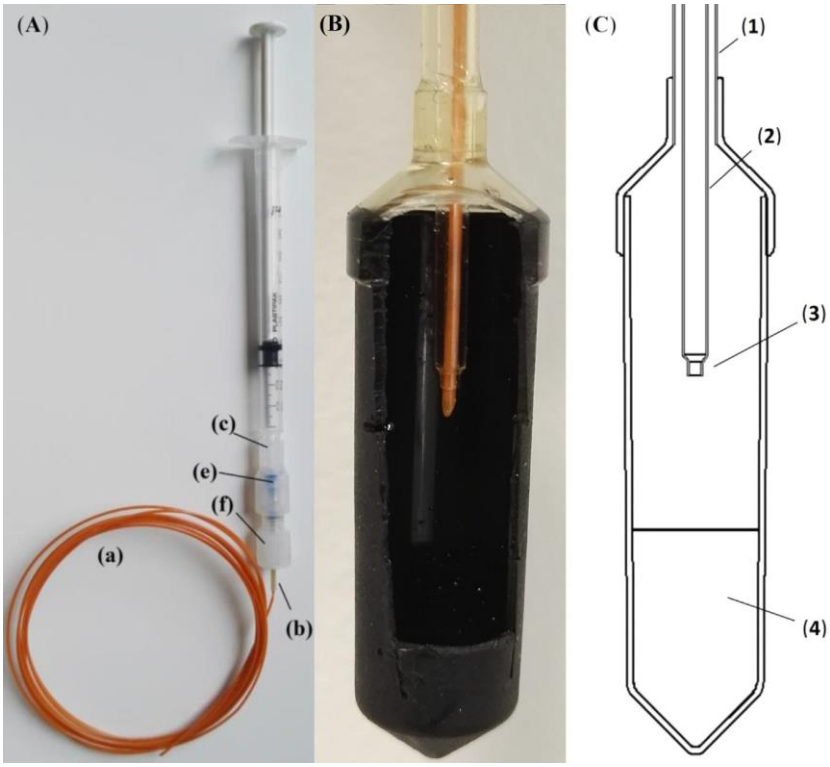

Fig. 2. (A) PEEK tube (a), sleeve (b), adapter (c), ferrule (e) and screw (f) assembled to result in the filling tube used for filling of the FP. (B) Filling tube placed in correct position in a demonstrational set-up (C) section of a vial with sample; (1) outer lumen, (2) inner tube, (3) nozzle, (4) sample (pyruvic acid).

of UV adhesive (Dymax 1161-M). On reuse, the FP part A was cleaned with 40 mL washing buffer (10% NM in distilled water), and then twice with 40 mL distilled water. Initially, the FP was thoroughly examined for any potential defects or irregularities. The FP was placed on a pressure check fixture and briefly flushed with Helium gas to secure unhindered flow. Reused FPs containing visible moisture were flushed for 10 min, or until dry, with compressed air or helium gas. Part B is not reused since it contains a small amount of HPTS (8-hydroxypyrene-1,3,6-trisulfonic acid, trisodium salt) dye used for the optical pH determination.

2.6 Filling tube for sample addition

For adding the sample, a syringe with a filling tube (Mikrolab Aarhus A/S, PEEK O.D. 1/32" I.D. 0.5 mm, 1.5 m, VI JRT5620M3) attached through an adapter, a ferrule and a screw (Tefzel P628, Tefzel P200 and Tefzel P215, Mikrolab Aarhus A/S, Denmark) were used. To fit into the adapter, a sleeve (Sealtight, 840 lm, F247, Mikrolab Aarhus A/S, Denmark) was glued (UV adhesive) onto the filling tube, Fig. 2. The end of the tube was cut in a slanted manner in order to pass the nozzle and minimize residual sample at the end of the tube. Before first use of the filling tube, it was inserted through the dissolution syringe valve bore and through the inner tube, all the way to the sample vial. When the tube reached the bottom of the empty vial, it was retracted such that the end of the tube just passed the nozzle of the inner tube (Fig. 2B). Thus no sample would contaminate the inner tube upon addition. A mark was put on the filling tube by the dissolution syringe valve bore, so the correct position would be easily found upon next use.

2.7 Addition of sample, DM and NM

2.7.1 Addition of large samples

Approx 0.5 mL of sample was pulled into a 3 mL single use plastic syringe (carefully avoiding air bubbles) after which the filling tube was attached. The sample was then pushed through the filling tube in order to fill the dead volume (approx. 380 µL). An Eppendorf tube with sample was placed on the balance, tared, and sample (1.47 g) was drawn into the syringe. Air (few centimeters) was then drawn into the tube to prevent contamination of the FP inner wall. The syringe and filling tube were weighted before and after addition, to confirm correct addition of sample. The surface of the filling tube was thoroughly cleaned for potential impurities and inserted through the inner tube of the FP until the tube reached the bottom of the vial. The slanted tip made it possible for the filling tube to pass the nozzle of the inner tube. The filling tube was then retracted to the correct position, as indicated by the mark. The sample was carefully added by push of the syringe piston. After addition, air was drawn into the filling tube, and it could then be retracted from the FP without contaminating the inner tube.

38.0 g of DM was added to the dissolution syringe. The outlet of the syringe was plugged and the syringe put on the filling stand purge. The sample vial was carefully submerged into liquid nitrogen (vertical position to avoid splashing) and allowed to freeze (2 min). The FP was then flushed with helium for 2 min after which the system was pressure tested (40 psi for 2 min without losing pressure). When the FP tests were completed, the valve rotor was inserted and put into the closed position. The dissolution syringe was then connected to a part B, Fig. 1. Ca. 15.0 g of NM and 26.2 g of DM were added to the receiver of part B, a Medrad power injector syringe was attached and the FP and receiver were ready to be inserted into the polarizer and QC module, respectively.

2.7.2. Addition of small samples

The filling tube was cleaned, dried and attached to a 1 mL syringe. Sample (40 µL) was placed in an Eppendorf tube, and drawn into the filling tube as a bolus, followed by ca. 10 cm air (Supplementary data Video 1). The filling tube was carefully inserted into the FP and pushed to the bottom of the vial. It was then retracted 0.5 cm. The syringe was removed, and helium was flushed through the filling tube (10 psi, 2 min) (Supplementary data Video 2). The filling tube was then removed from the FP. 13.3 g of DM and 138 µL NM were then added to the dissolution syringe. The FP was pressure tested as described for large samples. A short exit tube was attached (50 cm) and the FP was ready for being inserted into the polarizer. An empty 50 mL Falcon tube was used as a receiver for small samples.

2.8. SPINlab QC (online measurements; large sample only)

The QC module measures six parameters by methods that are non-contact with the product. The syringe valve is open for 10 s during the dissolution. The dissolution takes approx. 6 s. 5 s after the syringe valve closes, a part of the hyperpolarized sample is allowed to flow through a series of cavities by opening a valve in the bottom of the receiver. The QC parameters are measured in approx. 15 s, which means that the product (in the Medrad syringe) is released approx. 30 s after the dissolution is initiated. Pyruvate concentration is determined by absorbance at 360 nm, EPA concentration is determined by absorbance at 470 nm, pH is determined by ratio metric absorbance at 405 and 450 nm for a hydroxypyrene-1,3,6-trisulfonic acid (HPTS) dye in one of the cavities, polarization is measured by NMR and corrected for relaxation, temperature is measured by IR on the receiver and volume is a capacitance threshold sensor on the Medrad syringe. The QC module was calibrated prior to the experiments. Pyruvate concentration, EPA concentration and pH all required measurement of a dark, blank and several calibrants (GE Healthcare, USA) according to manufacturer's instructions. Polarization and flip angle calibration were performed by the use of a ^{13}C reference sample ($^{13}C_3$glycerol doped to shorten T_1, QC daily check sample, GE Healthcare, USA) according to manufacturer's instructions. Temperature was calibrated by the use of a receiver filled with water of known temperature.

2.9. Offline measurements

pH: LAQUA pH/ION meter F-72 (HORIBA) with pH electrode DJ 113662-1385 (VWR) or Knick Portamess pH-meter 913 with pH electrode Hamilton mini electrode (KLC). Polarization: measured on a 400 MHz NMR (Agilent Technologies, USA). Acquisition parameters: 3 flip angle every 2 s, starting approx. 10 s post dissolution. The thermal signal was acquired by adding Omniscan (15 lL) to reduce T_1 to <1 s. 2000 averages with repetition delay 0.5 s, 3 flip angle. Software for analysis: MestReNova 10.0 and MATLAB R2015a, by which polarization and T_1 were calculated. PA concentration: For large samples the concentration was measured by quantitative NMR. Sample: sample from receiver (450 µL), [^{13}C]urea (15 µL, 400 mM), D_2O (100 µL) and Omniscan (15 µL). Acquisition parameters: 90 flip angle, repetition delay 1.5 s. Software for analysis: TopSpin 3.2. For small samples the concentration was measured by absorbance on a BioTek EPOCH 2 microplate reader (Holm & Halby, Brøndby, Denmark) at wavelength 360 nm. Temperature was measured by the use of thermometers of type OMEGA HH804U Thermometer or Testo 110, AG Germany. EPA concentration: measured by absorbance at 465 nm (EPOCH plate reader with 10 mm cell). Output volumes were measured by weighing an empty Falcon tube before and after dissolution (Discovery Ohaus balance).

3. Results

3.1. Large samples

Eleven experiments were performed using four FP. The samples were polarized for 2.5 h on average to more than 90% of maximum polarization, followed by dissolution. The data from the QC module have been compared to offline measurements of the respective samples, Table 1. To secure a physiological acceptable pH, the NM in the receiver was adjusted accordingly to the amount of PA added (PA/NaOH ratio 1.6), which was in the range of 13.9– 14.6 g. The target concentration in the case of large samples was 250 mM, which mimics a human dose.

3.2. Small samples

To demonstrate filling of small samples, seven experiments were performed, Table 2, using the same four FP as in the large sample study. The experiments were designed to mimic a target concentration, suitable for small animal dose (80 mM). Polarization measurements were made for four of these.

4. Discussion

The study shows that the new filling method of the FP can be performed in a reproducible manner, validated by QC parameters from the SPINlab and offline measurements. The method is robust with small relative standard deviations. We have demonstrated two extreme conditions; filling of large samples mimicking a human clinical dose, and small samples suited for small animal studies. For the human dose, base is added to the receiver, in order for the radical to precipitate and be filtered off before entering the receiver.

Table 1

Results from dissolutions compared to the respective off-line measurements (n =11)

	Average	Standard deviation	Relative STD (%)
PA/EPA added (g)	1.47	0.02	1.4
DM in syringe (g)	38.0	0.1	
DM in receiver (g)	25.8	0.3	1.0
NM in receiver (g)	14.3	0.2	1.4
PA/NaOH mol ratio	1.6	0.002	0.1
Online results			
Pyruvate conc. (mM)	246	19	7.7
pH	7.71	0.17	2.2
EPA conc. (µM)	1.17	0.28	24
Temperature (C)	32.0	1.3	4.0
Volume (mL)	>40 mL		
Polarization (%)	34.2	2.9 (n = 3)*	8.5
Offline results			
Pyruvate conc. (mM)	247		8.3
pH	7.75	0.15	1.9
EPA conc. (µM)	0.68	0.21	31
Volume (mL) (product in Medrad syringe)	44.2	1.0	2.3
Temperature (C)	31.7	0.5	1.6

*The NMR flip angle was incorrectly calibrated in the first experiments leading to saturation of the receiver and incorrect estimation of the polarization.

Table 2
Results from dissolutions with small sample filling (n = 7).

	Average	Standard deviation	Relative STD (%)
PA/EPA added (mg)[a]	40		
DM in syringe (g)	13.4	0.2	1.6
NaOH (10 M) syringe (g)	0.138		
Pyruvate conc. (mM)	70	7.4	11
pH	7.8	0.1	2
EPA conc. (μM)	70.5	7.5	11
Product in receiver (g)	5.3	0.6	12
Temperature (C)	54	2.6	5
Polarization (%)	43.7	5.5 (n = 4)	13
T_1	53.8	2.0 (n = 4)	4
Recovery (%)	82	12	15

[a] 40 mg was assumed to be added with no loss under the addition process.

The acceptance criterion for residual EPA in the product is less than 3 μM [18]. The measured value is 1.2 ± 0.3 μM, well within specification, and demonstrating >99% removal. The mean value of the EPA concentration is five standard deviations below the acceptance criterion. The pyruvate concentration acceptance criteria are 220–280 mM [18], which is also achieved with three standard deviations margin. The acceptance criteria for pH are 6.7–8.2 [18]. The study was not perfectly centered in the range, which could be achieved by changing the volume of NM in the receiver. However, the range is about ten standard deviations in this study. pH is a critical safety parameter, demonstrating that filling and process performed very well and is robust. Since only approx. 44 mL are transferred to the Medrad syringe, recovery has been disregarded in the large sample case, since some of the sample is used in the QC and thereby trapped in the dead volume of the system. However, the volume transferred to the Medrad syringe is four standard deviations above the acceptance criterion. The FP's have been reused for demonstrational purposes and are not sterile, but we believe the approach could be translated into a low bioburden version by appropriate cleaning of the FP before filling. Sterility assurance can then be achieved by a validated, in-line sterile filter. The filling procedure should be compatible with normal pharmacy clean room environments.

For small samples, base is added to the dissolution syringe, which means that all the PA and EPA is transferred to the receiver upon dissolution, and recovery can thereby be estimated. Recovery is calculated from the product of pyruvate concentration and volume, and assume that the full 40 mg was deposited in the sample vial. Most of the 15–20% loss of sample is likely due to loss in the filling process. The pyruvate concentration in the receiver is highly linked to the performance of the fluid path, since the dead volume vary. The variability of 11% for the pyruvate concentration is acceptable for most animal studies. We have not systematically studied the minimal possible sample amount that can be deposited in the vial by our method, but we have tested volumes down to 10 mg. This could have significance for e.g. cell or perfused organ studies that only require dilute substrate concentrations. More important is the minimal volume that can be applied in the dissolution. We believe that the product volume of app 5 mL achieved in this study, is close to the minimum volume that can be reached without loss of polarization and reduced recovery. This is close to the same performance as e.g. the Hypersense optimized for small sample polarization. It would be reasonable to expect that the use of two-phase dissolution could reduce the effective dissolution volume even further as previously demonstrated [19].

The lower temperature of the solvent in the dissolution allows the use of all plastic components. Plastic components eliminates leaching of paramagnetic ions from e.g. stainless steel components and potential enhanced relaxation from these ions. The polyphenylsulfone that is used in the fluid path is a plastic with high toughness and impact strength, good long-term hydrolytic stability and chemical resistance. It withstands steam sterilization without any significant loss of properties. For other solvents than water, the chemical resistance at the given temperature and pressure conditions needs to be taken into consideration and tested.

The SPINlab corrects the polarization to the start of dissolution by assuming a T_1 of 65 s. This means that the measured polarization is corrected by a factor of approx. 1.5 in this study. The polarization for low dose is the actual measurement without any correction. However, the delay is only approx. 10 s from start of dissolution to measurement. The difference in polarization for the two situations is partly due to the higher magnetic field strength of the prototype polarizer (6.7 T vs 5.0 T), but also that some polarization loss is known to occur in the QC system.

The reusability of the FP's means reduced cost for research purposes, and no failed FP were observed within the ten times reuse that we arbitrarily defined as the maximum number of reuses on the SPINlab. The filling method has been tested extensively (>100 dissolutions) at Aarhus University Hospital, Skejby on the SPINlab, without failure of the fluid path during dissolution that have led to contamination of the polarizer. Failure in dissolution can happen due to e.g. moisture in the tubing that lead to blockage and prevention of flow. This happens at a low rate depending on operator skills. In our laboratory we use the fluid paths until failure since contamination of the polarizer is easier to clean. However, most failures occur during handling as fatigue of glue joints, typically after 20–50 uses. Wear and tear can also lead to failure in the pressure test and discard of the fluid path. More rarely the FP fails early in use due to defects in the plastic. The failures due to defects in the plastic appear to be unrelated to the filling method, but can lead to a burst inside the polarizer during dissolution depending on location of the defect. With the hundreds of dissolutions that we have performed with this method, there does not seem to be a higher frequency of fatal incidents than by single use.

5. Conclusion

The principle of the fluid path for dissolution-DNP enables independent control of solvent temperature and flow rate. The benefit is efficient dissolution at lower solvent temperature and use of all plastic components. The reproducibility of the dissolution process is high on all parameters relevant for clinical use. The fluid path can be used for any sample size from 10 μL to 1.1 mL, and produces a minimum product volume of approx. 5 mL up to the full volume of 44 mL for a patient.

Acknowledgements

Rigshospitalet, Copenhagen, Denmark, is acknowledged for providing access to the SPINlab. Aarhus University Hospital, Skejby, Denmark, is acknowledged for testing the procedure and confirming reliability and performance. Furthermore, the authors wish to thank Danish National Research Foundation [grant number DNRF124] for financial support.

Appendix A. Supplementary material

Supplementary data associated with this article can be found, in the online version, at http://dx.doi.org/10.1016/j.jmr.2016.09.015.

References

[1] J.H. Ardenkjær-Larsen, B. Frindlund, A. Gram, G. Hansson, L. Hansson, M.H. Lerche, R. Servin, M. Thaning, K. Golman, Increase in signal-to-noise ratio of >10,000 times in liquid state NMR, PNAS 100 (18) (2003) 10158–10163.

[2] S. Kohler, Y. Yen, J. Wolber, A. Chen, M. Albers, R. Bok, V. Zhang, J. Tropp, S. Nelson, D. Vigneron, J. Kurhanewicz, R. Hurd, In vivo 13 carbon metabolic imaging at 3 T with hyperpolarized ^{13}C-1-pyruvate, Magn. Reson. Med. 58 (2007) 65–69.

[3] H. Gutte, A.E. Hansen, H.H. Johannesen, A.E. Clemmensen, J.H. ArdenkjærLarsen, C.H. Nielsen, K. Andreas, The use of dynamic nuclear polarization (13) C-pyruvate MRS in cancer, Am. J. Nucl. Med. Mol. Imaging 5 (2015) 548–560.

[4] K. Golman, R. in't Zandt, M. Lerche, R. Pehrson, J.H. Ardenkjaer-Larsen, Metabolic imaging by hyperpolarized ^{13}C magnetic resonance imaging for in vivo tumor diagnosis, Cancer Res. 66 (22) (2006) 10855–10860.

[5] S. Meier, P.R. Jensen, J.Ø. Duus, Real-time detection of central carbon metabolism in living Escherichia coli and its response to perturbations, FEBS Lett. 585 (2011) 3133–3138.

[6] F.A. Gallagher, M.I. Kettunen, D.-E. Hu, P.R. Jensen, R. in't Zandt, M. Karlsson, A. Gisselsson, S.K. Nelson, T.H. Witney, S.E. Bohndiek, G. Hansson, T. Peitersen, M. H. Lerche, K.M. Brindle, Production of hyperpolarized [1,4-^{13}C2]malate from [1,4-^{13}C2]fumarate is a marker of cell necrosis and treatment response in tumors, PNAS 106 (47) (2009) 19801–19806.

[7] F.A. Gallagher, M.I. Kettunen, K.M. Brindle, Imaging pH with hyperpolarized ^{13}C, NMR Biomed. 24 (2011) 1006–1015.

[8] C. von Morze, P.E. Larson, S. Hu, H.A. Yoshihara, R.A. Bok, A. Goga, J.H. Ardenkjær-Larsen, D.B. Vigneron, Investigating tumor perfusion and metabolism using multiple hyperpolarized ^{13}C compounds: HP001, pyruvate and urea, Magn. Reson. Imaging 30 (2012) 305–311.

[9] K.W. Lipsø, P. Magnusson, J.H. Ardenkjær-Larsen, Hyperpolarized ^{13}C MR angiography, Curr. Pharm. Des. 22 (2016) 90–95.

[10] J. Ardenkjaer-Larsen, S. Macholl, H. Jóhanneson, Dynamic nuclear polarization with trityls at 1.2 K, Appl. Magn. Reson. 34 (2008) 509–522.

[11] L. Lumata, S.J. Ratnakar, A. Jindal, M. Merritt, A. Comment, C. Malloy, A.D. Sherry, Z. Kovacs, BDPA: an efficient polarizing agent for fast dissolution dynamic nuclear polarization NMR spectroscopy, Chem. Eur. J. 17 (2011) 10825–10827.

[12] B.v.d. Brandt, E. Bunyatova, P. Hautle, J. Konter, DNP with the free radicals deuterated TEMPO and deuterated oxo-TEMPO, Nucl. Instrum. Meth. A 526 (2004) 53–55.

[13] S.J. Nelson, J. Kurhanewicz, D.B. Vigneron, P.E.Z. Larson, A.L. Harzstark, M. Ferrone, M. van Criekinge, J.W. Chang, R. Bok, I. Park, G. Reed, V.K. Weinberg, J. H. Ardenkjær-Larsen, A.P. Chen, R.E. Hurd, L.-I. Odegardstuen, F.J. Robb, J. Tropp, J.A. Murray, Metabolic imaging of patients with prostate cancer using hyperpolarized [1-^{13}C]pyruvate, Sci. Transl. Med. 5 (198) (2013) 1–11.

[14] A. Comment, J. Rentsch, F. Kurdzesau, S. Jannin, K. Uffmann, R. van Heeswijk, P. Hautle, J. Konter, B. van den Brandt, J. van der Klink, Producing over 100 ml of highly concentrated hyperpolarized solution by means of dissolution DNP, J. Magn. Reson. 194 (2008) 152–155.

[15] S. Bowen, J.H. Ardenkjaer-Larsen, Enhanced performance large volume dissolution-DNP, J. Magn. Reson. 240 (2014) 90–94.

[16] J.H. Ardenkjær-Larsen, A.M. Leach, N. Clarke, J. Urbahn, D. Anderson, T.W. Skloss, Dynamic nuclear polarization polarizer for sterile use intent, NMR Biomed. 24 (2011) 927–932.

[17] J. Jain, S. Dey, L. Muralidharan, A.M. Leach, J.H. Ardenkjær-Larsen, Jet impingement melting with vaporization: a numerical study, in: ASME Heat Transfer Summer Conference, Jacksonville, Florida, 2008.

[18] ''Hyperpolarized [13C] Pyruvate Documentation Page," National Cancer Institute – the National Institute of Health, (Online), Available: <http://imaging.cancer.gov/programsandresources/cancer-tracer-synthesisresources/hyperpolarized-C13-pyruvate-documentation> (accessed 28.06.2016).

[19] T. Harris, C. Bretschneider, L. Frydman, Dissolution DNP NMR with solvent mixtures: substrate concentration and radical extraction, J. Magn. Reson. 211 (2011) 96–100, http://dx.doi.org/10.1016/j.jmr.2011.04.001.

Paper II

Journal of Magnetic Resonance

Large dose hyperpolarized water with dissolution-DNP at high magnetic field

Kasper Wigh Lipsø[1], Sean Bowen[1], Oleksandr Rybalko[1] and Jan Henrik Ardenkjær-Larsen[1,2]

[1]Department of Electrical Engineering, Technical University of Denmark, Kgs. Lyngby, Denmark.

[2]GE Healthcare, Brøndby, Denmark.

In Press, Accepted Manuscript

Available online 18 November 2016

Abstract

We demonstrate a method for the preparation of hyperpolarized water by dissolution Dynamic Nuclear Polarization at high magnetic field. Protons were polarized at 6.7 T and 1.1 K to >70% with frequency modulated microwave irradiation at 188 GHz. 97.2 ± 0.7% of the radical was extracted from the sample in the dissolution in a two-phase system. 16 ± 1 mL of 5.0 M ^{1}H in D_2O with a polarization of 13.0 ± 0.9% in the liquid state was obtained, corresponding to an enhancement factor of 4,000 ± 300 compared to the thermal equilibrium at 9.4 T and 293 K. A longitudinal relaxation time constant of 16 ± 1 s was measured.

The sample was polarized and dissolved in a fluid path compatible with clinical polarizers. The volume of hyperpolarized water produced by this method enables angiography and perfusion measurements in large animals, as well as NMR experiments for studies of e.g. proton exchange and polarization transfer to other nuclei.

Keywords: hyperpolarized water; dissolution-DNP; hyperpolarization

---

Corresponding author and Reprint info: Jan Henrik Ardenkjær-Larsen, DTU Electrical Engineering, Ørsteds Plads, Building 349, room 126, 2800 Kgs. Lyngby, Denmark. Tel (0045) 4525 3918. E-mail: jhar@elektro.dtu.dk

Grant support: This work was supported by the Danish Research Council [grant number 12-127232] and the Danish National Research Foundation [grant number DNRF124].

The authors confirm that this article content has no conflict of interest.

Graphical Abstract

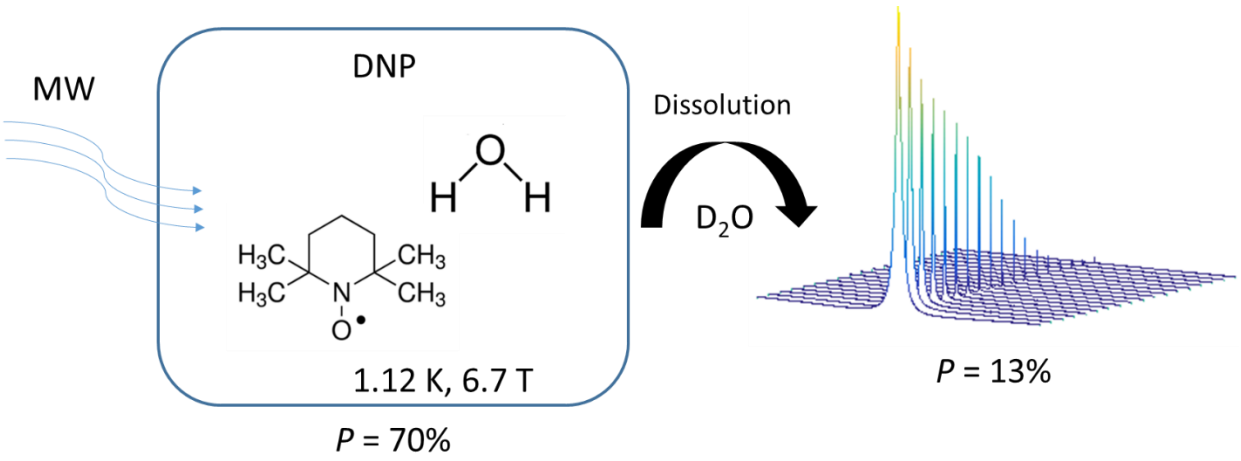

Highlights:

- 16 mL of 5.0 M ^{1}H in D_2O is hyperpolarized to 13% with a T_1 of 16 s.
- Solid state polarization of 71.5% at 6.7 T with a time constant of 23 min using dynamic nuclear polarization with frequency modulation.
- Dissolution in a two-phase system of D_2O and organic solvents yields rapid radical extraction of 97.2% ± 0.7%.

Introduction

NMR is an important analytical tool for e.g. structure analysis, chemical quantification, and investigation of biochemical pathways. Similarly, MRI is a valuable and safe diagnostic tool in medical applications. However, both techniques share a key weakness – poor sensitivity caused by low polarization of nuclear spins. Through the use of hyperpolarization, the signal can be enhanced by several orders of magnitude; leading directly to an increase in sensitivity. This increase in signal obviates the need for time-consuming signal averaging, permitting real-time experiments with unprecedented time resolution. An especially promising application of this capability is the study of chemical and biochemical reactions both in vitro and in vivo.

The field of dissolution-Dynamic Nuclear Polarization (d-DNP) has developed rapidly since the first demonstration in 2003 [1]. The main focus has been on hyperpolarization of ^{13}C nuclei for metabolic imaging, where preclinical studies of hyperpolarized ^{13}C labelled pyruvic acid was injected for characterization of cancer [2–4] or other metabolic diseases in animal models [5,6]. Hyperpolarization has also been used for angiographic and perfusion imaging [7–9] with agents that are not metabolically active. Concurrently, hyperpolarized ^{13}C has been applied for signal enhancement in NMR experiments, such as kinetic studies of metabolism [10–12] or structure analysis of biochemical compounds [13,14].

In recent years, the interest in hyperpolarization of protons diluted in heavy water has increased [15,16]. Due to the high gyromagnetic ratio of the proton and the high proton concentration in water, the achievable magnetization may exceed what is possible with hyperpolarized ^{13}C or other nuclei. Furthermore, hyperpolarized proton imaging is facilitated by already existing MRI coils and sequences, in contrast to hyperpolarized ^{13}C that requires non-standard equipment. In one approach, water, polarized by the Overhauser effect at 0.35 T, was applied for MRI [17,18]. However, the Overhauser effect typically achieves an enhancement of 100 times at 0.35 T for pure water, corresponding to a polarization of only 0.001%. Secondly, the short T_1 of pure water, 3.6 s, limits the available time window significantly. Both of these limitations can be overcome by d-DNP. A 3.35 T HyperSense polarizer was used to produce angiographic images in the rat venous system and head with ^{1}H polarization of 3.5% and ^{1}H concentration of 3.9 M [19], and hyperpolarized water has been used for signal enhancement in NMR experiments [20,21]. Hyperpolarized protons have been applied to enhance the inherent low sensitivity of larger biomolecules, and proton exchange has facilitated increased sensitivity leading to large reduction in scan time [22], or to accommodate studies of protein-ligand interactions for drug discovery [23]. Polarization, dissolution and radical extraction for water/DMSO-d_6 samples was shown to give polarization of approximately 25% and T_1 > 40 s [24]. 6% proton polarization and T_1 of >36 s has been demonstrated by attaching nitroxide radicals to polymer-based backbones that could be filtered out at dissolution [25].

In this work we study the hyperpolarization of ^{1}H in D_2O with d-DNP at 6.7 T and 1.2 K using the fluid path of [26]. The aim of the study was to investigate the polarization and dissolution at these experimental conditions.

Theory

DNP relies on the presence of electron spins, from which polarization is transferred to nuclear spins by microwave (MW) irradiation. An increase in performance has recently been demonstrated when the MW field is frequency modulated [27,28]. The unpaired electron spins are typically added to the system in the form of stable organic radicals such as nitroxides or trityls. Paramagnetic species, such as radicals, efficiently promote nuclear spin relaxation, yet they are a key requirement in the DNP process. A key challenge in dissolution-DNP is supplying sufficient paramagnetic agent to perform DNP, without negatively influencing the relaxation properties of the sample after dissolution. This trade-off is more pronounced due to the high gyromagnetic ratio of ^{1}H that renders it more susceptible to paramagnetic relaxation. Hence, the radical should be segregated from the nuclei upon serving its purpose.

Nitroxides are well suited for DNP of protons due to their broad electron paramagnetic resonance (EPR) lines [29]. With a reported relaxation rate contribution of 0.55 s^{-1} mM^{-1} at 25 °C in low field [30], the dissolved sample would lose the enhanced polarization in a few seconds with the radical present. Thus, radical extraction is a crucial element for achieving long T_1 and, ultimately, high polarization after the dissolution and transfer process. Small animal angiography with hyperpolarized water has been demonstrated in a 3.35 T polarizer [19], where the radical induced relaxation was eliminated by scavenging with ascorbic acid, as demonstrated earlier in [31]. However, the ascorbic acid needs to be hundreds of mM to quench the radical effectively, and the quenching process takes a significant amount of time, during which relaxation occurs. Furthermore, the ascorbic acid undergoes thermal degradation that leads to browning during the solvent heating process, complicating the process further. Hence, we describe a system where the nonpolar nitroxide radical is rapidly extracted into an organic phase immediately after dissolution, as previously demonstrated in [32].

In addition, the T_1 is sensitive to the proton concentration. A high proton concentration will enhance the final magnetization, but will concurrently increase the dipolar relaxation between proton nuclei, and thus cause faster relaxation. A proton concentration of 5.0 M is determined to achieve a high signal in the injectable sample, giving rise to a relaxation rate contribution of less than 0.04 s^{-1} at 21.5 °C [33]. A final relaxation contributor is the temperature, where a warmer sample will have higher proton diffusivity, and thus retain polarization longer, within the relevant temperature range [34].

Rapid dissolution and radical extraction are crucial for maintaining a high solution state polarization. We accelerate the dissolution by addition of Nonafluorobutyl methyl ether (NFBME) with boiling point of 60 °C and density ρ = 1.529 g/mL to the dissolution medium syringe. The low boiling point results in a high pressure to drive the flow in the fluid path, and the density ensures that the sample will be dissolved and diluted in D_2O rapidly, and that the denser NFBME will follow, due to the vertically aligned, upwards facing syringe. Another feature of addition of an immiscible solvent in the dissolution medium syringe is reduction of variation in the volume reaching the sample, because all dissolution medium is flushed out of the tubes, while the dead volume consists of the organic solvent only.

The oxygen in the system originating from air in the fluid path and dissolved in the solvents contributes to the relaxation rate with 0.0094 L/mg/s [35]. The concentration of dissolved oxygen in air saturated water at 25 °C is around 8.6 mg/L, which leads to a relaxation rate contribution of 0.081 s^{-1}. The corresponding oxygen concentrations in heptane and NFBME, are a factor of 10 and 20 higher, respectively [36,37]. The system thus requires degassing of the solvents, as well as flushing of the entire fluid path and receiver system with inert gas.

Radiation damping: The precession of the transverse magnetization of the protons after excitation induces a current in the NMR coil that contributes to restoring the magnetization to the longitudinal direction. Considering the large magnetization of hyperpolarized water protons, this mechanism will have a significant effect on the transverse relaxation rate. In addition to the magnetization, the contribution to the reduced time constant of the free-induction-decay (FID) is affected by parameters such as the Q-factor and the filling factor of the coil [38], or it can be treated by the reciprocity principle [39]. The observable transverse relaxation time T_2^{obs} is given by $\frac{1}{T_2^{obs}} = \frac{1}{T_2^*} + \frac{1}{\tau_{RD}}$, where T_2^* is the time constant of the FID in the absence of radiation damping (typically due to field inhomogeneity) and τ_{RD} is the radiation damping time constant. We show that the radiation time constant, τ_{RD}, can be used as a measure of polarization, with a series of concentration dependent, thermally polarized radiation damping time constants as reference. The method complements quantification of polarization by comparison of integrals for spectra that are hyperpolarized and at thermal equilibrium.

Methods

DNP: All experiments were performed using a homebuilt DNP polarizer (6.7 T magnet from Magnex, Oxford, UK) with a flow-type variable temperature insert. The DNP probe was conceptually based on the idea introduced in 2003 [1]. Microwaves were provided by a microwave source VCOM-10/94-WPT (ELVA-1, St. Petersburg, Russia) and a 200X2R4 frequency doubler (VDI, Charlottesville, VA, USA), which provided an

output power of 55 mW at 188 GHz. The source had a tuning range of ±0.6 GHz. The output power after transmission through the 800 mm circular waveguide and the microwave window [40] was measured to 5 ± 1 mW using a horn and an Ericsson power meter (VDI, Charlottesville, VA, USA). Solid state NMR was performed with a saddle coil formed around a polytetrafluoroethylene (PTFE) former connected to a nonmagnetic coaxial cable (type Stainless Steel 304/Beryllium Copper, SCB Service and Consulting, Neuss, Germany) and a tune and match box. NMR measurements were performed with a Varian INOVA console (Palo Alto, CA, USA). The polarizer was fitted with a heater-pressure module, airlock and insertion module to allow use of the fluid path (both described in [26]). The microwave frequency was sinusoidally swept with a rate of f_{mod} and amplitude a_{mod}. The samples were polarized for 60 min.

Solid state NMR: The build-up of polarization was monitored by acquisition of NMR spectra every 120 s from initiation of MW irradiation. A pulse of 1 μs at 2.7 W corresponding to a flip angle of approximately 0.3° was used for excitation, and 1024 complex points with a spectral width of 5 MHz were acquired. Short MW frequency sweeps were measured with the same parameters, except only with 60 s between each MW frequency step and increased receiver gain. The magnetization was saturated before each MW frequency step by a train of 3000 pulses of 30° flip angle. Long MW frequency sweeps were monitored for one hour at each MW frequency. The NMR signal was destroyed by a train of saturating pulses before each build-up (MW frequency), and then measured every 120 s. Similar for long MW power sweeps. The build-up curve for each MW frequency or power setting was fitted to a mono-exponential function to obtain asymptotic value and time constant. Polarization was quantified by allowing a 30 mM water/glycerol sample to polarize towards thermal equilibrium in the magnetic field at 1.12 K over 19 h, and fitting of the build-up curve of spectra acquired every 300 s. The background signal from the DNP probe was measured with an empty sample cup and subtracted from the data to determine the thermal signal from the sample. 100 kHz exponential line broadening was applied to the data, which were analyzed in MATLAB (Mathworks, Natick, MA, USA).

Sample preparation: Solutions of 20 and 30 mM TEMPO (2,2,6,6-Tetramethylpiperidine 1-oxyl, 98%, Sigma Aldrich, Denmark) in H_2O/glycerol (both Sigma Aldrich, Denmark) 1:1 (w/w), and 30 mM TEMPO in H_2O/DMSO-d_6 (Dimethyl sulfoxide-d6, Sigma Aldrich, Denmark) 1:1 (w/w), was prepared. Dissolution medium consisted of D_2O (99.90%, Euriso-top, Saint-Aubin, France) with 1 mM calcium disodium ethylenediaminetetraacetic acid (EDTA) and 9 g/L NaCl. Sodium chloride was added to provide an isotonic solution.

Fluid path filling: The fluid path consists of a syringe, two concentric tubes leading to a sample vial and an exit tube. The dissolution medium is heated in the syringe, and transferred via the inner tube to the sample

vial for dissolution of the sample, before being flushed back to the syringe via the outer lumen and a three-way valve. The exit tube leads the dissolved sample from the syringe valve to a receiver.

The 1100 mg (~1 mL) sample was injected into the sample vial by the large sample filling method introduced in [41]. This procedure resulted in actual sample mass of 1099.8 ±12.6 mg (N = 5). 7.6 g (5 mL) NFBME (≥99%, Sigma Aldrich, Denmark) and 17.72 g (16 mL) dissolution medium was filled in the syringe and degassed by bubbling with helium gas for 10 minutes by inserting a tube through an adapter that led the moist gas away from the fluid path openings. In experiments without NFBME, another 12 mL of dissolution medium was added. The fluid path syringe was closed off before freezing the sample vial in liquid nitrogen for 2 minutes to avoid cryo pumping of moisture into the fluid path. Samples to be degassed were exposed to vacuum and sealed off before melting and sonicating the sample vial. The sample was frozen again; the cycle was repeated three times (freeze-pump-thaw). After freezing, the fluid path was flushed with helium gas for 2 minutes to remove air and provide a helium atmosphere. The sample vial was rapidly transferred from the liquid nitrogen bath to the polarizer.

Dissolution: The syringe was inserted into a heater/pressure module, where the dissolution medium and NFBME were heated to a temperature of 130 °C over 30 min at 2.75 bar. The sample was raised 140 mm out of the helium bath before the dissolution medium syringe three-way valve was switched, releasing the piston in the syringe driven with 16 bar pressure. The 50 cm outlet tube was inserted into a closed 150 mL separatory funnel containing 25 mL degassed heptane (≥99%, Sigma Aldrich, Denmark), which was shaken vigorously during dissolution and a further 10 s. The aqueous phase was drawn into a syringe, and 1.5 mL was rapidly injected into an injection line entering a 5 mm NMR tube situated in the NMR spectrometer, which had been flushed with helium gas and sealed before the experiment. The dead volume of the injection line was 0.6 mL. Temperature was measured with an RTD thermometer (OMEGA HH804U, Stamford, CT, USA) within 30 s from dissolution.

Liquid state NMR: NMR measurements of the dissolved sample were performed on a 400 MHz spectrometer (Agilent, Palo Alto, CA). A series of 200 spectra were acquired at 1 s intervals with 31200 points, sweep width of 50 kHz and a 1° flip angle of pulse length 1 µs at approximately 0.4 W. The integral was measured as the first point in the FID, and the decay was fitted to estimate the radiation damping time constant. A spectrum of the fully relaxed sample with identical acquisition parameters was measured to quantify the enhancement factor, and thus polarization. The longitudinal relaxation time constant, T_1, was obtained from the decay of the hyperpolarized signal. The T_1 for the same sample was subsequently confirmed by measuring the NMR signal build-up at 9.4 T when quickly inserting the nonpolarized (earth field) sample. from the build-up of the magnetization after relaxation outside the magnet. Quantitative

NMR measurements were performed to determine the final proton concentration in the dissolved sample. 0.2 M potassium formate in D_2O was added for reference. With the probe used, this concentration did not significantly change the 90° flip angle. Data were analyzed using VnmrJ (Agilent Technologies, Palo Alto, CA, USA) and MATLAB (Mathworks, Natick, MA, USA).

Radiation damping in thermal experiments: Solutions of equally distributed water/D_2O volume ratios from 10% to 100%, corresponding to 11.08 M to 110.82 M, were prepared. A series of 10 NMR experiments with parameters identical to those of the hyperpolarized experiments was measured, and the linewidth was determined.

Optical absorbance measurements: The final concentration of TEMPO radical was determined by optical absorbance measurements with an Ocean Optics DH-2000 Deuterium-Halogen light source and an Ocean Optics USB2000+UV-VIS spectrometer in quartz cuvettes of 10 mm path length. The absorbance at λ = 240 nm was compared to a reference curve of TEMPO in water at 125, 250, 375 and 500 µM.

Clinical polarizer compatibility: Organic solvents tend to weaken the fluid path syringe when heated for longer periods, as when inserted in clinical polarizers. To avoid syringe damage during these experiments, the protocol was modified by leaving out the NFBME. Additional dissolution medium was added to a total volume of 28.0 mL. Experiments were performed on a 5 T SPINlab (GE Healthcare, Brøndby, Denmark).

Results

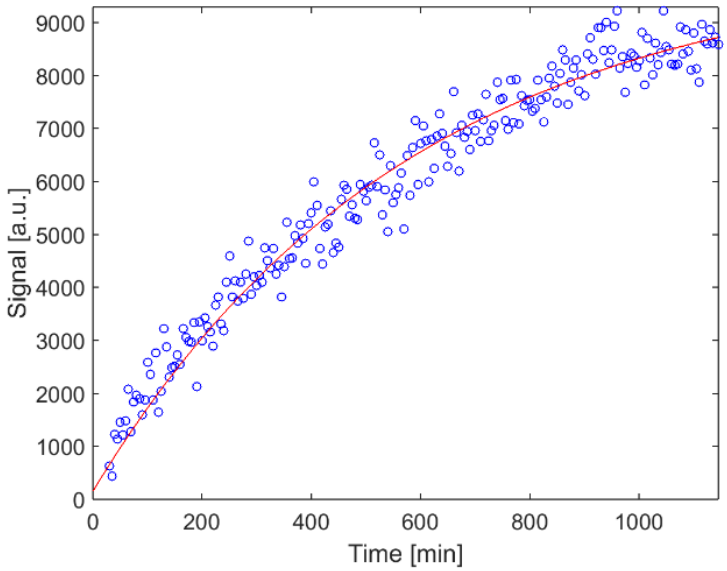

Figure 1: Build-up of the 1H NMR signal to thermal equilibrium for a 30 mM TEMPO in water/glycerol 1:1 (w/w) sample at 6.7 T after subtraction of background signal. The T_1 was 583 min.

The solid state polarization from an 1100 mg 30 mM TEMPO in H_2O/glycerol 1:1 (w/w) sample was measured (Figure 1), and showed a T_1 of 583 ± 62 min. The asymptotic value corresponds to a thermal polarization of 0.61%, and was used for quantification of the DNP enhanced polarization.

Short MW frequency sweeps for three different samples are shown in Figure 2. The polarization of the 30 mM TEMPO in water/glycerol 1:1 (w/w) sample in Figure 2a increases by 30% at the optimal MW frequency and modulation amplitude of 50 MHz. The maximum of the DNP profile left shifts for increasing modulation amplitude, as the MW frequencies giving rise to negative polarization are irradiated. A similar picture is seen for a 20 mM sample (Figure 2b). However, the lower concentration appears to benefit from larger modulation amplitudes. This trend is even more pronounced for samples using DMSO-d_6 as glassing agent, Figure 2c. An increase in polarization at optimum MW frequency is observed up to a_{mod} of 125 MHz. The effect of frequency modulation is more pronounced for this sample. Without modulation, the DNP enhancement is significantly lower.

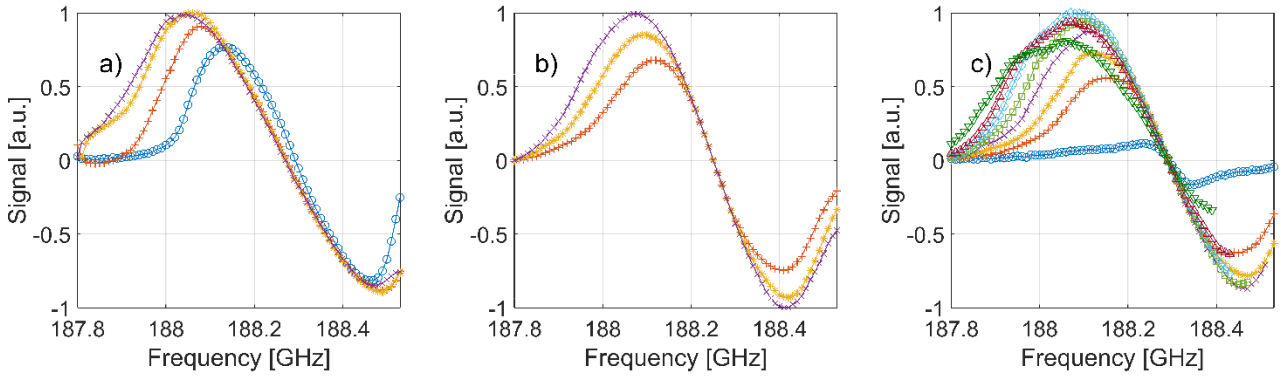

Figure 2: Short MW frequency sweeps. a) 30 mM TEMPO in water/glycerol 1:1 (w/w) with no frequency modulation (○) and modulation amplitude of 25 MHz (+), 50 MHz (*) and 75 MHz (x). b) 20 mM TEMPO in water/glycerol 1:1 (w/w) with modulation amplitude of 25 MHz (+), 50 MHz (*) and 75 MHz (x). c) 30 mM TEMPO in water/DMSO-d_6 1:1 (w/w) with no frequency modulation (○) and modulation amplitude of 25 MHz (+), 50 MHz (*), 75 MHz (x), 100 MHz (□), 125 MHz (◊), 150 MHz (Δ) and 200 MHz (▽). Modulation frequency f_{mod} = 1 kHz.

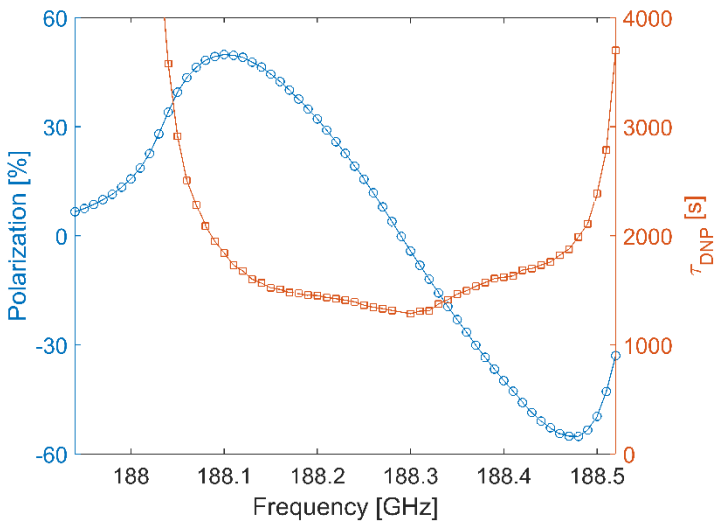

Figure 3: Long MW frequency sweep without modulation. Final polarization (○) and DNP time constant (□) of build up for 30 mM TEMPO in water/glycerol 1:1 (w/w) sample.

A long MW frequency sweep without frequency modulation is shown in Figure 3, for the 30 mM TEMPO in glycerol/water 1:1 (w/w) sample. The polarization resembles the short build-ups of Figure 2a. However, the optima are shifted towards the center in short sweeps due to the faster build up in the central region (τ_{DNP} curve).

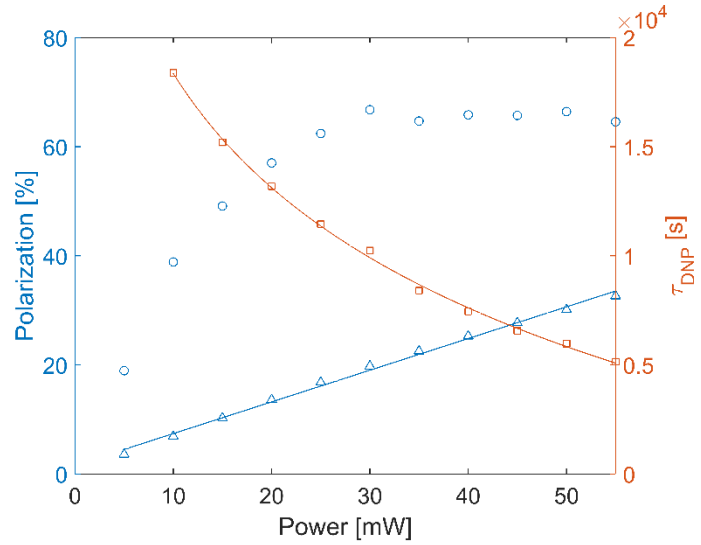

Figure 4: DNP power sweep of 20 mM TEMPO in water/glycerol 1:1 (w/w) for microwave power 5 to 55 mW at 188.06 GHz with modulation amplitude 50 MHz and frequency 1 kHz. Polarization after 1 hr DNP (Δ), asymptotical max polarization (○) with linear fit and DNP time constant estimated from a fit of 60 min polarization (□, build up at 5 mW was too slow to estimate time constant) with fit of inverse square root.

A long power sweep is shown in Figure 4. The asymptotical maximum polarization is reached for 30 mW power. The DNP polarization after 1 hr increases linearly with the available MW power and the DNP build-up time constant decreases with MW power with a square-root of power dependence. The linear relation between MW power and polarization is valid over the entire DNP spectrum, Figure 5, i.e. the data confirms that build-up rate constant is independent of MW frequency.

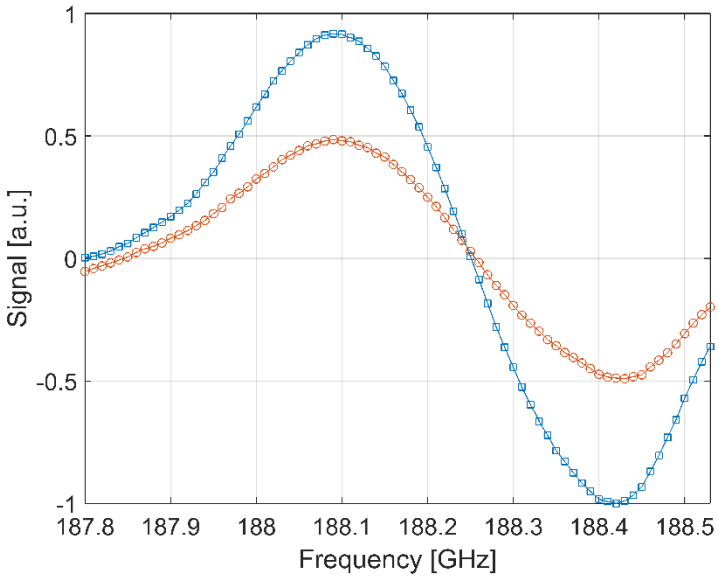

Figure 5: Short MW frequency sweep for 20 mM TEMPO in water/glycerol 1:1 (w/w) at 60 mW (□) and 30 mW MW power (○). 60 s MW irradiation with frequency modulation of a_{mod} = 50 MHz and f_{mod} = 1 kHz was applied. The data confirms that build-up rate constant is independent of MW frequency.

The build-up curves of several sample compositions have been measured to study the radical concentration, removal of dissolved oxygen and glassing matrix. The build-up time constants and polarizations after 60 min DNP are presented in Table 1.

Experiment	***N***	***P* (1 hr) [%]**	**DNP time const.**
20 mM TEMPO in water/glycerol at 188.12 ± 0.05 GHz	6	48.1 ± 4.9	37 ± 5 min
30 mM TEMPO in water/glycerol at 188.12 ± 0.05 GHz	4	63.1 ± 3.7	24 ± 4 min
Degassed 30 mM TEMPO in water/glycerol at 188.06 ± 0.05 GHz	5	71.5 ± 4.5	23 ± 2 min
Degassed 30 mM TEMPO in water/DMSO-d_6 at 188.06 ± 0.05 GHz	3	42.8 ± 1.7	41 ± 2 min

Table 1: DNP results for various sample compositions and polarization parameters.

The dissolution resulted in 16 ± 1 mL (*N* = 8) aqueous phase entering the heptane bath, to reach a common temperature of 50 ± 2 °C (*N* = 6). The total time of dissolution, extraction and transferring of sample from separatory funnel via syringe and tubing to acquisition in NMR spectrometer was less than 25 s. The first

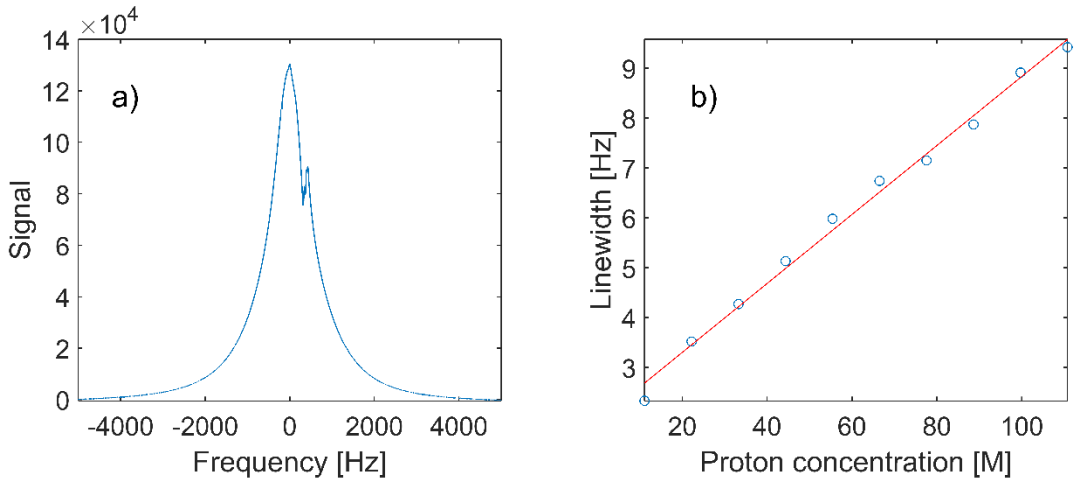

Figure 6: a) Spectrum of hyperpolarized 30 mM TEMPO in water/glycerol 1:1 (w/w) sample after dissolution. The small shoulder represents the glycerol protons. 50% linewidth of 1166 Hz. b) Linear regression of linewidth of thermal spectra from samples of varying H_2O:D_2O ratio.

spectrum is shown in Figure 6a. The water peak has a line width of 1166 Hz due to the radiation damping caused by the large magnetization of the sample. The peak of the glycerol aliphatic protons is apparent in the spectrum, indicating that these protons are hyperpolarized along with the water protons.

In this particular experiment, we achieved an enhancement factor of 3,761 at 9.4 T, corresponding to a polarization of 12.1%. A signal time series is shown in Figure 7. The estimated T_1 after correction for signal loss from previous excitations is 17.0 s. The relation between linewidth (full with at half maximum, *FWHM*) due to radiation damping and water concentration was found to be $FWHM(c_W) = 0.0691\ \text{Hz} \cdot c_W + 1.92\ \text{Hz}$, where c_W is the proton concentration in the sample (Figure 6b). Thus, the linewidth of 1,166 Hz corresponds to an polarization of 11.7%, when corrected for the 111 M proton concentration in water and the 4.6 M proton concentration in the dissolved sample, in close agreement with the time domain integral estimate. The thermal signal and T_1 was measured by acquiring the NMR signal from the sample as it was introduced into the 9.4 T magnet, Figure 7. The measurement was done 5 min after dissolution when the sample was fully relaxated. A consistent T_1 of 16.6 s was measured.

The polarizations and T_1's in the liquid state at 9.4 T for several samples are shown in Table 2. The 30 mM TEMPO in water/glycerol 1:1 (w/w) sample showed large fluctuations in the observed polarization, with an average of 7.8%. The polarization was significantly lower when the NFBME was omitted, where the standard fluid path exit tube set-up yielded polarizations below 3%. However, a significant increase in polarization was achieved when the exit tube was reduced from 210 cm to 50 cm – a setup that requires minor modifications of a SPINlab. Shortening the exit tube increased the temperature in the dissolved

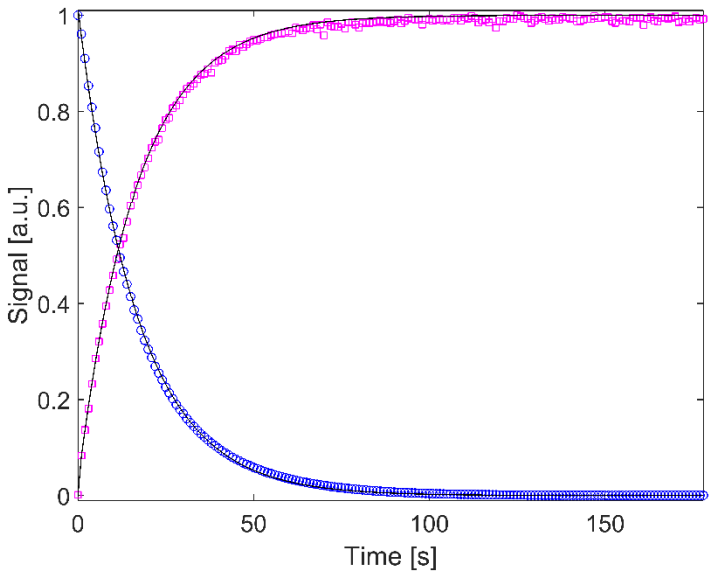

Figure 7: Normalized NMR signal of hyperpolarized water sample (○) (30 mM TEMPO in water/glycerol 1:1 (w/w)) and build-up of relaxed sample at 9.4 T to validate T_1 (□). The initial hyperpolarized signal is 3,761 times that at thermal equilibrium. The T_1 for the hyperpolarized sample was 17.0 s, whereas the build-up to thermal equilibrium had a T_1 of 16.6 s (sample at room temperature).

sample with approximately 10 °C, which we believe to be the main reason for the increased polarization. In addition, the shorter time from dissolution to extraction may also play a role.

Larger enhancements were achieved when the 30 mM TEMPO in water/glycerol 1:1 (w/w) sample was degassed in the fluid path before polarization, which can be attributed to the increased solid state polarization (Table 1). However, the degassing only increased the solid state polarization by 13%, whereas the liquid state polarization increased by more than 50%. The amount of oxygen removed from the sample has insignificant impact on the liquid state relaxation rate, and no further T_1 prolongation was observed.

The liquid state polarization of the degassed water/DMSO-d_6 1:1 (w/w) sample was 7.2%, significantly lower than the degassed water/glycerol 1:1 (w/w) sample of 13.0%. The difference is explained by the significantly lower solid state polarization of the water/DMSO-d_6 sample.

The method was tested with a sample of half size (550 mg) (30 mM TEMPO in water/glycerol 1:1 (w/w)) dissolved in half the volume of dissolution medium (8 mL) and the standard 5 mL NFBME. Polarization of 12% and T_1 of 17.0 s confirm that the method scales to smaller samples.

Experiment	*N*	Pol. [%]	T_1 [s]
20 mM TEMPO in water/glycerol 1:1 (w/w)	5	8.6 ± 1.5	16.1 ± 1
30 mM TEMPO in water/glycerol 1:1 (w/w)	6	7.8 ± 3.3	17.0 ± 0.9
Degassed 30 mM TEMPO in water/glycerol 1:1 (w/w)	3	13.0 ± 0.9	15.7 ± 1.2
Degassed 30 mM TEMPO in water/DMSO-d_6 1:1 (w/w)	2	7.2 ± 1.3	18.8 ± 1.6
30 mM TEMPO in water/glycerol 1:1 (w/w) without NFBME, long exit tube	2	2.4 ± 0.6	19.6 ± 0.8
30 mM TEMPO in water/glycerol 1:1 (w/w) without NFBME, short exit tube	2	4.8 ± 0.5	20.1 ± 1.3
SPINlab polarization	4*	5.3 ± 0.9	24.1 ± 1.0

*Table 2: Liquid state polarization and T_1 at 9.4 T. *Measured at 3 T, from* [42].*

The partition coefficient of TEMPO in water/heptane, water/NFBME and water/[NFBME/heptane 1:3 (V/V)] were similar. The scheme of extraction in the separatory funnel was investigated by a series of dissolutions with varying shaking time. An equilibrium was observed for approx. 5 s vigorous shaking, and 10 s shaking time was chosen to ensure complete equilibrium in all experiments. With 10 s shaking in 25 mL heptane, we observed a final TEMPO concentration of 50 ± 12 µM (30 mM TEMPO in water/glycerol 1:1 (w/w), N = 5) and 35 ± 6 µM (20 mM TEMPO in water/glycerol 1:1 (w/w), N = 5), corresponding to relaxation rate contributions of $R_{30\,mM}$ = 0.028 s^{-1} and $R_{20\,mM}$ = 0.019 s^{-1}, respectively.

The average final proton concentration in the dissolved glycerol/water 1:1 (w/w) sample was measured to 5.0 ± 0.5 M (N = 18), compared to the calculated value of 4.6 M. The proton concentration of the water/DMSO-d_6 sample was not measured, but should be 3.6 M if full recovery is assumed.

Discussion and Conclusion

The presented method enables experiments where large quantities of hyperpolarized water protons are required, e.g. imaging experiments in large animals. We demonstrate 13% ^{1}H polarization and T_1 of 16 s for a 16 mL sample with 5 M protons in D_2O on a polarizer operating at 6.7 T and 1.2 K. This is enabled by the fluid path that accommodates up to 2 mL of sample. The method has been used in a SPINlab (5 T/0.8 K) for hyperpolarized water studies in a pig model [42], where dynamic angiography time series and perfusion maps were produced. The fluid path is already used in clinical studies [43] and it is reasonable to expect that the presented method can be translated into a sterile operation. The safety of the formulation needs to be established.

At maximum power, the DNP time constant was 86 min, whereas the samples were polarized for 60 min. Thus, the reported liquid state polarization could have been increased further by a factor two by longer polarization time. The polarization after 1 hr showed a linear trend in the available power range (Figure 4),

indicating that higher polarization after 1 hr could be realized by increasing the microwave power above 55 mW through a shortening of the build-up time constant. The build-up time constant follows an inverse square-root of microwave power dependence, i.e. is inversely proportional to the microwave B_1 field. This is the expected dependence of the rate constant for both the solid-effect and thermal mixing [44]. The MW power at the entry to the cavity was measured to be approx. 5 mW, but since we do not have details about the power distribution within the cavity, all data has been referenced to the source output power.

The MW frequency modulation increased DNP efficiency for all tested samples. The 20 mM water/glycerol 1:1 (w/w) sample was tested for modulation amplitude of 25, 50, and 75 MHz, respectively, and 50 MHz gave the largest DNP gain. 75 MHz modulation amplitude was the optimal of the three for 30 mM water/glycerol 1:1 (w/w) sample, whereas the 30 mM water/DMSO-d_6 1:1 (w/w) sample polarized most efficiently at 125 MHz. Thus, both sample composition and radical concentration affect the frequency modulation performance. The modulation of the MW frequency is beneficial due to the inhomogeneous nature of the nitroxide EPR line at high magnetic field that restricts spectral diffusion. The inhomogeneity of the EPR line could probably have been overcome by increasing the nitroxide concentration further, but this may lead to shortening of T_1 in the liquid state and/or further loss in the dissolution.

Optimal MW frequencies were determined for several sample compositions at 6.7 T. Polarizers at other field strengths have other DNP frequency profiles, where optimal frequency modulation parameters are shifted. For polarizers without ^{1}H detection, the ^{13}C frequency sweeps can be used for localization of optimum EPR frequencies, and applied to protons due to the broad linewidth of the nitroxide radical. This is in principle how the SPINlab experiments were performed.

We have demonstrated that large volumes of hyperpolarized water can be produced with the fluid path technology. The 30 mM water/glycerol 1:1 (w/w) sample polarized 30% better than the corresponding 20 mM sample, whereas the dissolved state polarization was 10% higher for the 20 mM sample. The lower radical concentration in the dissolved state is the obvious reason. Degassing of the sample only increased the solid state polarization by 13%, but increased liquid state polarization by 51%. This is in good agreement with [24] where an approx. 50% increase of the liquid state enhancement is observed after degassing.

Some liquid state polarization measurements showed large deviations. Only small variance in the solid state polarization was observed, which means that the dissolution process, extraction and sample transfer are the dominating sources of variability. The manual extraction process, where a funnel was shaken by hand, is inevitably a variable operation. The variation in the transfer time should be a minor contribution if the measured T_1 values are constant during the process. However, the relaxivity of the nitroxide is about the

double in low field, and a shorter T_1 during the extraction and transfer should be expected. However, a more systematic variation in performance was also observed over time, possibly due to e.g. variation in microwave power delivery due to waveguide contamination.

Dissolving the frozen sample in heptane yielded low final polarizations. The low-density heptane places itself in the top in the dissolution medium syringe, and thus exits first. Thus, the sample was melted without being diluted until the aqueous phase appeared, causing a loss in polarization from relaxation by the high radical and proton concentration. Secondly, the fluid path plastic did not tolerate well the heated heptane and showed tendency of cracking. Instead, NFBME was determined to have TEMPO partition coefficient similar to that of heptane, and was tested with volume of 5, 8, 11 mL, where the lower volume yielded the most controlled and efficient dissolution, and highest polarization in the liquid state.

NFBME volumes above 5 mL resulted in uncontrolled dissolution, where the exit tube was blown out of the receiver or the sample was spurted out of the funnel due to high pressure sample and gas from the exit tube. An extraction system with a fixed, stirred receiver or application of a filter at the exit tube may allow larger NFBME volume, resulting in faster, warmer dissolutions. In addition, this would allow larger sample sizes, so the full potential of the 2 mL vial could be utilized. The water/glassing agent ratio was not investigated. Smaller glassing agent volume may yield faster sample melting and lower radical concentration in the dissolved state, but the glassing ability of such sample should be verified first.

The radical removal may be optimized, e.g. by automatization of the extraction, which could also reduce the variance in the dissolved state polarization. Although radical quenching can be done efficiently, removal is preferred for in vivo studies and future clinical applications. Thus, filtering, reverse phase or ion exchange extraction of the radical may prove useful.

We did not observe relaxation times above 40 s, as demonstrated in [24]. We believe that the decrease in temperature from dissolution to NMR acquisition is the main reason. In [24], the dissolved sample of 52 °C was transferred in a preheated transfer line into a preheated NMR tube at 60 °C , whereas the 50 °C dissolved sample of the present study was cooled in the transferring syringe, injection line and NMR tube at room temperature. Since the aim of our study was to enable in vivo studies, the sample temperature should be conditioned to 30-35 °C at time of injection. The slightly longer T_1 at 3 T support this, as the larger sample volume used in these experiments will stay at the higher solvent exit temperature of the polarizer during measurement.

The liquid state NMR signal yielded robust polarization quantification, and the radiation damping time constant was demonstrated to give consistent measure of polarization.

The T_1 of the hyperpolarized samples in the liquid state are in the range 15-20 s, with uncertainty of the temperature and field dependence during transfer. With a dissolution, extraction and transfer time of approx. 25 s, the relaxation loss amounts to approx. 70% ($e^{-25\ s/20\ s} = 0.3$). This explains most of the polarization loss from the solid state (P=70%) to the liquid state (P=13%), but probably not entirely. Further optimization and automation of the radical removal and transfer may reduce this loss further, e.g. by sample injection systems. Similarly, the ^1H concentration may be further reduced to prolong T_1 for the given transfer time.

Bibliography

[1] J.H. Ardenkjaer-Larsen, B. Fridlund, A. Gram, G. Hansson, L. Hansson, M.H. Lerche, R. Servin, M. Thaning, K. Golman, Increase in signal-to-noise ratio of > 10,000 times in liquid-state NMR., Proc. Natl. Acad. Sci. U. S. A. 100 (2003) 10158–10163. doi:10.1073/pnas.1733835100.

[2] S.E. Day, M.I. Kettunen, F.A. Gallagher, D.-E. Hu, M. Lerche, J. Wolber, K. Golman, J.H. Ardenkjaer-Larsen, K.M. Brindle, Detecting tumor response to treatment using hyperpolarized 13C magnetic resonance imaging and spectroscopy., Nat. Med. 13 (2007) 1382–1387. doi:10.1038/nm1650.

[3] M.J. Albers, R. Bok, A.P. Chen, C.H. Cunningham, M.L. Zierhut, V.Y. Zhang, S.J. Kohler, J. Tropp, R.E. Hurd, Y.F. Yen, S.J. Nelson, D.B. Vigneron, J. Kurhanewicz, Hyperpolarized 13C lactate, pyruvate, and alanine: Noninvasive biomarkers for prostate cancer detection and grading, Cancer Res. 68 (2008) 8607–8615. doi:10.1158/0008-5472.CAN-08-0749.

[4] H. Gutte, A.E. Hansen, H.H. Johannesen, A.E. Clemmensen, J.H. Ardenkjær-Larsen, C. Haagen, A. Kjær, The use of dynamic nuclear polarization 13 C-pyruvate MRS in cancer, Am. J. Nucl. Med. Mol. Imaging. 5 (2015) 548–560.

[5] R.E. Hurd, Y.-F. Yen, J. Tropp, A. Pfefferbaum, D.M. Spielman, D. Mayer, Cerebral dynamics and metabolism of hyperpolarized [1-(13)C]pyruvate using time-resolved MR spectroscopic imaging., J. Cereb. Blood Flow Metab. 30 (2010) 1734–1741. doi:10.1038/jcbfm.2010.93.

[6] C. Laustsen, K. Lipsø, J.A. Ostergaard, R. Nørregaard, A. Flyvbjerg, M. Pedersen, F. Palm, J.H. Ardenkjær-Larsen, Insufficient insulin administration to diabetic rats increases substrate utilization and maintains lactate production in the kidney, Physiol. Rep. 2 (2014) e12233–e12233. doi:10.14814/phy2.12233.

[7] L.E. Olsson, C.M. Chai, O. Axelsson, M. Karlsson, K. Golman, J.S. Petersson, MR coronary angiography in pigs with intraarterial injections of a hyperpolarized 13C substance, Magn. Reson. Med. 55 (2006) 731–737. doi:10.1002/mrm.20847.

[8] K. Golman, J.H. Ardenkjær-Larsen, J. Svensson, O. Axelsson, G. Hansson, L. Hansson, H. Jóhannesson, I. Leunbach, S. Månsson, J.S. Petersson, G. Pettersson, R. Servin, L.-G. Wistrand, 13C-Angiography, Acad. Radiol. 9 (2002) 507–510. doi:10.1016/S1076-6332(03)80278-7.

[9] K.W. Lipsø, P. Magnusson, J.H. Ardenkjær-Larsen, Hyperpolarized 13 C MR Angiography, Curr. Pharm. Des. 22 (2016) 90–95. doi:10.2174/1381612822666151109112415.

[10] S. Bowen, C. Hilty, Time-resolved dynamic nuclear polarization enhanced NMR spectroscopy, Angew. Chemie - Int. Ed. 47 (2008) 5235–5237. doi:10.1002/anie.200801492.

[11] C. Harrison, C. Yang, A. Jindal, R.J. Deberardinis, M.A. Hooshyar, M. Merritt, A. Dean Sherry, C.R. Malloy, Comparison of kinetic models for analysis of pyruvate-to-lactate exchange by hyperpolarized 13C NMR, NMR Biomed. 25 (2012) 1286–1294. doi:10.1002/nbm.2801.

[12] H. Allouche-Arnon, A. Gamliel, C.M. Barzilay, R. Nalbandian, J.M. Gomori, M. Karlsson, M.H. Lerche, R. Katz-Brull, A hyperpolarized choline molecular probe for monitoring acetylcholine synthesis, Contrast Media Mol. Imaging. 6 (2011) 139–147. doi:10.1002/cmmi.418.

[13] M.J. Bayro, G.T. Debelouchina, M.T. Eddy, N.R. Birkett, C.E. Macphee, M. Rosay, W.E. Maas, C.M. Dobson, R.G. Griffin, Intermolecular Structure Determination of Amyloid Fibrils with Magic-Angle Spinning and Dynamic Nuclear Polarization NMR, J. Am. Chem. Soc. 133 (2011) 13967–13974.

[14] A. Potapov, W.M. Yau, R. Tycko, Dynamic nuclear polarization-enhanced 13C NMR spectroscopy of static biological solids, J. Magn. Reson. 231 (2013) 5–14. doi:10.1016/j.jmr.2013.02.011.

[15] P. Mark D. Lingwood, B. Ting Ann Siaw, P. Napapon Sailasuta, M. Osama A. Abulseoud, M. Henry R. Chan, M. Brian D. Ross, P. Pratip Bhattacharya, P. Songi Han, Hyperpolarized Water as an MR Imaging Contrast Agent: Feasibility of in Vivo Imaging in a Rat Model, Radiology. 265 (2012) 418–425. doi:10.1148/radiol.12111804.

[16] R.E. Lenkinski, Science to Practice: Can Hyperpolarized Water Be Used to Enhance MR Angiography and Flow Measurement?, Radiology. 265 (2012) 325–326. doi:10.1148/radiol.12121642.

[17] E.R. McCarney, B.D. Armstrong, M.D. Lingwood, S. Han, Hyperpolarized water as an authentic magnetic resonance imaging contrast agent., Proc. Natl. Acad. Sci. U. S. A. 104 (2007) 1754–1759. doi:10.1073/pnas.0610540104.

[18] M.D. Lingwood, T.A. Siaw, N. Sailasuta, B.D. Ross, P. Bhattacharya, S. Han, Continuous flow Overhauser dynamic nuclear polarization of water in the fringe field of a clinical magnetic resonance imaging system for authentic image contrast, J. Magn. Reson. 205 (2010) 247–254. doi:10.1016/j.jmr.2010.05.008.

[19] J.H. Ardenkjaer-Larsen, C. Laustsen, S. Bowen, R. Rizi, Hyperpolarized H2O MR angiography, Magn. Reson. Med. 71 (2014) 50–56. doi:10.1002/mrm.25033.

[20] B.D. Armstrong, S. Han, Overhauser dynamic nuclear polarization to study local water dynamics., J. Am. Chem. Soc. 131 (2009) 4641–4647. doi:10.1021/ja809259q.

[21] J.-H. Ardenkjaer-Larsen, G.S. Boebinger, A. Comment, S. Duckett, A.S. Edison, F. Engelke, C. Griesinger, R.G. Griffin, C. Hilty, H. Maeda, G. Parigi, T. Prisner, E. Ravera, J. van Bentum, S. Vega, A. Webb, C. Luchinat, H. Schwalbe, L. Frydman, Facing and Overcoming Sensitivity Challenges in

Biomolecular NMR Spectroscopy, Angew. Chemie Int. Ed. 54 (2015) 9162–9185. doi:10.1002/anie.201410653.

[22] T. Harris, O. Szekely, L. Frydman, On the potential of Hyperpolarized Water in Biomolecular NMR Studies, J. Phys. Chem. B. 118 (2014) 3281–3290. doi:10.1021/jp4102916.

[23] Q. Chappuis, J. Milani, B. Vuichoud, A. Bornet, A.D. Gossert, G. Bodenhausen, S. Jannin, Hyperpolarized Water to Study Protein–Ligand Interactions, J. Phys. Chem. Lett. 6 (2015) 1674–1678. doi:10.1021/acs.jpclett.5b00403.

[24] G. Olsen, E. Markhasin, O. Szekely, C. Bretschneider, L. Frydman, Optimizing water hyperpolarization and dissolution for sensitivity-enhanced 2D biomolecular NMR, J. Magn. Reson. 264 (2016) 49–58. doi:10.1016/j.jmr.2016.01.005.

[25] B. Vuichoud, A. Bornet, F. de Nanteuil, J. Milani, E. Canet, X. Ji, P. Miéville, E. Weber, D. Kurzbach, A. Flamm, R. Konrat, A.D. Gossert, S. Jannin, G. Bodenhausen, Filterable Agents for Hyperpolarization of Water, Metabolites, and Proteins, Chem. Eur. J. 22 (2016) 1521–3765. doi:10.1002/chem.201602506.

[26] J.H. Ardenkjaer-Larsen, A.M. Leach, N. Clarke, J. Urbahn, D. Anderson, T.W. Skloss, Dynamic nuclear polarization polarizer for sterile use intent, NMR Biomed. 24 (2011) 927–932. doi:10.1002/nbm.1682.

[27] A. Bornet, J. Milani, B. Vuichoud, A.J. Perez Linde, G. Bodenhausen, S. Jannin, Microwave Frequency Modulation to Enhance Dissolution Dynamic Nuclear Polarization, Chem. Phys. Lett. 602 (2014) 63–67. doi:10.1016/j.cplett.2014.04.013.

[28] Y. Hovav, A. Feintuch, S. Vega, D. Goldfarb, Dynamic nuclear polarization using frequency modulation at 3.34 T, J. Magn. Reson. 238 (2014) 94–105. doi:10.1016/j.jmr.2013.10.025.

[29] V. Weis, M. Bennati, M. Rosay, J.A. Bryant, R.G. Griffin, High-field DNP and ENDOR with a novel multiple-frequency resonance structure, J. Magn. Reson. 140 (1999) 293–299. doi:10.1006/jmre.1999.1841.

[30] P. Höfer, G. Parigi, C. Luchinat, P. Carl, G. Guthausen, M. Reese, T. Carlomagno, C. Griesinger, M. Bennati, Field dependent dynamic nuclear polarization with radicals in aqueous solution, J. Am. Chem. Soc. 130 (2008) 3254–3255. doi:10.1021/ja0783207.

[31] P. Miéville, P. Ahuja, R. Sarkar, S. Jannin, P.R. Vasos, S. Gerber-Lemaire, M. Mishkovsky, A. Comment, R. Gruetter, O. Ouari, P. Tordo, G. Bodenhausen, Scavenging free radicals to preserve enhancement and extend relaxation times in NMR using dynamic nuclear polarization, Angew. Chemie - Int. Ed. 49

(2010) 6182–6185. doi:10.1002/anie.201000934.

[32] T. Harris, C. Bretschneider, L. Frydman, Dissolution DNP NMR with solvent mixtures: Substrate concentration and radical extraction, J. Magn. Reson. 211 (2011) 96–100. doi:10.1016/j.jmr.2011.04.001.

[33] J.T. Anderson, W. A.; Arnold, Proton Relaxation Times in H2O-D2O Mixtures, Phys. Rev. 101 (1956) 511–512. doi:10.1103/PhysRev.101.511.

[34] H.Y. Simpson, J. H.; Carr, Diffusion and Nuclear Spin Relaxation in Water, Phys. Rev. 111 (1958) 1201–1202. doi:10.1103/PhysRev.111.1201.

[35] N. Nestle, T. Baumann, R. Niessner, Oxygen determination in oxygen-supersaturated drinking waters by NMR relaxometry, Water Res. 37 (2003) 3361–3366. doi:10.1016/S0043-1354(03)00211-2.

[36] R. Battino, T.R. Rettich, T. Tominaga, The Solubility of Oxygen and Ozone in Liquids, J. Phys. Chem. Ref. Data. 12 (1983) 163–178. doi:10.1063/1.555680.

[37] Michael G. Costello, R.M. Flynn, J.G. Owens, 3M Company, Fluoroethers and Fluoroaminies, Kirk-Othmer Encyclopedia of Chemical Technology, 5th ed., John Wiley & Sons, 2005. doi:10.1002/0471238961.

[38] V. V. Krishnan, N. Murali, Radiation damping in modern NMR experiments: Progress and challenges, Prog. Nucl. Magn. Reson. Spectrosc. 68 (2013) 41–57. doi:10.1016/j.pnmrs.2012.06.001.

[39] J. Tropp, M. Van Criekinge, Radiation damping and reciprocity in nuclear magnetic resonance: The replacement of the filling factor, J. Magn. Reson. 206 (2010) 161–167. doi:10.1016/j.jmr.2010.06.001.

[40] O. Rybalko, S. Bowen, V. Zhurbenko, J.H. Ardenkjær-Larsen, Waveguide transition with vacuum window for multiband dynamic nuclear polarization systems, Rev. Sci. Instrum. 87 (2016) 54705. doi:10.1063/1.4948294.

[41] R.M. Malinowski, K.W. Lipsø, M.H. Lerche, J.H. Ardenkjær-larsen, Dissolution Dynamic Nuclear Polarization capability study with fluid path, J. Magn. Reson. 272 (2016) 141-146. doi:10.1016/j.jmr.2016.09.015.

[42] K.W. Lipsø, E.S. Szocska Hansen, R. Tougaard, C. Laustsen, J.H. Ardenkjær-Larsen, Renal MR Angiography and Perfusion in the Pig using Hyperpolarized Water, Magn. Reson. Med. In press (2016). doi:10.1002/mrm.26478.

[43] C.H. Cunningham, J.Y. Lau, A.P. Chen, B.J. Geraghty, W.J. Perks, I. Roifman, G.A. Wright, K.A.

Connelly, Hyperpolarized 13 C Metabolic MRI of the Human Heart: Initial Experience, Circ. Res. 119 (2016) 1177-1182. doi:10.1161/CIRCRESAHA.116.309769.

[44] T. Wenckebach, Essentials of Dynamic Nuclear Polarization, Spindrift Publications, The Netherlands, 9 May 2016. ISBN 9789075541182.

Paper III

Hyperpolarized ^{13}C MR Angiography

Kasper W. Lipsø[1,2], Peter Magnusson[2], and Jan Henrik Ardenkjær-Larsen[1,2,3*]

[1]Department of Electrical Engineering, Technical University of Denmark, Kgs. Lyngby, Denmark; [2]Danish Research Centre for Magnetic Resonance, Centre for Functional and Diagnostic Imaging and Research, Copenhagen University Hospital Hvidovre, Denmark; [3]GE Healthcare, Brøndby, Denmark

Abstract: Magnetic resonance angiography (MRA) is a non-invasive technology that can be used for diagnosis and monitoring of cardiovascular disease; the number one cause of mortality worldwide.

Hyperpolarized imaging agents provide signal enhancement of more than 10, 000 times, which implies large reduction in acquisition time and improved spatial resolution. We review the role of hyperpolarized ^{13}C agents for MR angiography and present the literature in the field. Furthermore, we present a study of the benefit of intra-arterial injection over intravenous injection of hyperpolarized agent for cerebral angiography in the rat, and compare the performance of two standard angiographic pulse sequences, the gradient echo (GRE) sequence and the balanced steady-state free precession (bSSFP).

2D coronal cerebral angiographies using intra-arterial injections were acquired with a GRE sequence with in-plane resolution of 0.27 mm and matrix size 256x128, and 2D coronal cerebral angiographies were acquired with a bSSFP sequence with in-plane resolution of 0.55 mm and matrix size 128x64.

The bSSFP sequence provides higher SNR in phantoms than the GRE sequence. Similarly, intravenous injections are imaged with higher SNR with the bSSFP sequence, where the signal destruction of the GRE sequence is avoided. However, for intra-arterial injections, the bSSFP sequence results in strong artefacts, and the GRE sequence is preferred.

Hyperpolarized MRA presents many challenges and cannot currently compete with conventional contrast enhanced MRA. Further research may change this since hyperpolarization is still an immature methodology.

Keywords: Magnetic resonance angiography, hyperpolarization, ^{13}C, HP001, DNP.

INTRODUCTION

Angiographic techniques are important in the diagnosis and treatment of medical conditions such as emboli, stenosis and intracranial aneurysms**.** The most frequently applied angiographic techniques are ultrasound imaging (US), computed tomography (CT), and nuclear medicine imaging such as PET [1]. US is non-invasive, but has its limitations in imaging of the cerebrovascular system, where cranium and tissue-bone interfaces cause attenuation and disturbance of the signal. CT provides high resolution images within short acquisition time, but the radiation exposure is a major limitation of repeated use. PET angiography can provide information about the functional metrics in the vascular system, however the low spatial resolution and the administration of radioactive contrast agent makes PET less preferable [2, 3]. Magnetic resonance angiography (MRA) is generally used with a contrast agent based on e.g. gadolinium [4] that reduces the T_1 of the blood, but flow dependent techniques such as time-of-flight (TOF) or phase contrast can also be employed without injections [5, 6]. One class of MRA contrast agents includes blood pool agents such as Clariscan™; ultra-small super paramagnetic iron oxide particles that stay in circulation for hours [7]. Thus, the arterial vascular system alone can be imaged during the first pass of the contrast agent, whereas the entire vascular system can be acquired in a large time window allowing signal averaging for high resolution. Time-resolved fast imaging can be applied to capture the dynamics [8].

Hyperpolarized ^{13}C MRA

Conventional coronary proton MRA acquisition time depends on parameters such as matrix size and repetition time, and is typically acquired over several minutes [9]. Thus, respiratory and cardiac motion, as well as movements of the patient will affect the image quality. The need for faster image acquisition has catalyzed research in hyperpolarized (HP) MRI, where the signal can be enhanced by orders of magnitude compared to the thermal signal [10]. The polarization is obtained via dissolution Dynamic Nuclear Polarization (DNP). The sample is mixed with an Electron Paramagnetic Agent (EPA) and cooled to low temperature in a magnetic field, by which the unpaired electrons of the EPA reach a polarization of unity. The polarization of the electrons is transferred to the nuclear spins by irradiating with microwaves at the resonance frequency of the electrons. The high polarization of the nuclear spins are preserved to the liquid phase by rapidly dissolving in a dissolution medium, before the agent is injected. The polarization of the injected volume is more than 4 orders of magnitude larger than the thermal signal of ^{13}C. Therefore, the signal in a ^{13}C image obtained after injection of a hyperpolarized substance is proportional to the concentration of the agent in question, and the image acts as a qualitative map of perfusion [11-14]. Likewise, the conversion of hyperpolarized ^{13}C-labelled compounds such as pyruvate can be followed with Magnetic Resonance Spectroscopic Imaging (MRSI) [15-17], and the metabolic activity monitored [18].

Hyperpolarized MRA provides imaging of the injected substance in the vascular system, and thus provides a direct signal from the hyperpolarized spins in the blood. In addition, hyperpolarized MRA is not dependent on flow velocity as e.g. TOF-imaging, where flow close to the vessel walls appears with a low signal due to low flow velocity. In 2002 Golman *et al.* demonstrated that angiography in rats using hyperpolarized ^{13}C is possible with bis-1, 1(hydroxymethyl)-[1-^{13}C]cyclopropane-D8 (HP001) as imaging agent and demonstrated that both ParaHydrogen-Induced Polarization (PHIP) [19] and dissolution DNP [20] can be used for hyperpolarized ^{13}C angiography with i.v. agent administration (Fig. **1**).

*Address correspondence to this author at the DTU Electrical Engineering,
Ørsteds Plads, Building 349, room 106, 2800 Kgs. Lyngby, Denmark;
Tel: (0045) 4525 3918; E-mail: jhar@elektro.dtu.dk

Svensson *et al*. [21] studied ^{13}C cerebral MRA in the rat and found that high SNR can be obtained in both the head and neck area (Fig. **2**) and in the thoracic/abdominal region using the balanced steady state
free precision pulse sequence (bSSFP). Later, Olsson *et al.* [22] presented a study on hyperpolarized ^{13}C coronary MRA in a pig model with i.a. injection. Recently, hyperpolarized H_2O has been applied in angiography with the advantage of applicability on clinical scanners with ^{1}H channels only, as well as higher achievable magnetization due to a larger magnetic moment [23].

Fig. (1). Angiographic image of the rat heart region after i.v. injection in the tail vein. Acquired with a gradient spoiled, gradient echo sequence (TE/TR = 4 ms/9.5 ms, α = 10°, FOV = 70x70 mm^2, matrix = 128x128, slice = 30 mm, scan time = 2 s). With permission from [19] and Elsevier.

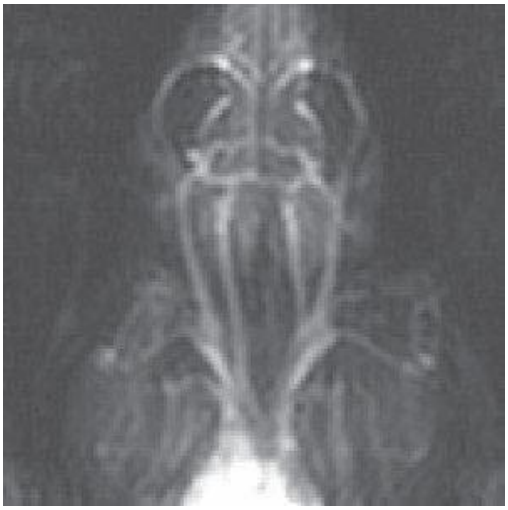

Fig. (2). First image in a series of angiograms covering the head and neck region. The image has been acquired on a 2.35 T animal MRI system with a trueFISP sequence (TE/TR = 1.8 ms/3.6 ms, FOV = 70x70 mm^2, and matrix = 64x64, with read oversampling). Major vessels appear with SNR of 74-76, but some enhancement of other tissue is observed as well. With permission from [21] and John Wiley and Sons.

For cerebral angiography in the rat, the hyperpolarized substance is typically injected using either intravenous (i.v.) injection through one of the tail veins, or intra-arterial (i.a.) injection where a catheter is operated into one of the carotid arteries. The injection method affects the system in various ways and *e.g*. movement of the catheter and the reaction of the vessels to increased pressure will result in difference in signal-to-noise ratio (SNR) and artefacts in the images. Thus, the

MR sequence must be chosen and optimized in accordance with the injection method. Furthermore, the injection type will enhance specific characteristics of the arterial and venous network. An even distribution in the vasculature should be observed with an intravenous injection when the hyperpolarized substance is distributed through the heart of the animal. When the substance is injected in a carotid artery, only arteries branching from that specific carotid artery as well as the corresponding veins are highlighted.

^{13}C Agent and MRI Considerations

The ^{13}C-labelled agent HP001 is chosen for its long T_1 (*in vitro*, 2.35 T: $T_1 \approx$ 82 s, $T_2 \approx$18 s; *in vivo*, 2.35 T: $T_1 \approx$ 38 s, $T_2 \approx$ 1.3 s) [21]. This means that the signal decay should be caused mainly by dilution in the vasculature and extravasation of the agent to the surrounding tissue, and to a smaller extent by relaxation processes.

The bSSFP imaging technique has been demonstrated to be a rapid, high-SNR technique for angiography and spectroscopic applications using hyperpolarized substances (Fig. **2**) [21, 22, 24, 25]. The gradient echo (GRE) technique has been used extensively for single resonance HP lung imaging [26-28], but less for HP- angiography using ^{13}C-labeled substances. A theoretical basis and *in vitro* measurement comparison between bSSFP and GRE for the HP angiography application was performed by Svensson *et al.* [21], but *in vivo* comparisons between the combinations of the two imaging techniques (bSSFP and GRE) and the two injection techniques (i.v. and i.a.) is to our knowledge not performed.

In this review we demonstrate the current possibilities of a hyperpolarized ^{13}C-labelled agent for MRA and investigate the difference between intravenous and intra-arterial injection with the GRE and bSSFP imaging sequences.

METHODS

Polarization

Bis-1, 1-(hydroxymethyl)-[1-^{13}C]cyclopropane-D8 (HP001) was used as the imaging agent to obtain long relaxation times of the ^{13}C nuclei. Trityl OX063 (Oxford Instruments, Abingdon UK) was used as paramagnetic agent. A batch consisting of 18.0 mg OX063, 500 mg HP001, 180 mg water and 15 L Dotarem (1: 10 dilution, Guerbet, Paris, France) was prepared. 100 L sample was polarized using an Oxford Instruments Hypersense, 3.35 T, 1.4 K, by irradiation with microwaves at 94.112 GHz for one hour. The polarization time constant was 1800 s. The sample was dissolved in 1 mL PBS buffer with 0.01 g/L EDTA diluted in 3 mL NaCl (9 g/L). The ^{13}C concentration in the final solution was 100 mmol/L. The solution temperature was approximately 37 °C

and the pH 7.5-8. The time from dissolution to injection start was 14-18 s and the polarization was 20-25% at time of injection.

Animal Preparation

All animal experiments were carried out in compliance with the guidelines for use and care of laboratory animals and were approved by the Danish Inspectorate of Animal Experiments, approval 2012-15-2934-00244.

Male Sprague Dawley rats weighing 240-320 g were anaesthetized with 1.8% isoflurane in air mixed with 5 % oxygen adjusted to a respiration rate of 75±10 min^{-1} and mounted in an animal holder. The body temperature was kept at 38±1 °C with hot air flow.

Tail vein catherization: A catheter was inserted in a tail vein for i.v. contrast agent administration. A volume of 1.5 mL was injected over 6-9 s.

Carotid artery catherization: Carotid artery injections were prepared by incision in the ventral neck of the rat and isolation of the right carotid artery, before inserting and securing the catheter in the artery. The catheter was fixed to the skin with tape. A volume of 1.0 mL was injected over 6-9 s.

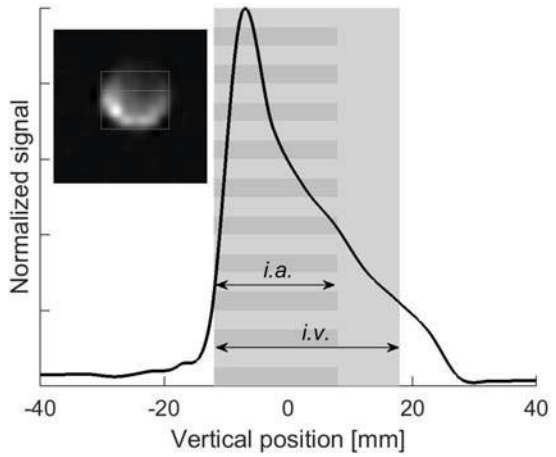

Fig. (3). The vertical sensitivity profile of the coil from a sum of squares CSI image of a spherical bicarbonate phantom (small insert). The FOV and slab position of the i.v. (bSSFP) acquisitions and the thinner slab of the i.a. (GRE) acquisitions are indicated.

MR Scanner System and Pulse Sequences

Data was acquired on a 4.7 T imaging system (Agilent, Direct Drive, VnmrJ 4.0) using a $^{13}C/^{1}H$ RF volume coil combined with a ^{13}C 4-channel surface array coil (receive-only, 50 mm inner diameter, RAPID Biomedical GmbH, Germany). The receiver coil was placed dorsal with the animal supine. Fig. **3** shows the profile of the coil sensitivity measured as the sum-of-squares image of a CSI acquisition of a spherical bicarbonate phantom. The position of the GRE slab is indicated as the shaded area. The bSSFP slab is overlapping, but extends 10 mm in the anterior direction. The sensitivity is highest in the region closest to the coil elements, thus the sensitivity of the vessels in this region is more than twice the sensitivity in the outer region of the slab. The system was shimmed to a proton line width of less than 110 Hz over the field-of-view (FOV). The image reconstruction applied the sum-of-squares algorithm where the signal in each pixel is the square root of the sum of the squares of the signal from each individual array coil element. The background noise is measured in a ROI of 20x20 pixels in an area away from the hyperpolarized signal.

Coil Sensitivity measurements: The coil sensitivity is assessed with a CSI pulse sequence with FOV 80x80 mm^2, matrix size 16x16, α = 10°, TR = 75 ms on a spherical phantom of 1.0 M bicarbonate (38 mm diameter).

HP-^{13}C-MRA - bSSFP: The hyperpolarized signals were acquired using a single-shot bSSFP sequence with 110° flip angle (α). An /2-pulse preparation pulse was implemented at time TR/2 before the first excitation pulse to approach a steady state like situation faster and a corresponding flip-back pulse was implemented at the end of each image acquisition to restore the longitudinal magnetization for the following time frame. The angiographic images had a Field-Of-View (FOV) of 70x35 mm^2 and a slab thickness of 30 mm placed coronal in the head and neck region. The matrix size was 128x64. The repetition time and echo time were set to minimum, TR/TE = 6.95/3.48 ms. A bandwidth of 50 kHz yielded a total image acquisition of 450 ms for each image. The sequence was started when the solution had been fully injected to capture the maximum possible signal.

HP-^{13}C-MRA, GRE: The GRE sequence was applied with an FOV of 70x35 mm^2, a slab thickness of 20 mm and with matrix size 256x128. The pulse length was 2 ms and the repetition and echo times were TR/TE = 10.16/5.10 ms. The total acquisition time for an image was 1300 ms with α = 5° and imaging was repeated over 30 time frames. Acquisition was started when injection was initiated to capture the maximum signal strength.

^{1}H MRA: Proton angiographic images were acquired with a 1H quadrature coil (M2M imaging corporation, Cleveland, Ohio, USA) with inner diameter of 35 mm. A 3D GRE sequence with TR/TE = 90/2.47 ms, α = 40°, FOV of 30x35x20 mm^3, matrix size 256x256x64 was used after an intravenous injection of 50 L Clariscan™ (NC100150, NYCOMED IMAGING AS, Oslo, Norway). The total acquisition time was 25 minutes.

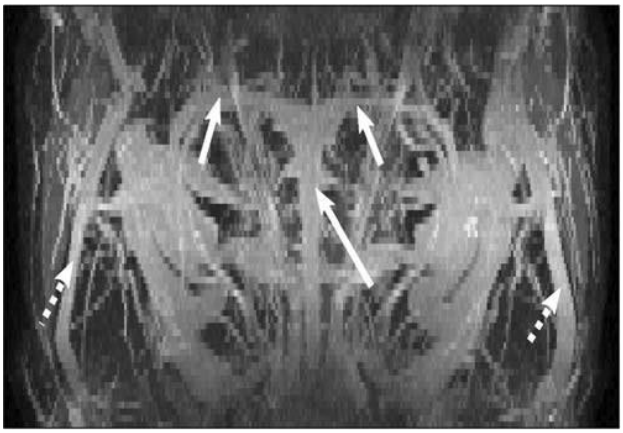

Fig. (4). Coronal image of cerebral vessel structure acquired with a 3D gradient echo sequence after injection of NC100150. The large arrow indicates the superior sagittal sinus, the small arrows indicate the transverse sinuses, and the dotted arrows indicate the superficial temporal vein.

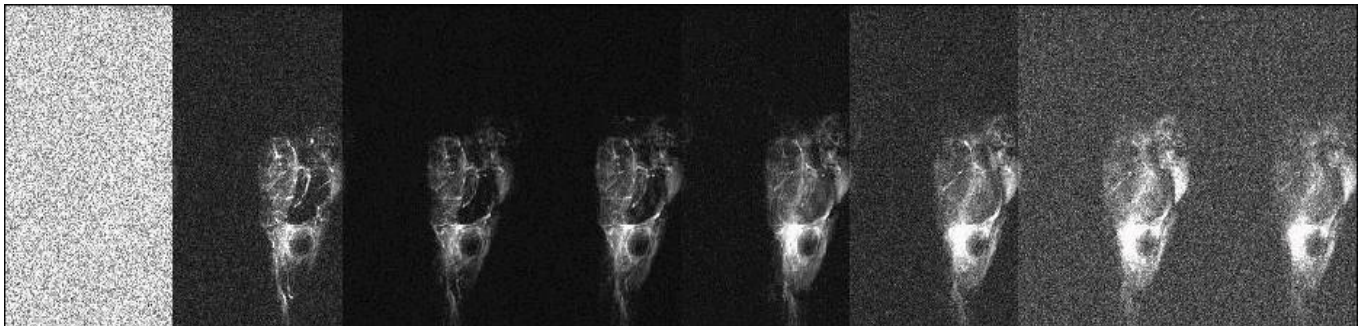

Fig. (5). Time series of GRE images initiated after injection of hyperpolarized HP001 through the right carotid artery. 1.3 s between each frame.

Fig. (6). Image of GRE sequence (4th frame) initiated after injection of hyperpolarized HP001 through the right carotid artery as overlay on the proton image of Fig. **4**. The veins SSS, TRS (right) and STEMV (right) coincide and the structure of finer vessels appear in the overlay.

RESULTS

^{1}H MRA: Fig. 4 shows a contrast enhanced H 3D GRE image of the cerebral vascular system. The large arrow indicates the superior sagittal sinus (SSS), the small arrows indicate the transverse sinuses (TRS) and the dotted arrows indicate the superficial temporal vein (STEMV), posterior facial.

HP-^{13}C-MRA, GRE: An excitation pulse flip angle of 5° was found the optimal compromise between signal strength and conversion of magnetization during the time series in a separate study (data not shown). A time series of 8 frames during intra-arterial injection is shown in Fig. **5**. The best image is the 4th time frame. The rat brain was centered in the FOV, and arteries and veins of the right side of the head appear with the largest denseness around the brain and towards the nose region. Only a few veins appear in the left half of the image, and only minor signal contribution is visible in the eye region of the right side. Fig. **6** shows the 4th frame as overlay on the proton image. Though the two angiographies are obtained on different animals and positioning, the images are in agreement and major venal structures (SSS, TRS, STEMV) of the right side are identified.

A series of 3 consecutive intra-arterial injections of hyperpolarized HP001 in an animal with intervals of approximately one hour gave SNR 26, 19 and 20, as measured as the ratio between the largest signal observed and the background noise, and demonstrates reproducibility of the result.

18 injections in 10 animals yielded SNR of 17.6±4.5 (Mean±SD).

The corresponding GRE acquisition after an intravenous injection yielded signal from the larger veins but with SNR lower than 10 (acquired in 3 animals, image not shown).

HP-^{13}C-MRA, bSSFP: The signal acquisition bandwidth was studied in the range of 20-100 kHz, and we found 50 kHz to be the optimal balance between high signal and minimal flow artefacts. The sequence was started when the solution had been fully injected to capture the maximum possible signal. In separate experiments (data not shown), the flip angle for the bSSFP- sequence was optimized on thermal phantom experiments where a flip angle of 110° yielded a 22% higher SNR than the corresponding experiment with 60° flip angle and where flip angles higher than 110° did experiments on HP *in vivo* experiments with the bSSFP (data not shown). A time series of bSSFP acquired images with one second intervals is shown in Fig. **7**. SNR of 36 is observed in the first frame and the signal decays rapidly in the following frames. The larger veins (SSS, TRS, STEMV) identified from the overlay appear distinctly in a symmetrical shape, and smaller venal structure appears towards the nose region.

5 injections in 4 different animals yielded SNR of 31.3±20.0 (Mean±SD).

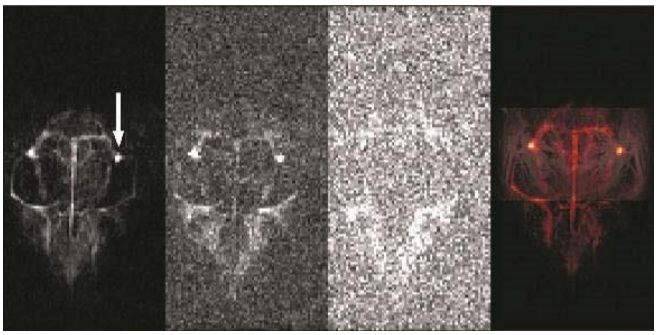

Fig. (7). bSSFP time series after finished injection of hyperpolarized HP001 though the tail vein, 1 s between frames. Right image shows the first image as overlay on the proton image of Fig. **4**. The veins SSS, TRS and STEMV coincide while smaller vessels are not distinguishable.

DISCUSSION

In this study we injected a dose close to the anticipated clinical dose of ca. 0.4 mmol/kg, which is only 25-50% of the dose used in previous studies with a similar polarization. We obtained results similar to Golman *et al.*, where an SNR of 34 was demonstrated in a 128x128 matrix (70x70 mm^2) in the rat heart with an injection of 2-3 mL of 200 mM (ca. 1.5 mmol/kg) solution with polarization of ca. 15% [19]. Svensson *et al.* obtained SNR of 74-76 in a lower resolution of a 64x64 matrix (70x70 mm^2) placed in the rat head and neck region with injection of 3-3.5 mL of 200 mM solution with a polarization of ca. 15% [21].

The bSSFP sequence proved best for injections through the tail vein where the physiological and physical reactions of the animal are negligible, in contrary to injections through a carotid artery, which caused minor mechanical movements of the neck and head region where the catheter is inserted, as well as possible physiological reactions in the imaged region due to the injected bolus' impact on the vessels due to pressure, pH, temperature and tonicity. These movements caused motion artefacts in the bSSFP acquisition, whereas a GRE sequence was more robust to displacements and hence better suitable. Images of carotid artery injection acquired with bSSFP (Fig. **8**) showed a very high SNR of 137. Even though this large signal from the high agent concentration in the arteries was observed, the details of the vascular system were indistinguishable. The sequence was applied with TR/TE = 6.95/3.48 ms, $\alpha = 60°$ in a 128x128 matrix with FOV 60x60 mm^2 in a 30 mm slab.

The strong artefacts may be caused by motion due to the injection as well as B_0-field disturbances caused by the large difference in oxygenated blood and the water introduced with the injection [29].

The contrast agent is further diluted for tail vein injections. The combination of small flip angle GRE acquisition and large dilution in the vascular system resulted in SNR below 10. Therefore, a bSSFP sequence with high flip angle is preferred.

The bSSFP-sequence had a slab thickness of 30 mm. In some experiments, the transverse sinuses align orthogonally to the slice and thus contribute with a large signal in the projection (arrow in Fig. **7**). These outliers cause the large variance where single pixels have yielded signal strength much larger than the rest of the vasculature.

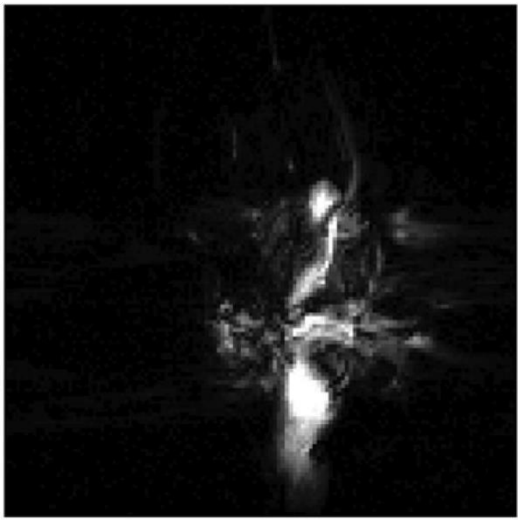

Fig. (8). bSSFP acquired image after intra-arterial injection demonstrates high SNR of 137 and artefacts due to motion and susceptibility change.

Large parts of the image characteristics in Fig. **5** are observed throughout the series, while some features are vanishing in the later time steps. The fact that the operated carotid has been sealed off beneath the catheter explains that some of the branches have closed off during several hours of occlusion in the scanner. The image series and the consistency in the SNR indicate that polarization, injection and data acquisition is reproducible.

When the bSSFP sequence was applied following an intraarterial injection, we observe motion artefacts in the phase encoding direction as shown in Fig. **8**.

Polarizers for DNP have now been installed in several clinics around the world, and studies of HP ^{13}C in humans initiated [30]. As this equipment is being implemented, the application of hyperpolarized agents for angiography will be further studied, and a potential translation towards application in clinical practice explored.

In conclusion, intravenous and intra-arterial injection techniques were used in combinations with optimized GRE- and bSSFP-imaging, respectively, for rat cerebral MRA with a hyperpolarized ^{13}C-labelled agent, and resulted in bSSFP-imaging being preferable for intravenous injections, and GRE-imaging being preferable for the intra-arterial injection technique.

Hyperpolarized ^{13}C MRA is currently unable to compete with contrast enhanced MRA. Considering the complexity of the method (primarily the need for polarizer hardware and the short life time of the signal) it is unlikely that it will become an attractive method. However, hyperpolarization is still an immature methodology, and there are areas where current MRA falls short. With further research into hyperpolarization to

increase the available signal, and possibly increase the life time, there are opportunities for significant improvement.

CONFLICT OF INTEREST

The authors confirm that this article content has no conflict of interest.

ACKNOWLEDGEMENTS

The authors want to thank Sascha Gude for her assistance with the animal preparations.

We acknowledge funding from the Danish Research Council grant 12-127232.

REFERENCES

[1] MacDonald ME, Frayne R. Cerebrovascular MRI: a review of state-of-the-art approaches, methods and techniques. NMR Biomed 2015; 28(7): 767-91.

[2] Schroeder MA, Clarke K, Neubauer S, Tyler DJ. Hyperpolarized magnetic resonance: A novel technique for the *in vivo* assessment of cardiovascular disease. Circulation 2011; 124: 1580-94.

[3] O'Leary DH, Bots ML. Imaging of atherosclerosis: carotid intimamedia thickness. Eur heart J 2010; 31(14): 1682-9.

[4] Kinner S, Maderwald S, Parohl N, *et al.* Contrast-enhanced magnetic resonance angiography in rabbits: evaluation of the gadolinium-based agent P846 and the iron-based blood pool agent P904 in comparison with gadoterate meglumine. Invest Radiol 2011; 46: 524-9.

[5] Beckmann N. High resolution magnetic resonance angiography non-invasively reveals mouse strain differences in the cerebrovascular anatomy *in vivo*. Magn Reson Med 2000; 44: 252-8.

[6] Reese T, Bochelen D, Sauter A, Beckmann N, Rudin M. Magnetic resonance angiography of the rat cerebrovascular system without the use of contrast agents. NMR Biomed 1999; 12: 189-96.

[7] Howles GP, Ghaghada KB, Qi Y, Mukundan S, Johnson GA. Highresolution magnetic resonance angiography in the mouse using a nanoparticle blood-pool contrast agent. Magn Reson Med 2009; 62: 1447-56.

[8] Riederer SJ, Haider CR, Borisch EA, Weavers PT, Young PM. Recent advances in 3D time-resolved contrast-enhanced MR angiography. J Magn Reson Imaging 2015; 42: 3-22.

[9] Kim WY, Danias PG, Stuber M, *et al.* Coronary magnetic resonance angiography for the detection of coronary stenoses. N Engl J Med 2001; 345: 1863-9.

[10] Ardenkjær-Larsen JH, Fridlund B, Gram A, *et al.* Increase in signal-to-noise ratio of >10, 000 times in liquid-state NMR. Proc Natl Acad Sci USA 2003; 100: 10158-63.

[11] Grant AK, Vinogradov E, Wang X, Lenkinski RE, Alsop DC. Perfusion imaging with a freely diffusible hyperpolarized contrast agent. Magn Reson Med 2011; 66: 746-55.

[12] Johansson E, Månsson S, Wirestam R, *et al.* Cerebral perfusion assessment by bolus tracking using hyperpolarized ^{13}C. Magn Reson Med 2004; 51: 464-72.

[13] Johansson E, Olsson LE, Månsson S, *et al.* Perfusion assessment with bolus differentiation: A technique applicable to hyperpolarized tracers. Magn Reson Med 2004; 52: 1043-51.

[14] Lau AZ, Miller JJ, Robson MD, Tyler DJ. Cardiac perfusion imaging using hyperpolarized ^{13}C urea using flow sensitizing gradients.
Magn Reson Med 2015, May 20. [Epub ahead of print].

[15] Day SE, Kettunen MI, Gallagher FA, *et al.* Detecting tumor response to treatment using hyperpolarized ^{13}C magnetic resonance imaging and spectroscopy. Nat Med 2007; 13: 1382-7.

[16] Albers MJ, Bok R, Chen AP, *et al.* Hyperpolarized ^{13}C lactate, pyruvate, and alanine: Noninvasive biomarkers for prostate cancer detection and grading. Cancer Res 2008; 68(20): 8607-15.

[17] Lauritzen MH, Søgaard LV, Madsen PL, Ardenkjær-Larsen JH. Hyperpolarized metabolic MR in the study of cardiac function and disease. Curr Pharm Des 2014; 20: 6162-70(9).

[18] Dodd MS, Ball V, Bray R, *et al. In vivo* mouse cardiac hyperpolarized magnetic resonance spectroscopy. J Cardiovasc Magn Reson 2013; 15: 19.

[19] Golman K, Ardenkjær-Larsen JH, Svensson J, *et al.* ^{13}Cangiography. Acad Radiol 2002; 9(suppl 2): 507-10.

[20] Golman K, Axelsson O, Jóhannesson H, Månsson S, Olofsson C, Petersson. Parahydrogen-induced polarization in imaging: Subsecond ^{13}C angiography. Magn Reson Med 2001; 46: 1-5.

[21] Svensson J, Månsson S, Johansson E, Petersson JS, Olsson LE. Hyperpolarized ^{13}C MR angiography using trueFISP. Magn Reson Med 2003; 50: 256-62.

[22] Olsson LE, Chai C-M, Axelsson O, Karlsson M, Golman K, Petersson JS. MR coronary angiography in pigs with intraarterial injections of a hyperpolarized ^{13}C substance. Magn Reson Med 2006; 55: 731-7.

[23] Ardenkjær-Larsen JH, Laustsen C, Bowen S, Rizi R. Hyperpolarized H_2O MR angiography. Magn Reson Med 2014; 71: 50-6.

[24] Leupold J, Månsson S, Petersson JS, Hennig J, Wieben O. Fast multiecho balanced SSFP metabolite mapping of ^{1}H and hyperpolarized ^{13}C compounds. Magn Reson Mater Phy 2009; 22: 251-6.

[25] Leupold J, Wieben O, Månsson S. Fast chemical shift mapping with multiecho balanced SSFP. Magn Reson Mater Phy 2006; 19: 26773.

[26] Kauczor HU. Hyperpolarized helium-3 gas magnetic resonance imaging of the lung. Top Magn Reson Imaging 2003; 14: 223-30.

[27] Deninger AJ, Månsson S, Petersson JS. Quantitative measurement of regional lung ventilation using ^{3}He MRI. Magn Reson Med 2002; 48: 223-32.

[28] Mugler JP, Altes TA. Hyperpolarized ^{129}Xe MRI of the human lung. J Magn Reson Imaging 2013; 37: 313-31.

[29] Jain V, Abdulmalik O, Propert KJ, Wehrli FW. Investigating the magnetic susceptibility properties of fresh human blood for noninvasive oxygen saturation quantification. Magn Reson Med 2012; 68: 863-7.

[30] Nelson SJ, Kurhanewicz J, Vigneron DB, *et al.* Metabolic imaging of patients with prostate cancer using hyperpolarized [1-^{13}C]pyruvate. Sci Transl Med 2013; 5(198): 198. ra108.

Received: July 19, 2015 **Accepted: November 5, 2015**

Paper IV

FULL PAPER

Magnetic Resonance in Medicine 00:00–00 (2016)

Renal MR Angiography and Perfusion in the Pig Using Hyperpolarized Water

Kasper Wigh Lipsø,[1] Esben Søvsø Szocska Hansen,[2,3] Rasmus Stilling Tougaard,[2,4] Christoffer Laustsen,[2] and Jan Henrik Ardenkjær-Larsen[1,5]*

Purpose: To study hyperpolarized water as an angiography and perfusion tracer in a large animal model.
Methods: Protons dissolved in deuterium oxide (D_2O) were hyperpolarized in a SPINlab dissolution dynamic nuclear polarization (dDNP) polarizer and subsequently investigated in vivo in a pig model at 3 Tesla (T). Approximately 15 mL of hyperpolarized water was injected in the renal artery by hand over 4–5 s.
Results: A liquid state polarization of 5.3±6 0.9% of 3.8 M protons in 15 mL of deuterium oxide was achieved with a T_1 of 24±6 1 s. This allowed injection through an arterial catheter into the renal artery and subsequently high-contrast imaging of the entire kidney parenchyma over several seconds. The dynamic images allow quantification of tissue perfusion, with a mean cortical perfusion of 504 ± 123 mL/100 mL/min.
Conclusion: Hyperpolarized water MR imaging was successfully demonstrated as a renal angiography and perfusion method. Quantitative perfusion maps of the kidney were obtained in agreement with literature and control experiments with gadolinium contrast.

Key words: perfusion; magnetic resonance angiography; hyperpolarization; DNP

INTRODUCTION

Magnetic resonance angiography (MRA) is an important tool for diagnosing various medical conditions such as emboli, stenosis, and aneurysms. More specifically, renal artery MRA allows detection of renal vascular diseases such as fibromuscular dysplasia, venous thrombosis, and arterial dissection (1). Submillimeter resolution can be obtained with proton imaging, and further optimization can be obtained by employing vascular contrast agents such as gadolinium (Gd) based blood pool agents (2) or nanoparticles (3). Despite significant improvement in scanner technology and reconstruction methods (4–6), MRA evaluation of small vessels is still challenging. This is primarily due to the inherent low sensitivity of MR, in which the signal is proportional to the polarization of protons in the blood stream.

It has been demonstrated that this sensitivity problem can be overcome by hyperpolarizing nuclear spins (7). The method has recently been introduced in patients using [1-^{13}C]pyruvate (8). By enhancing the polarization of ^{13}C by many orders of magnitude, the detected signal is increased dramatically, allowing in situ conversion of metabolic ^{13}C-containing compounds to be imaged. The procedure of increasing polarization beyond thermal level, hyperpolarization (HP), can be achieved by dissolution dynamic nuclear polarization (dDNP), in which the high polarization of the high-gamma electrons, at cryogenic temperature and high magnetic field strength, is transferred to the nuclei by irradiation with microwaves. By rapid dissolution in a hot medium, the hyperpolarized nuclei can be brought to liquid state and injected into the patient before the polarization is lost as a result of longitudinal relaxation (7). Alternatively, metabolically inert ^{13}C-labeled molecules can be used for angiographic imaging (9–11), as demonstrated in rodent and porcine models, and for perfusion of rodent organs (12–15) or of tumor models (16,17). ^{13}C or ^{15}N-labeled molecules for angiography and perfusion imaging exploits the long T_1 for selected ^{13}C and ^{15}N molecules and the low signal background (18). Despite these advantages, these molecules exhibit partial permeability and active transport limitations.

A more accurate technique for water perfusion measurements is therefore necessary (19,20). A way to measure the perfusion of water molecules directly exists, using ^{15}O-labeled water as a tracer for positron emission tomography (PET) imaging (21,22), with the main drawbacks being the use of a radioactive tracer and the limited spatial and temporal resolution of PET. Using hyperpolarized water for angiographic and perfusion imaging overcomes several of these limitations. Water protons for imaging have previously been hyperpolarized by use of the Overhauser effect (23). However, the maximum achievable magnetization is limited. Typically, an enhancement of 100 times at 0.35T can be obtained for pure water (H_2O), corresponding to a polarization of 0.001%. Higher polarizations have been reached with dissolution-DNP using the 3.35T HyperSense polarizer, in which 3–4mL of 5M ^{1}H in D_2O with a polarization of 3–5% have been applied to biomolecular NMR studies

[1]Department of Electrical Engineering, Technical University of Denmark, Kgs, Lyngby, Denmark.

[2]Department of Clinical Medicine, MR Research Centre, Aarhus University, Aarhus, Denmark.

[3]Danish Diabetes Academy, Odense, Denmark.

[4]Department of Cardiology - Research, Aarhus University Hospital, Aarhus, Denmark.

[5]GE Healthcare, Brøndby, Denmark.

Grant sponsor: Danish Research Council; Grant number: 12-127232; Grant sponsor: Danish National Research Foundation; Grant number: DNRF124.

*Correspondence to: Jan Henrik Ardenkjær-Larsen, Ph.D., DTU Electrical Engineering, Ørsteds Plads, Building 349, Room 126, 2800 Kgs. Lyngby, Denmark. Tel: (0045) 4525 3918; E-mail: jhar@elektro.dtu.dk.

Received 28 June 2016; revised 8 August 2016; accepted 1 September 2016

DOI 10.1002/mrm.26478

Published online 00 Month 2016 in Wiley Online Library (wileyonlinelibrary. com).

(24) or MR angiographies in the rat (25). Correcting for the difference in proton concentration, this corresponds to an available signal of two orders of magnitude larger than the Overhauser experiments. Imaging of hyperpolarized protons allows for the use of coils and pulse sequences already available in the clinical setting. Much more effort has gone into optimizing pulse sequences for optimal performance for proton imaging than for other nuclei. Moreover, the magnetization achievable with hyperpolarized water is superior to other nuclei, because of its large gyromagnetic ratio ($\gamma_{1H} \approx 4 \cdot \gamma_{13C}$) and the potentially high proton concentration. As a tracer for perfusion, hyperpolarized water has additional interesting properties. Water diffuses freely in the vascular bed and intracellularly, hence providing information not obtainable with larger compounds such as Gd-based MR contrast agents or larger nuclear tracers. Compared with the slow washout rate of conventional MR contrast agents (26), the T_1 value of hyperpolarized tracers hampers image acquisition, as well as reduces the spatial range of measurable perfusion. However, the signal enhancement of hyperpolarization facilitates higher resolution and faster image acquisition, which allow us to trace the permeable protons in detail—with the stated limitations.

The purpose of this study was to demonstrate that hyperpolarized water can be used as a tracer to provide subsecond, high-resolution angiographies in pigs by intra-arterial injection in the renal artery, and that accurate perfusion maps can be obtained with good signal-to-noise ratio (SNR).

METHODS

The polarizer and fluid path have been described in detail in (27). Briefly, the dDNP polarizer operates at 5T and approximately 0.9 K. The sample and solvent was loaded into a fluid path that allows the sample to be polarized in the magnetic field at low temperature under microwave irradiation. The solvent was contained in a syringe that connects to the vial using two concentric tubes (inner and outer tube) and a valve. The syringe was placed in a heater/pressure module outside the polarizer cryostat. During dissolution, the hyperpolarized solution leaves the polarizer through an exit tube.

Sample and Solvent Preparation

A sample of 1mL 30mM TEMPO (2,2,6,6-Tetramethylpiperidine 1-oxyl, 98%, Sigma Aldrich, Copenhagen, Denmark) in H_2O/glycerol 1:1 (w/w) was prepared. The sample was placed in the fluid path vial and frozen in liquid nitrogen. Dissolution medium (DM) consisted of D_2O with 1mM calcium disodium ethylenediaminetetraacetic acid (EDTA) and 9g/L NaCl (both Sigma Aldrich, Denmark).

31.01g DM (28mL) was filled in the syringe and degassed by bubbling with helium gas for 10min. The fluid path was flushed with helium gas for 2min to remove air and ensure clear passage.

Polarization

The sample vial was rapidly transferred from the liquid nitrogen bath to the 5T magnet in the polarizer (SPINlab, GE Healthcare, Brøndby, Denmark). The sample was irradiated with approximately 50 mW microwaves at 139.923 GHz for 1h.

Dissolution

The syringe containing the DM was heated to 130C for 1h before dissolution while being under pressure. The piston of the syringe was driven with 16-bar pressure during dissolution. The dissolved sample was injected through the exit tube into a separatory funnel (100mL) containing 25mL of heptane (>99%, Sigma Aldrich, Copenhagen, Denmark) to extract the radical from the aqueous phase. The heptane had been degassed by flushing with helium gas in the funnel for 10min. The funnel was shaken heavily during dissolution for a total of 10 s from dissolution start. The lower, aqueous phase was extracted into a syringe before transferring to the scanner room. The proton concentration in the dissolved sample was analyzed by NMR after the addition of 2M formate solution as reference.

Animal Protocol

All animal experiments were carried out in compliance with the guidelines for use and care of laboratory animals and were approved by the Danish Inspectorate of Animal Experiments. Four healthy 30-kg female Danish domestic pigs were presedated with intramuscular injection of Stressnil (1mL/kg) and Midazolam (1mL/kg), and anesthesia was maintained by continuous infusion of Propofol (0.4mg/kg/h) and Fentanyl (8mg/kg/h). The animals were intubated and mechanically ventilated with a 60% O_2-air mix.

A 6-F introducer sheath was positioned in the left common femoral artery by ultrasound guidance to allow access for a 6F, JR 4.0 angiography catheter to be placed in the left main renal artery using X-ray guidance. The angiography catheter was repeatedly flushed with heparinized sterile water to avoid occlusion. 15mL HP water was injected over 5 s, initiated approximately 22 s after dissolution.

Through a vein access in the right ear, a bolus of 0.2 mmol/kg Gd-DTPA (Gadobutrol, Gadovist, Bayer Schering Pharma, Berlin, Germany) was administered manually for conventional T_1-DCE-MRI.

MRI Acquisition

MRI detection was performed on a 3T GE HDx with an eight-channel cardiac array receiver coil (GE Healthcare, Milwaukee, Wisconsin, USA). Phantom experiments were performed with a gradient echo sequence using a flip angle of 1°, matrix size 128 x 128, field of view (FOV)=$(24mm)^2$ in a slab of 40 mm with repetition time (TR)=3 ms, echo time (TE)=0.784 ms. The acquisition time of each frame was 450 ms, and images were acquired with a time delay of 1 s.

Axial and coronal images were acquired to cover both kidneys to allow for planning of the angiography slice

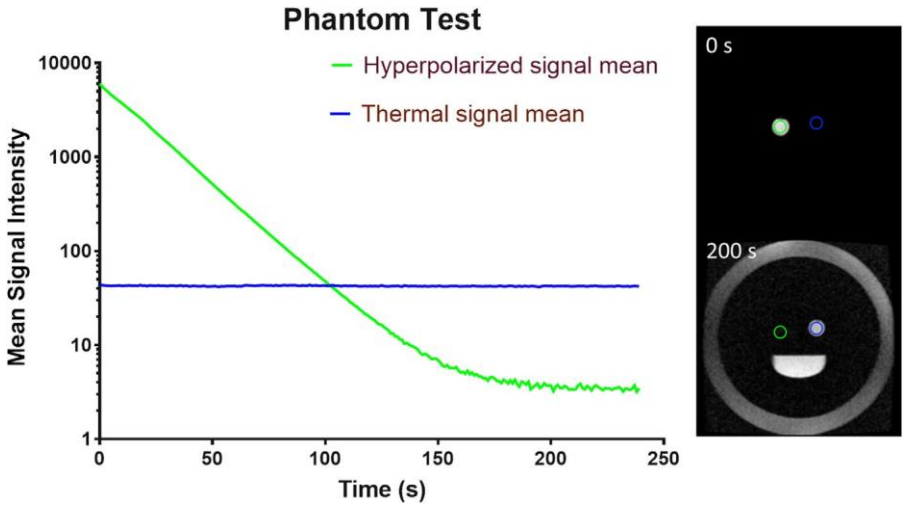

FIG. 1. ROI signal means of the hyperpolarized ^1H in D_2O (green, decaying signal) and the H_2O thermal phantoms (blue, steady signal). The phantoms consist of two syringes inside a loading phantom (ring structure). Images (individually scaled) are shown at 0 and 200 s. The hyperpolarized MR signal is initially 211 times stronger than the thermal H_2O signal, and the T_1 of the decay is 24 s. The hyperpolarized signal decays into the noise, as the ^1H density is approximately 20 times lower than the thermal H_2O sample.

for hyperpolarized water imaging. The planning sequence (before injection of hyperpolarized water) was as follows: a standard steady-state free precession sequence (TE=1.1 ms, TR=2.7 ms, flip angle (FA) of 35°, image matrix of 256×256, FOV=340×340 mm^2, in-plane resolution = 1.3 mm, slice thickness = 3 mm).

Angiographies (during injection of the hyperpolarized water) were acquired in the coronal plane of the left kidney using a gradient echo sequence with 5° FA, slice thickness 40 mm, TR=3.4 ms, TE=0.984 ms, 256×256 matrix, FOV=140×140mm^2. The acquisition time was 870 ms. The Gd-perfusion sequence was executed with the following parameters: spoiled gradient echo, inversion time = 850 ms, 10° FA, slice thickness 50 mm, TR=2 s, TE=1.4 ms, 128×128 matrix, FOV = 290×290 mm^2.

MRI Postprocessing

Phantom data were analyzed using MATLAB (MathWorks, Natick, Massachusetts, USA). Renal perfusion maps were calculated in OsiriX (Pixmeo, Geneva, Switzerland) using an open source OsiriX plug-in for DCE-MRI perfusion analysis (29). A pixel-by-pixel model-free fast deconvolution was applied, assuming a direct signal enhancement of the hyperpolarized water, a hematocrit of 0.45 and a regularization of 0.15. The hyperpolarized arterial input function (AIF) was fixed at the end of the arterial bolus (7 s in Fig. 2), to avoid the injection characteristics of the AIF. The Gd-T_1-DCE contrast was similarly analyzed by a pixel-by-pixel model-free fast deconvolution, assuming a relative signal enhancement accounting for the signal modulations by the contrast agent.

RESULTS

The average proton concentration in the dissolved sample was 3.846±0.22 M (n=10). 18±1 mL of dissolved sample was produced. The polarization was measured by placing a syringe with dissolved hyperpolarized sample next to a similar syringe of saline and image a slice of 40 mm (same sequence as for the angiographies). The signal obtained from the phantoms is plotted in Figure 1.

The initial hyperpolarized signal was 211 times the mean signal in the thermal phantom (110M ^1H) of Boltzmann polarization (10.5 ppm). Thus, after correction for the proton concentration, the polarization was 5.3±0.9% (n=4). A T_1 of 24±1 s was measured.

Angiographies of the arterial system of the left kidney were produced with hyperpolarized water in four animals (Fig. 2). Perfusion maps were calculated for the four animals (Fig. 3). A mean cortical perfusion of 504±123mL/100mL/min was found. Some folding of the signal from the catheter appears in the images in Figure 3c and 3d. The arterial input function is shown in Figure 2 along with the cortical signal curve. The arterial input function is heavily modulated by the direct injection, as seen by the flat top of the input from 3–7 s. Trimming the AIF to the end of the injection was found to reproducibly reflect the average perfusion found by Gd-T_1DCE analysis of 450 mL/100mL/min (n=2).

DISCUSSION

The main finding of this study was the demonstration of a feasible method for acquiring reproducible renal angiograms and perfusion maps using hyperpolarized water with both high resolution and high SNR in a large animal model resembling human renal anatomy and physiology. The produced volume of 15mL exceeds the previously demonstrated volumes of 4mL produced on the HyperSense (25), and the SPINlab and fluid path technology facilitates sterile samples for clinical applications (27). Good agreement was found between the calculated hyperpolarized water perfusion and both the reported Gd-based perfusion values in healthy porcine models (30) and with our Gd-based perfusion measurements (average of 450mL/100mL/min). Further optimization of MRI sequence, sample preparation, radical extraction, as well as automation and consistency of the injection process are likely to enhance image quality and applicability further. A longer bolus injection to approximate a Heaviside input function may improve accuracy. The primary limitation is the short lifetime of the hyperpolarized water, reducing its applicability to highly perfused organs. The use of direct arterial injection imposes

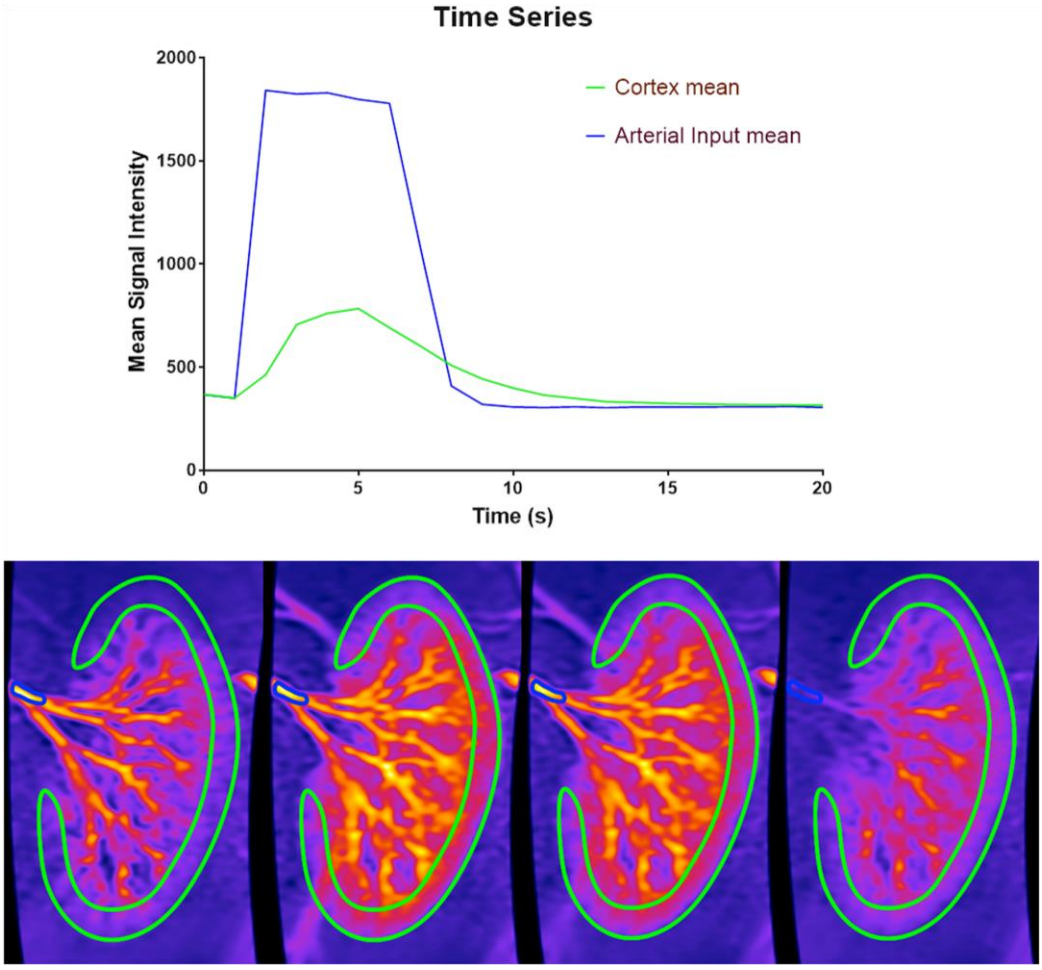

FIG. 2. Image intensity in the arterial input ROI and cortex ROI for the same pig. Images visualize time steps at 3, 5, 7, and 9 s.

challenges on both animal handling (future clinical usability) and on the modeling of the perfusion information. The angiograms are of excellent quality; however, Gd-based and noncontrast angiography of the renal arteries is currently providing sufficient diagnostic quality. In contrast, since the discovery of Nephrogenic Systemic

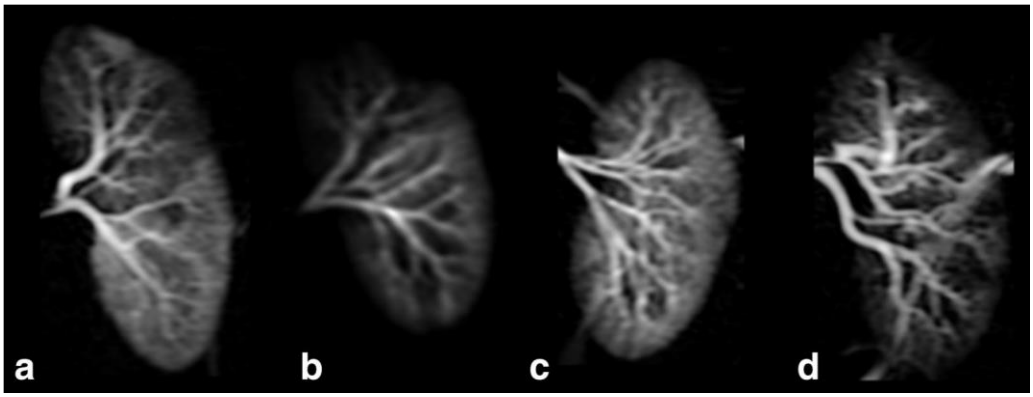

FIG. 3. A, B, C, D show perfusion maps generated from four individual pigs with a mean cortical perfusion of 504 ± 123 mL/100 mL/min. C is the same pig as shown in Figure 2.

Fibrosis, new MR methods to measure perfusion may have a role. In addition to the specific extravasation properties of water relative to any other molecule, the signal that can be created by hyperpolarized ^{1}H exceeds that of any other magnetic nucleus (eg, ^{13}C).

Both the radical and molecular oxygen in the sample induce dipolar relaxation that reduces the longitudinal relaxation time T_1. Thus, the radical extraction in the organic phase as well as the oxygen removal during preparation are crucial elements for achieving long T_1 and, ultimately, high polarization after substance transferring. TEMPO was chosen without optimization as a good compromise between water solubility and preferential partitioning to the heptane phase. The proton concentration was chosen as an optimal compromise between the limitation of the intermolecular dipolar relaxation between proton nuclei and achievement of high signal in the injectable sample. We believe that the 1 H signal (polarization) can be further increased by a factor of five by optimization of the solid-state DNP polarization and the reduction of losses in the dissolution.

The ability to hyperpolarize water protons in a polarizer designed for clinical use, with sufficient polarization to allow ultrafast angiographic and perfusion assessment, shows great promise for future clinical translation.

REFERENCES

1. Attenberger UI, Morelli JN, Schoenberg SO, Michaely HJ. Assessment of the kidneys: magnetic resonance angiography, perfusion and diffusion. J Cardiovasc Magn Reson 2011;13:1–13.
2. Kinner S, Maderwald S, Parohl N, Albert J, Corot C, Robert P, Barkhausen J, Vogt FM. Contrast-enhanced magnetic resonance angiography in rabbits: evaluation of the gadolinium-based agent p846 and the iron-based blood pool agent p904 in comparison with gadoterate meglumine. Invest Radiol 2011;46:524–529.
3. Howles GP, Ghaghada KB, Qi Y, Mukundan S, Johnson GA. High-resolution magnetic resonance angiography in the mouse using a nanoparticle blood-pool contrast agent. Magn Reson Med 2009;62:1447–1456.
4. Addy NO, Ingle RR, Wu HH, Hu BS, Nishimura DG. High-resolution variable-density 3D cones coronary MRA. Magn Reson Med 2015;74: 614–621.
5. Koktzoglou I, Murphy IG, Giri S, Edelman RR. Quiescent interval low angle shot magnetic resonance angiography of the extracranial carotid arteries. Magn Reson Med 2016;75:2072–2077.
6. Nezafat M, Henningsson M, Ripley DP, Dedieu N, Greil G, Greenwood JP, Bornert P, Plein S, Botnar RM. Coronary MR angiography at 3T: fat suppression versus water-fat separation. Magn Reson Mater Physics Biol Med 2016. doi: 10.1007/s10334-016-0550-7.
7. Ardenkjær-Larsen JH, Fridlund B, Gram A, Hansson G, Hansson L,Lerche MH, Servin R, Thaning M, Golman K. Increase in signal-to-noise ratio of>10,000 times in liquid-state NMR. Proc Natl Acad Sci U S A 2003;100:10158–10163.
8. Nelson SJ, Kurhanewicz J, Vigneron DB, et al. Metabolic imaging of patients with prostate cancer using hyperpolarized [1- ^{13}C] pyruvate. Sci Transl Med 2013:5;198ra108.
9. Golman K, Axelsson O, Johannesson H, Månsson S, Olofsson C, Petersson JS, Parahydrogen-induced polarization in imaging: subsecond 13C angiography. Magn Reson Med 2001;46:1–5.
10. Svensson J, Månsson S, Johansson E, Petersson JS, Olsson LE. Hyperpolarized 13C MR angiography using trueFISP. Magn Reson Med 2003;50:256–262.
11. Lipsø KW, Magnusson P, Ardenkjær-Larsen JH. Hyperpolarized (13)C MR angiography. Curr Pharm Des 2016;22:90–95.
12. Qi H, Nørlinger TS, Nielsen PM, Bertelsen LB, Mikkelsen E, Xu Y,Stødkilde-Jørgensen H, Laustsen C. Early diabetic kidney maintains the corticomedullary urea and sodium gradient. Physiol Rep 2016;4:1–6.
13. Lau AZ, Miller JJ, Robson MD, Tyler DJ. Cardiac perfusion imaging using hyperpolarized (13)C urea using flow sensitizing gradients. Magn Reson Med 2016;75:1474–1483.
14. Lau AZ, Miller JJ, Robson MD, Tyler DJ. Simultaneous assessment of cardiac metabolism and perfusion using copolarized [1-(13) C]pyruvate and (13) C-urea. Magn Reson Med 2016. doi: 10.1002/mrm. 26106.
15. Von Morze C, Bok RA, Reed GD, Ardenkjær-Larsen JH, KurhanewiczJ, Vigneron DB. Simultaneous multiagent hyperpolarized 13C perfusion imaging. Magn Reson Med 2014;72:1599–1609.
16. Park I, von Morze C, Lupo JM, Ardenkjær-Larsen JH, Kadambi A, Vigneron DB, Nelson SJ. Investigating tumor perfusion by hyperpolarized ^{13}C MRI with comparison to conventional gadolinium contrast-enhanced MRI and pathology in orthotopic human GBM xenografts. Magn Reson Med 2016. doi: 10.1002/mrm.26155.
17. Von Morze C, Larson PEZ, Hu S, Yoshihara HAI, Bok RA, Goga A, Ardenkjær-Larsen JH, Vigneron DB. Investigating tumor perfusion and metabolism using multiple hyperpolarized 13C compounds: HP001, pyruvate and urea. Magn Reson Imaging 2012;30:305–311.
18. Durst M, Chiavazza E, Haase A, Aime S, Schwaiger M, Schulte RF. α-trideuteromethyl[15N]glutamine: A long-lived hyperpolarized perfusion marker. Magn Reson Med 2016. doi: 10.1002/mrm.26104.
19. Bergmann SR, Herrero P, Markham J, Weinheimer CJ, Norine M. Noninvasive quantitation of myocardial blood flow in human subjects with oxygen-15-labeled water and positron emission tomography. J Am Coll Cardiol 1989;14:639–652.
20. De Langen AJ, van den Boogaart VEM, Marcus JT, Lubberink M. Useof H2(15)O-PET and DCE-MRI to measure tumor blood flow. Oncologist 2008;13:631–644.
21. Herscovitch P, Markham J, Raichle ME. Brain blood flow measured with intravenous H215O. I: Theory and error analysis. J Nucl Med 1983;24:782–789.
22. Raichle ME, Martin WRW, Herscovltch P, Mintun MA, Markham J.Brain blood flow measured with intravenous H215O: II: Implementation and validation. J Nucl Med 1983;24:790–798.
23. McCarney ER, Armstrong BD, Lingwood MD, Han S. Hyperpolarized water as an authentic magnetic resonance imaging contrast agent. Proc Natl Acad Sci U S A 2007;104:1754–1759.
24. Harris T, Szekely O, Frydman L. On the potential of hyperpolarized water in biomolecular NMR studies. J Phys Chem B 2014;118:3281– 3290.
25. Ardenkjær-Larsen JH, Laustsen C, Bowen S, Rizi R. HyperpolarizedH2O MR angiography. Magn Reson Med 2014;71:50–56.
26. Schoenberg SO, Rieger J, Weber CH, Michaely HJ, Waggershauser T,Ittrich C, Dietrich O, Reiser MF. High-spatial-resolution MR angiography of renal arteries with integrated parallel acquisitions: comparison with digital subtraction angiography and US. Radiology 2005;235: 687–698.
27. Ardenkjær-Larsen JH, Leach AM, Clarke N, Urbahn J, Anderson D, Skloss TW. Dynamic nuclear polarization polarizer for sterile use intent. NMR Biomed 2011;24:927–932.
28. Zollner FG, Weisser G, Reich M, Kaiser S, Schoenberg SO, Sourbron SP, Schad LR. Ummperfusion: an open source software tool towards quantitative MRI perfusion analysis in clinical routine. J Digit Imaging 2013;26:344–352.
29. Wentland AL, Artz NS, Fain SB, Grist TM, Djamali A, Sadowski EA.MR measures of renal perfusion, oxygen bioavailability and total renal blood flow in a porcine model: noninvasive regional assessment of renal function. Nephrol Dial Transplant 2012;27:128–135.

Paper V

Manuscript in preparation

Dynamic Coronary MR Angiography in the Pig using Hyperpolarized Water

Kasper Wigh Lipsø, M.Sc.[1], Esben Søvsø Szocska Hansen M.Sc[2,3], Rasmus Stilling Tougaard, MD[2,4], Christoffer Laustsen, PhD[2] and Jan Henrik Ardenkjær-Larsen, PhD[1,5]

[1]Department of Electrical Engineering, Technical University of Denmark, Kgs. Lyngby, Denmark.

[2]Department of Clinical Medicine, MR Research Centre, Aarhus University, Aarhus, Denmark

[3]Danish Diabetes Academy, Odense, Denmark

[4]Department of Cardiology - Research, Aarhus University Hospital, Aarhus, Denmark

[5]GE Healthcare, Brøndby, Denmark.

Abstract

Rationale: Magnetic resonance imaging is a safe modality providing high-resolution images of soft tissue. However, the inherent low sensitivity limits the achievable signal and contrast. Hyperpolarization has been shown to increase the signal several orders of magnitude, and recently been translated to human cardiac application. The use of hyperpolarization suggests that large reductions in scan time can be achieved, enabling the high temporal resolution required to acquire dynamic cardiac images without motion artifacts for coronary flow and tissue perfusion assessment.

Objective: To demonstrate the first dynamic coronary magnetic resonance angiographies using hyperpolarized water.

Methods and Results: Water was hyperpolarized using dissolution dynamic nuclear polarization at 5 T to a polarization of >5% in a clinical polarizer. Sample was injected into the coronary arteries of Danish landrace pigs (N = 9, 3 injections in 3 different animals) over 6 s. MRI images were acquired with a gradient echo sequence of 5° flip angle in a tilted slab covering the main right coronary arteries. The acquisition time of each frame was 870 ms.

Conclusions: High signal-to-noise MR angiography of the coronary arteries of a large animal model with high spatial resolution and temporal resolution was demonstrated. The dynamic first pass nature of the positive contrast examination, allows perfusion analysis of the water movement from the arteries to the capillary bed of the cardiac tissue.

Key words: Coronary Angiography, Cardiac Perfusion, Magnetic Resonance Angiography, Hyperpolarization, dissolution-DNP

Name and complete address for correspondence: Jan Henrik Ardenkjær-Larsen, DTU Electrical Engineering, Ørsteds Plads, Building 349, room 126, 2800 Kgs. Lyngby, Denmark. Tel (0045) 4525 3918. E-mail: jhar@elektro.dtu.dk

Sources of Funding: This work was supported by the Danish Research Council (grant number 12-127232) and the Danish National Research Foundation (grant number DNRF124).

Disclosures: The authors report no conflicts.

Introduction

Magnetic Resonance Angiography (MRA) for coronary artery imaging has so far failed to translate into widespread clinical use[1,2]. This is partly due to the inherent low sensitivity of current MRA methods, extending the acquisition time to several minutes and multiple respiration and heart cycles[3]. Coronary arteries are challenging structures to image with MRI due to the small and tortuous vessel structures and motion. Therefore, successful coronary MRA requires high-resolution, whole-heart imaging, and effective motion suppression. Current free-breathing protocols use segmented acquisitions with prospective electrocardiography (ECG) and navigator gating to suppress cardiac and respiratory motion artefacts and blurring. The current strategy for cardiac gating means that the acquisition window is well within one of the quiescent periods, leaving the remaining time (80-90%) unused.

Today, the typical first-line test for evaluation of Coronary Artery Disease (CAD) is stress SPECT Myocardial Perfusion Imaging (MPI) or contrast-enhanced Coronary CT coronary Angiography (CCTA)[4]. Increasing evidence support the altered myocardial perfusion as an accurate diagnostic marker of CAD[4]. Water perfusion is of particular interest and has been demonstrated with ^{15}O-labeled water in positron emission tomography (PET)[5–8]. To date, MR contrast agents consist of other compounds (primarily Gadolinium-based chelates), with different permeability dynamics than water[9,10]. Recent advances have introduced Arterial Spin Labeling (ASL) to map the perfusion of blood in the myocardial tissue[11,12], however, common to these methods is the inherent low sensitivity, and thus lack of robustness and diagnostic quality.

One way to dramatically increase the sensitivity of MRI is hyperpolarization. In hyperpolarization, we detect the magnetic resonance signal from a molecule that has gone through an activation process, hyperpolarization, to enhance the nuclear spin polarization by many orders of magnitude[13]. The hyperpolarized state decay at a rate that is slow enough to allow us to follow the fate of the molecule for seconds to minutes. Hyperpolarization is typically performed on endogenous, metabolically active ^{13}C labelled molecules, such as [1-^{13}C]pyruvate. The method that has recently been translated to human use for characterization of cancer[14] or assessment of myocardial metabolism[15]. Imaging of hyperpolarized inert ^{13}C labelled molecules for angiography and perfusion has been demonstrated in both rodent and large animal models[16–20]. The direct detection of signal from injected molecules, improves the quantification of the perfusion compared to conventional perfusion methods[21–27].

MRI of hyperpolarized carbon-13 suffers from needing specialized scanner hardware and coils and a lack of optimized pulse sequences. Instead, hyperpolarization of the protons of water molecules would allow the use of conventional MR hardware and pulse sequences. In addition to compatibility with existing equipment, protons have the advantage of a four times higher magnetic moment than that of ^{13}C, resulting in a larger magnetization, and hence signal. The main drawback of hyperpolarized water is the short relaxation time. After hyperpolarization, during handling, transfer and injection, the relaxation time is 20-30 s[28,29], but as soon as the water protons have been injected into the blood stream, the relaxation time reduces to a few seconds[30] requiring intra-arterial injection. Hyperpolarized water has been demonstrated for MRI angiographies in small animal models, where the cerebral network and the vena cava were imaged[30], and was recently applied for angiographies of the pig renal arteries, and perfusion measurements of the kidney tissue[29]. In this study, we hypothesize that high resolution dynamic coronary MRA and myocardial perfusion can be acquired using hyperpolarized water. This may be combined with the metabolic assessment as demonstrated by Cunningham et al.[13] to provide both metabolic and hemodynamic information within the same scan session.

Methods

Sample and medium preparation: A sample of 1 mL 30 mM TEMPO (2,2,6,6-Tetramethylpiperidine 1-oxyl, 98%) in H_2O/glycerol 1:1 (w/w) was prepared. Dissolution medium consisted of D_2O with 1 mM calcium disodium ethylenediaminetetraacetic acid (EDTA) and 9 g/L NaCl (all from Sigma Aldrich, Denmark).

Fluid path filling: The fluid path consisted of a syringe, from which the heated dissolution medium was transferred in an inner concentric tube to the sample vial for dissolution of the sample. The dissolved sample was transferred out of the magnetic field in the outer concentric tube.

The sample was placed in the vial using a 150 cm filling tube[31] and frozen in liquid nitrogen. 31.01 g dissolution medium (28 mL) was filled in the syringe and degassed by bubbling with helium gas for 10 minutes. The fluid path was flushed with helium gas for 2 minutes in order to remove air and ensure clear passage.

Polarization: The sample vial was rapidly transferred from the liquid nitrogen bath to the 5 T magnet in the polarizer (SPINlab, GE Healthcare, Brøndby, Denmark). The sample was irradiated with app. 50 mW microwaves at 139.923 GHz for one hour.

Dissolution: The syringe containing the dissolution medium was heated to 130 °C one hour before dissolution. The piston in the syringe was driven with 16 bar pressure. The dissolved sample was injected into a sealed separatory funnel (150 mL) containing 25 mL of heptane (>99%, Sigma Aldrich, Denmark). The heptane had been degassed by flushing with helium gas in the funnel for 10 minutes. The funnel was shaken heavily during dissolution for a total of 10 s from dissolution start. The lower, aqueous phase was extracted into a syringe before transferring to the scanner room. The proton concentration in the dissolved sample was analyzed by NMR after addition of 0.2 M potassium formate (Sigma Aldrich, Denmark) as reference.

Animal protocol: All animal experiments were carried out in compliance with the guidelines for use and care of laboratory animals and were approved by the Danish Inspectorate of Animal Experiments. Three healthy 30 kg female Danish domestic pigs were pre-sedated with intramuscular injection of Stressnil (1 mL/kg), and Midazolam (1 mL/kg), and anesthesia was maintained by continuous intravenous infusion of Propofol (0.4 mg/kg/h) and Fentanyl (8 ng/kg/h). The animals were intubated and mechanically ventilated with a 60 % O_2-air mix.

A 6 F introducer sheath was positioned in the left common femoral artery by ultrasound guidance to allow access for a 6F, JR 4.0, angiography catheter to be placed in the left LAD coronary artery via x-ray guidance. The angiography catheter was repeatedly flushed with heparinized sterile water to avoid occlusion. 15 mL hyperpolarized water was injected over 5 s, initiated approximately 22 s after dissolution.

MRI acquisition: MRI detection was performed on a 3 T GE HDx with an 8-channel cardiac array receiver coil (GE Healthcare, Milwaukee, WI, USA). Axial and coronal images were acquired to cover the heart to allow for planning of the angiography slab for hyperpolarized water imaging. The sequence was as follows: a 3D T_1 weighted sequence with a standard steady state free precession sequence (TE = 1.1 ms, TR = 2.7 ms, FA = 35°, image matrix 256x256, FOV = 340x340 mm^2, in-plane resolution of 1.3 mm and slice thickness of 3 mm). Angiographies were acquired in a tilted plane covering the left anterior descending artery (LAD) using a gradient echo sequence with FA = 5°, slice thickness of 40 mm, TR = 3.4 ms, TE = 0.984 ms, matrix size 256x256 and FOV = 140x140 mm^2. The acquisition time was 870 ms.

ROI analysis of the images were performed in OsiriX (Pixmeo, Geneva, Switzerland). Apparent signal-to-noise ratio (aSNR) and coronary sharpness were measured to quantify image performance[32]. aSNR was measured at the left main stem coronary artery where the catheter was positioned (signal at bolus peak / SD prior injection) and coronary sharpness was measured in the proximal LAD at bolus peak – reported as mean and standard deviation between the individual shots (N = 8).

Results

A water proton polarization of 5.3 ± 0.9 % and relaxation time T_1 = 24 ± 1 s (N = 4) was estimated by injecting the sample into a phantom placed in the 3 T scanner next to a thermally polarized water reference sample, Figure 1, recently published elsewhere[29].

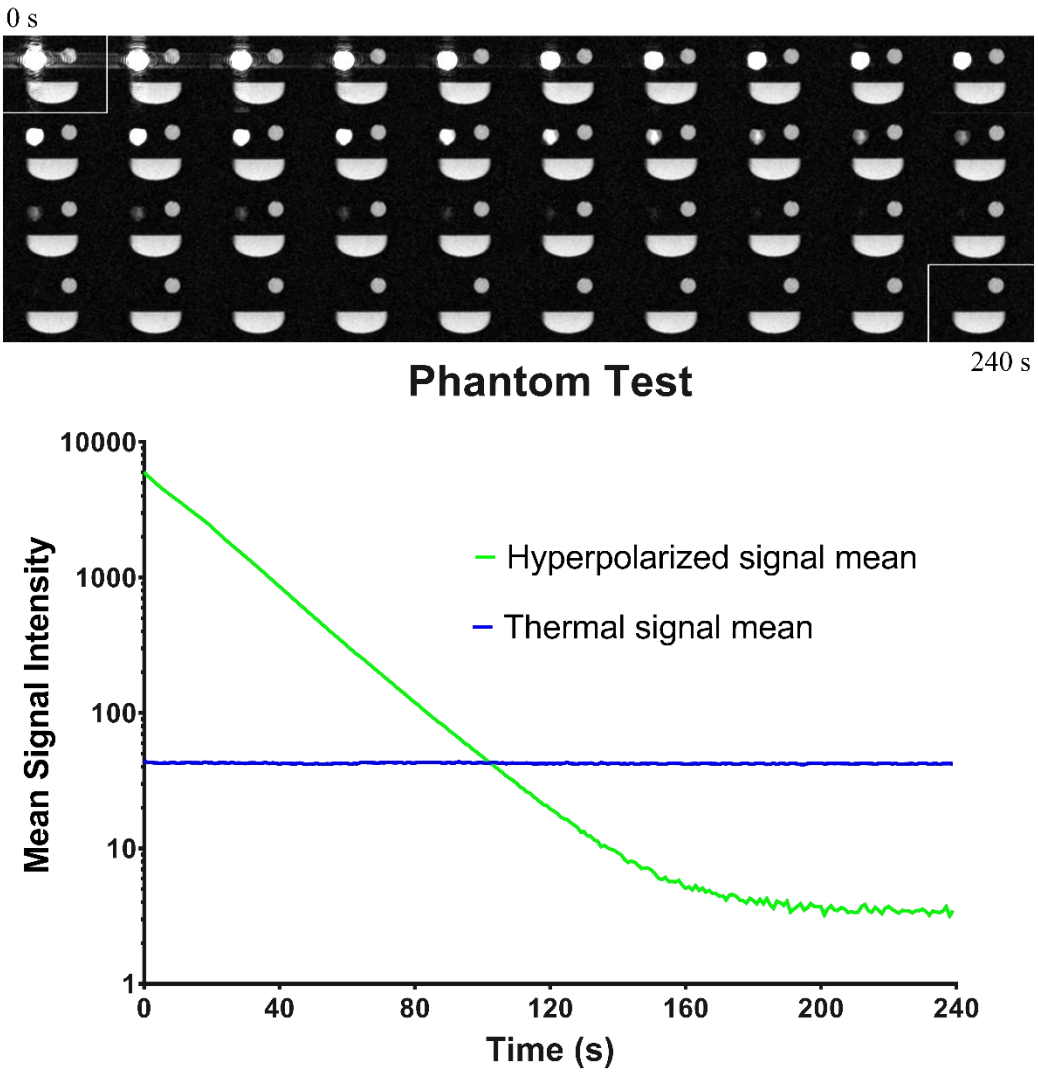

Figure 1: The graph shows ROI signal means of the hyperpolarized ^1H in D_2O (green, decaying signal) and the H_2O thermal phantoms (blue, steady signal). The phantoms consist of two syringes. Stacked images (same scale) are shown from 0 to 240 s with an image every 6 s. The hyperpolarized MR signal is initially 211 times stronger than the thermal H_2O signal, and the T_1 of the decay is 24 s. The hyperpolarized signal decays into the noise since the ^1H density is ca 20 times lower than the thermal H_2O sample. Data published in [29].

Reproducible hyperpolarized MRA examinations in healthy pigs (N=3) were demonstrated with three successive acquisitions of coronal angiographies (Figure 2). The aorta injection site, the LAD and the left circumflex appear with the highest intensity, and their branches with smaller diameter and lower intensity. The presented images are acquired 5 s after injection of hyperpolarized sample, and some leaking into the vascular

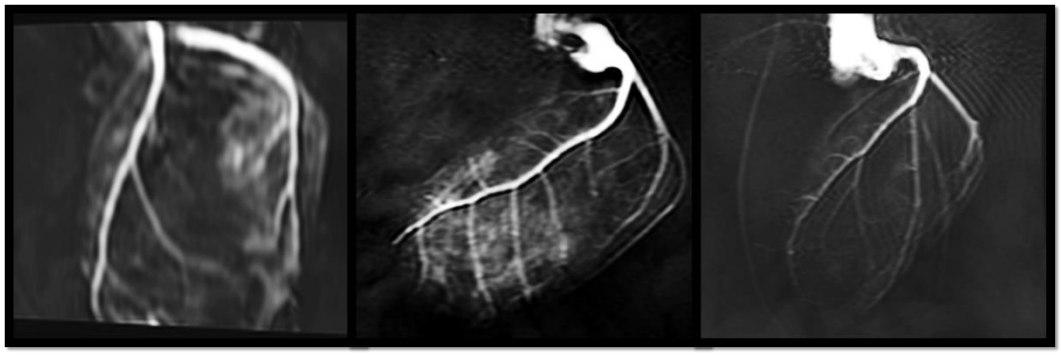

Figure 2: Coronary angiographies after hyperpolarized water injections in three different animals. Images 5 s after injection of sample.

bed is observed in between arteries. The orientation and projection are different in the three animals, but the images in each individual animal were reproducible. aSNR from the left main stem was 269±169 and coronary sharpness from proximal LAD was 0.31±0.086 mm^{-1}.

A time series of angiographies is presented in Figure 3, initiated from the first observed hyperpolarized signal and 11 additional time steps of 1 s each. High intensity signal was evident in the main coronary arteries in frames 3-7, during which fresh sample was injected. After that, the maximum intensity decreased due to relaxation and wash out of the sample. No hyperpolarized signal was observed after 14 s. Frames 3, 4, 6, 7 and 12 of the series suffers from motion artefacts, possibly from cardiac contractions.

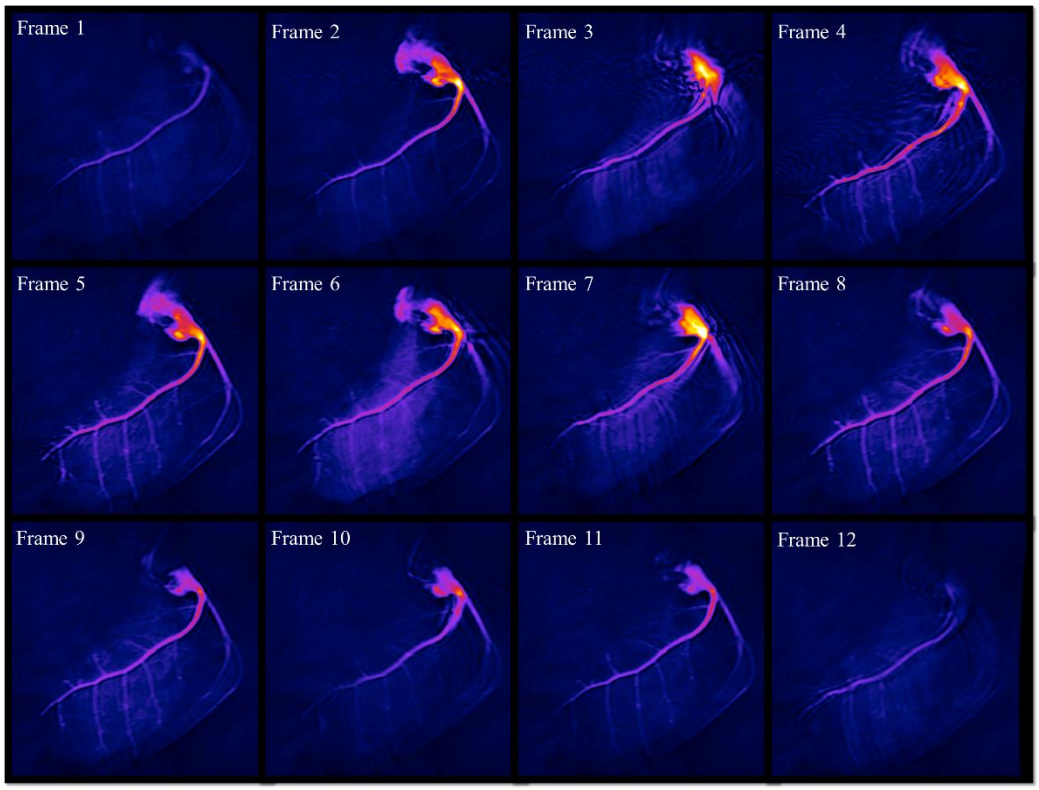

Figure 3: Time series of consecutive images acquired every second from injection of sample. Major and minor vessels of the coronary tree can easily be identified.

The signal in the minor branch arteries appeared after the first few time steps, and appeared increasingly more distinct throughout the series until vanishing due to relaxation and washout. Similarly, the signal in the tissue occurred with a time delay from the arterial signal. The temporal profile is shown in Figure 4, where the average signal intensity in regions of interest (ROI) in the proximal LAD, medial LAD and at a distal branch of LAD. The signal increase is first observed in the proximal LAD, and later in the medial and distal branch of the LAD, describing the perfusion from injection site into the vasculature.

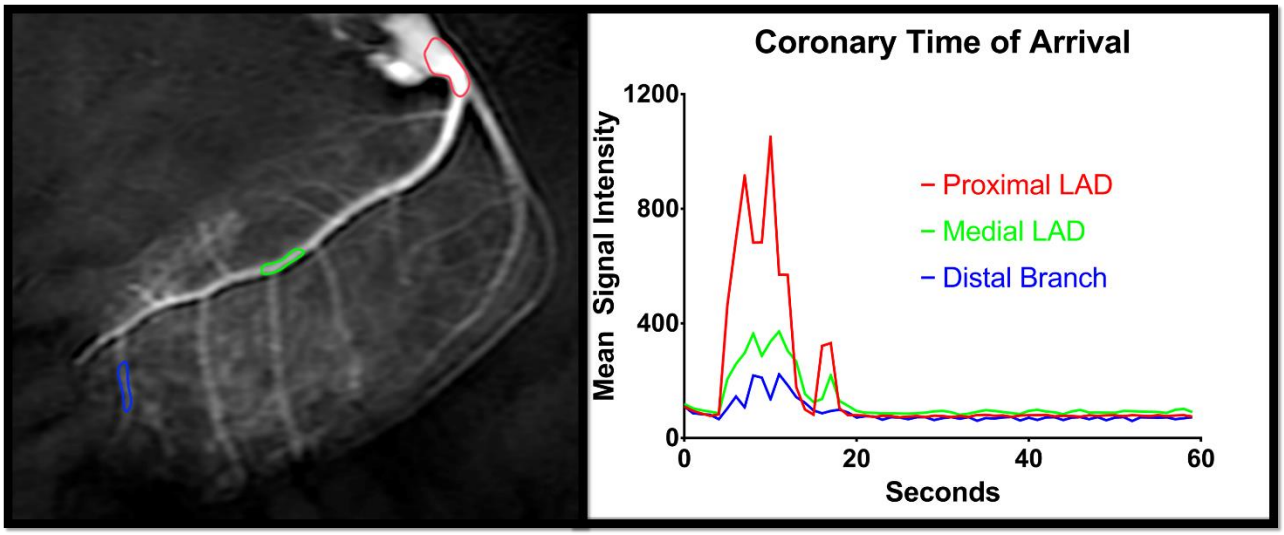

Figure 4: Time of arrival of hyperpolarized water at proximal LAD, medial LAD and at a distal branch of LAD.

Discussion

The main finding of this study was the demonstration of the feasibility of using hyperpolarized water for dynamic coronary angiography and perfusion mapping. The high reproducibility and quality of the images in a large animal model shows great promise for future applications in humans. The coronary arteries in the porcine model resembles human cardiac anatomy, and thus portrays the clinical situation well. The coronary arteries were imaged with high resolution and SNR. The angiograms are of high quality, and is superior to coronary MRA available in today's clinical practice. A main drawback of the method is the invasive nature of the catheterization.

The images are acquired in less than one second, providing series of high temporal resolution. Thus the perfusion of the cardiac tissue can be evaluated by fitting the signal with a model function, where also the relaxation of the signal is accounted for. This technique would provide perfusion values of water, contrary to most established perfusion measurement techniques, where the perfusion of contrast enhancing compounds is recorded, without exposing patients to ionizing irradiation. The high perfusion of the cardiac muscle as well as its importance in cardiovascular disease makes it an obvious organ for hyperpolarized water perfusion imaging. The motion of the heart is a key challenge for authentic measurements. Thus, ECG triggered acquisition and respiratory control is required for automated perfusion data analysis, something we do not have access to in the current setup. In general, the scanner used in this study is not optimized for cardiac imaging and the performance inferior to current state of the art[33–35].

The hyperpolarization method yielded consistent, reproducible sample properties; MR signal in particular. The images in this study were obtained with 5% proton polarization. We believe that ten times higher polarization is achievable, dramatically improving the image quality over what is presented here.

The method presented in this study should be translational to clinical use. The same polarizer (SPINlab) used for clinical studies with [1-13C]pyruvate was used, providing the possibility of producing sterile samples. The safety profile of the formulation needs to be established, and the catheterization of coronary arteries may be the largest challenge for clinical translation.

References

1. Kato S, Kitagawa K, Ishida N, Ishida M, Nagata M, Ichikawa Y, Katahira K, Matsumoto Y, Seo K, Ochiai R, Kobayashi Y, Sakuma H. Assessment of Coronary Artery Disease Using Magnetic Resonance Coronary Angiography. *J Am Coll Cardiol*. 2010;56:983–991.

2. W. Yong Kim, M.D. PD, Peter G. Danias, M.D. PD, Matthias Stuber PD, Scott D. Flamm MD, Sven Plein MD, Eike Nagel MD, Susan E. Langerak MS, Oliver M. Weber PD, Erik M. Pedersen, M.D. PD, Matthias Schmidt MD, René M. Botnar PD, Warren J. Manning MD. Coronary Magnetic Resonance Angiography for the Detection of Coronary Stenoses. *N Engl J Med*. 2011;345:1863–1869.

3. Kramer CM, Narula J. Atherosclerotic Plaque Imaging: The Last Frontier for Cardiac Magnetic Resonance. *JACC Cardiovasc Imaging*. 2009;2:916–918.

4. Takx RAP, Blomberg BA, El Aidi H, Habets J, de Jong PA, Nagel E, Hoffmann U, Leiner T. Diagnostic accuracy of stress myocardial perfusion imaging compared to invasive coronary angiography with fractional flow reserve meta-analysis. *Circ Cardiovasc Imaging*. 2015;8.

5. Herscovitch P, Markham J, Raichle ME. Brain Blood Flow Measured with Intravenous H215O.: I. Theory and Error Analysis. *J Nucl Med*. 1983;24:782–789.

6. Raichle ME, Martin WRW, Herscovltch P, Mintun MA, Markham J. Brain Blood Flow Measured with Intravenous H215O.: II. Implementation and Validation. *J Nucl Med*. 1983;24.

7. Rosen BR, Belliveau JW, Vevea JM, Brady TJ. Perfusion imaging with NMR contrast agents. *Magn Reson Med*. 1990;14:249–265.

8. Bergmann SR, Herrero P, Markham J, Weinheimer CJ, Norine M. Noninvasive Quantitation of Myocardial Blood Flow in Human Subjects With Oxygen-15 Labeled Water and Positron Emission Tomography. *J Am Coll Cardiol*. 1989;14:639–652.

9. Prompona M, Cyran C, Nikolaou K, Bauner K, Reiser M, Huber A. Contrast-Enhanced Whole-Heart MR Coronary Angiography at 3.0 T Using the Intravascular Contrast Agent Gadofosveset. *Invest Radiol*. 2009;44:369–374.

10. Bi X, Carr JC, Li D. Whole-heart coronary magnetic resonance angiography at 3 Tesla in 5 minutes with slow infusion of Gd-BOPTA, a high-relaxivity clinical contrast agent. *Magn Reson Med*. 2007;58:1–7.

11. Schwitter J, Wacker CM, Wilke N, Al-Saadi N, Sauer E, Huettle K, Schönberg SO, Luchner A,

Strohm O, Ahlstrom H, Dill T, Hoebel N, Simor T. MR-IMPACT II: Magnetic Resonance Imaging for Myocardial Perfusion Assessment in Coronary artery disease Trial: perfusion-cardiac magnetic resonance vs. single-photon emission computed tomography for the detection of coronary artery disease: a comparative. *Eur Heart J*. 2013;34:775–81.

12. Kober F, Jao T, Troalen T, Nayak KS. Myocardial arterial spin labeling. *J Cardiovasc Magn Reson*. 2016;18:22.

13. Ardenkjaer-Larsen JH, Fridlund B, Gram A, Hansson G, Hansson L, Lerche MH, Servin R, Thaning M, Golman K. Increase in signal-to-noise ratio of > 10,000 times in liquid-state NMR. *Proc Natl Acad Sci U S A*. 2003;100:10158–10163.

14. Nelson SJ, Kurhanewicz J, Vigneron DB, Larson PEZ, Harzstark AL, Ferrone M, Criekinge M Van, Chang JW, Bok R, Park I, Reed G, Carvajal L, Small EJ, Munster P, Weinberg VK, Ardenkjaer-larsen JH, Chen AP, Hurd RE, Odegardstuen L, Robb FJ, Tropp J, Murray J a. Metabolic Imaging of Patients with Prostate Cancer Using Hyperpolarized [1- 13 C]Pyruvate. *Sci Transl Med*. 2013;5:198ra108.

15. Cunningham CH, Lau JY, Chen AP, Geraghty BJ, Perks WJ, Roifman I, Wright GA, Connelly KA. Hyperpolarized 13 C Metabolic MRI of the Human Heart: Initial Experience. *Circ Res*. 2016;In press.

16. Golman K, Axelsson O, Jóhannesson H, Månsson S, Olofsson C, Petersson JS. Parahydrogen-induced polarization in imaging: Subsecond 13C angiography. *Magn Reson Med*. 2001;46:1–5.

17. Golman K, Ardenkjær-Larsen JH, Svensson J, Axelsson O, Hansson G, Hansson L, Jóhannesson H, Leunbach I, Månsson S, Petersson JS, Pettersson G, Servin R, Wistrand L-G. 13C-Angiography. *Acad Radiol*. 2002;9:507–510.

18. Svensson J, Månsson S, Johansson E, Petersson JS, Olsson LE. Hyperpolarized 13C MR angiography using trueFISP. *Magn Reson Med*. 2003;50:256–262.

19. Lipsø KW, Magnusson P, Ardenkjær-Larsen JH. Hyperpolarized 13 C MR Angiography. *Curr Pharm Des*. 2016;22:90–95.

20. Olsson LE, Chai CM, Axelsson O, Karlsson M, Golman K, Petersson JS. MR coronary angiography in pigs with intraarterial injections of a hyperpolarized 13C substance. *Magn Reson Med*. 2006;55:731–737.

21. Von Morze C, Larson PEZ, Hu S, Yoshihara H a I, Bok R a., Goga A, Ardenkjaer-Larsen JH, Vigneron DB. Investigating tumor perfusion and metabolism using multiple hyperpolarized 13C compounds: HP001, pyruvate and urea. *Magn Reson Imaging*. 2012;30:305–311.

22. Von Morze C, Bok RA, Reed GD, Ardenkjaer-Larsen JH, Kurhanewicz J, Vigneron DB. Simultaneous multiagent hyperpolarized 13C perfusion imaging. *Magn Reson Med*. 2014;72:1599–1609.

23. Grant AK, Vinogradov E, Wang X, Lenkinski RE, Alsop DC. Perfusion imaging with a freely diffusible hyperpolarized contrast agent. *Magn Reson Med*. 2011;66:746–755.

24. Johansson E, Månsson S, Wirestam R, Svensson J, Petersson JS, Golman K, Ståhlberg F. Cerebral Perfusion Assessment by Bolus Tracking Using Hyperpolarized 13C. *Magn Reson*

Med. 2004;51:464–472.

25. Lau AZ, Miller JJ, Robson MD, Tyler DJ. Cardiac perfusion imaging using hyperpolarized 13 c urea using flow sensitizing gradients. *Magn Reson Med*. 2016;75:1474–1483.

26. Lau AZ, Miller JJ, Robson MD, Tyler DJ. Simultaneous assessment of cardiac metabolism and perfusion using copolarized [1-(13) C]pyruvate and (13) C-urea. *Magn Reson Med*. 2016;0:1–8.

27. Park I, von Morze C, Lupo JM, Ardenkjaer-Larsen JH, Kadambi A, Vigneron DB, Nelson SJ. Investigating tumor perfusion by hyperpolarized 13C MRI with comparison to conventional gadolinium contrast-enhanced MRI and pathology in orthotopic human GBM xenografts. *Magn Reson Med*. 2016;0:n/a-n/a.

28. Olsen G, Markhasin E, Szekely O, Bretschneider C, Frydman L. Optimizing water hyperpolarization and dissolution for sensitivity-enhanced 2D biomolecular NMR. *J Magn Reson*. 2016;264:49–58.

29. Lipsø KW, Szocska Hansen ES, Tougaard R, Laustsen C, Ardenkjær-Larsen JH. Renal MR Angiography and Perfusion in the Pig using Hyperpolarized Water. *Magn Reson Med*. 2016;In press.

30. Ardenkjaer-Larsen JH, Laustsen C, Bowen S, Rizi R. Hyperpolarized H2O MR angiography. *Magn Reson Med*. 2014;71:50–56.

31. Malinowski RM, Lipsø KW, Lerche MH, Ardenkjær-Larsen JH. Dissolution Dynamic Nuclear Polarization capability study with fluid path. *J Magn Reson*. 2016;272:141–146.

32. Li D, Carr JC, Shea SM, Zheng J, Wielopolski PA, Finn JP. Coronary Arteries: Magnetization-prepared Contrast-enhanced Three- dimensional Volume-targeted Breath-hold MR Angiography. *Radiology*. 2001;219:270–277.

33. Henningsson M, Hussain T, Vieira MS, Greil GF, Smink J, Ensbergen G v, Beck G, Botnar RM. Whole-heart coronary MR angiography using image-based navigation for the detection of coronary anomalies in adult patients with congenital heart disease. *J Magn Reson Imaging*. 2016;43:947–55.

34. Addy NO, Ingle RR, Wu HH, Hu BS, Nishimura DG. High-resolution variable-density 3D cones coronary MRA. *Magn Reson Med*. 2015;74:614–621.

35. Nezafat M, Henningsson M, Ripley DP, Dedieu N, Greil G, Greenwood JP, Börnert P, Plein S, Botnar RM. Coronary MR angiography at 3T: fat suppression versus water-fat separation. *Magn Reson Mater Physics, Biol Med*. 2016;5–10.